Understanding and Optimising the Mechanical Effects of Textured Indentation in Cold Roll Metal Forming

David Scholtz

A thesis submitted to the University of Sussex for the degree of Doctor of Philosophy in Engineering

March 2020

Declaration

I hereby declare that this thesis has not been and will not be submitted in whole or in part to another University for the award of any other degree.

David Scholtz

Signature: _____

Date: _____

Abstract

Textures are commonly applied to steel sheet for the mechanical benefits produced however, the mechanisms responsible for these benefits are not well understood, causing undesirable variation in the results. This thesis aims to investigate these mechanisms and their impact on the mechanical behaviour of dimpled steel.

Investigating UltraSTEEL®, developed by Hadley Industries, the possibility of grain boundary strengthening was explored; microstructural examination of dimpled sheet revealed possible grain size reductions resulting from the dimpling process. It was noted that this should result in a correlation between Lüders elongation in the plain steel and the strengthening due to dimpling.

To test this and understand how the mechanical response of dimpled steel differs from that of the plain steel source material, numerous tensile tests were conducted. This enabled statistical analysis to identify correlations such as the aforementioned. Confirming the Lüders elongation – strengthening link, an expression predicting strengthening based on Lüders elongation in the plain steel was established.

Investigating the stiffness implications of dimpling, the geometric effects were assessed using FEA of plain and dimpled cross-sections. This illustrated that dimpled geometry necessitates a reduction in stiffness. However, the material property changes due to dimpling counteract this reduction.

Observing that standard measures for yield strength are not representative of the behaviour of dimpled steel, alternatives were explored. The inapplicability of these measures was attributed to macroscopic geometric non-uniformity, leading to the proposal of the novel derivative yield criterion. This novel criterion was applied

successfully to both plain and dimpled steel (discontinuous and continuous yield, respectively) and the implications for the predictive expression developed here have been addressed.

FEA was used to apply new understanding to optimise the dimple tooth profile. Existing and novel tooth geometries and configurations were assessed based on plastic strain distributions and thinning. Consequently, the novel star profile was proposed for experimental evaluation.

Acknowledgements

Firstly, I would like to thank my supervisor, Dr Chang Jiang Wang, for his support and guidance throughout this research. His expertise in the related methodologies and experience in the doctoral process have been crucial to the completion of this thesis. I would also like to thank my second supervisors, Dr Romeo Glovnea and Prof Diane Mynors for their feedback and advice.

I am grateful for the support and input from Dr Martin English and Robert Ng along with the entire research team at the Hadley Group. I am particularly grateful to Robert Ng for his continued work in supporting and, in some cases, conducting the testing required to complete this thesis as well as the suggestions and observations he has made that were critical to findings contained herein. Further to this, I thank the University of Sussex, the Hadley Group, and the EPSRC for this studentship.

I extend my sincerest gratitude to Dr Jennifer Mankin at the University of Sussex who took the time to teach me the basics and intricacies of statistical modelling alongside completion of her own PhD and starting a full-time position as lecturer at the university. She has also provided invaluable support through the difficulties of the doctoral process. This thesis would not have been possible without her support and guidance.

Special thanks go to my family and friends who have supported me in innumerable ways through my studies. I could not have completed this thesis without all of you.

Table of Contents

List of Figures

List of Tables

List of Symbols

Δ_ε	Strain range from 0.2% offset yield to UTS
Δ_σ	Stress range from 0.2% offset yield to UTS
ε_{eng}	Engineering Strain
ε_{true}	True Strain
ε_{UTS}	Strain to UTS (total strain as measured at UTS)
$\varepsilon_{y,0.2}$	Strain to Yield (total strain as measured at 0.2% offset yield)
$\varepsilon_{y,\Delta}$	Strain to Derivative Yield (total strain as measured at $\sigma_{\Delta Y}$)
σ_0	Material constant (Hall-Petch)
$\sigma_{\Delta Y}$	Derivative Yield Stress
σ_{eng}	Engineering Stress
σ_{EUL}	Extension-Under-Load Yield Stress
σ_{LY}	Lower Yield Stress
σ_{true}	True Stress
σ_{UY}	Upper Yield Stress
σ_y	Yield Stress
$\sigma_{Y,0.2}$	0.2% Offset Yield Stress
cov_{xy}	Covariance of variables ‘x’ and ‘y’
d	Average grain diameter (Hall-Petch)
DX51D	Mild steel specification
E	Elastic Modulus
k_y	Material constant (Hall-Petch)
r	Pearson’s correlation coefficient
R^2	Coefficient of determination
S_x	Standard Deviation of variable ‘x’
T_m	Tangent Modulus
Y_d	Yield Drop
Y_e	Lüders Elongation (or Yield-Point Elongation)
Y_{inc}	Yield Increase (as a percentage of the relevant plain steel yield)

List of Acronyms

AS	Standards Australia
ASTM	American Society for Testing and Materials
BSI	British Standards Institution
CEN	European Committee for Standardization
DGPM	Dimpled-Geometry-Plain-Material
ECAP	Equal-channel-angular-pressing
FE / FEA	Finite Element / Finite Element Analysis
GTN	Gurson-Tvergaard-Needleman yield criterion
ISO	International Organization for Standardization
LYS	Lower Yield Stress
SD	Standard Deviation
SEM	Scanning Electron Microscopy
SPD	Severe plastic deformation
US	UltraSTEEL®
UTS	Ultimate Tensile Strength
UYS	Upper Yield Stress
w-EDM	Wire electrical discharge machine
YPE	Yield-Point Elongation (or Lüders Elongation)

Chapter 1 Introduction

1.1 Cold Roll Forming

Cold roll forming is the process by which coiled sheets of metal are incrementally formed into a desired cross-section as defined based on the intended application of the product. Commonly used to produce lighter, stronger substitutes for wooden beams, this process is often configured to form C- or Z-shaped cross-sections [1]. As illustrated in Figure 1.1, this is achieved by arranging a series of forming rolls in tandem, collectively known as a 'rolling mill' [2].

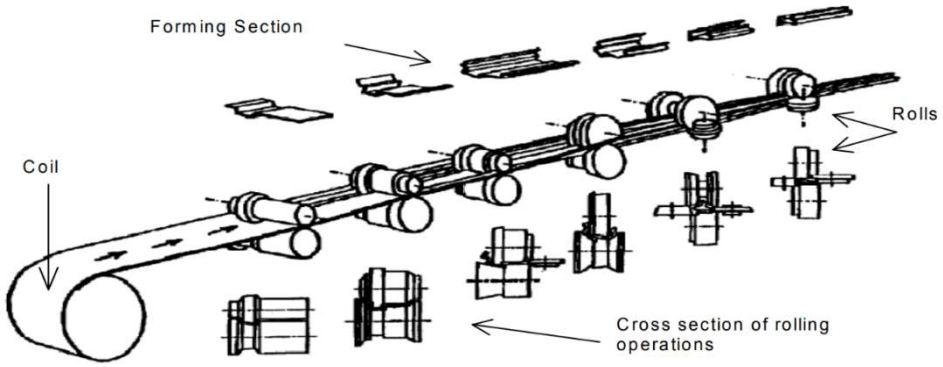

Figure 1.1 - Schematic representation of the cold roll forming process (rolling mill) [3]

1.2 UltraSTEEL®

Ever increasing demands for strength of materials with minimal cost increases have led to the use of 'stiffeners' in products such as those mentioned above. These are geometric deviations from an otherwise uniform cross-section whose primary purpose is the increase of the relevant measure of strength of the product [2, 4]. Where tensile yield strength is the measure of concern, these stiffeners may take the form of a pattern of small dimples covering the surface of the product. Hadley Industries has developed one such form known as UltraSTEEL® [5, 6]. Non-processed material (i.e. flat sheet) is hereafter referred to as 'plain'.

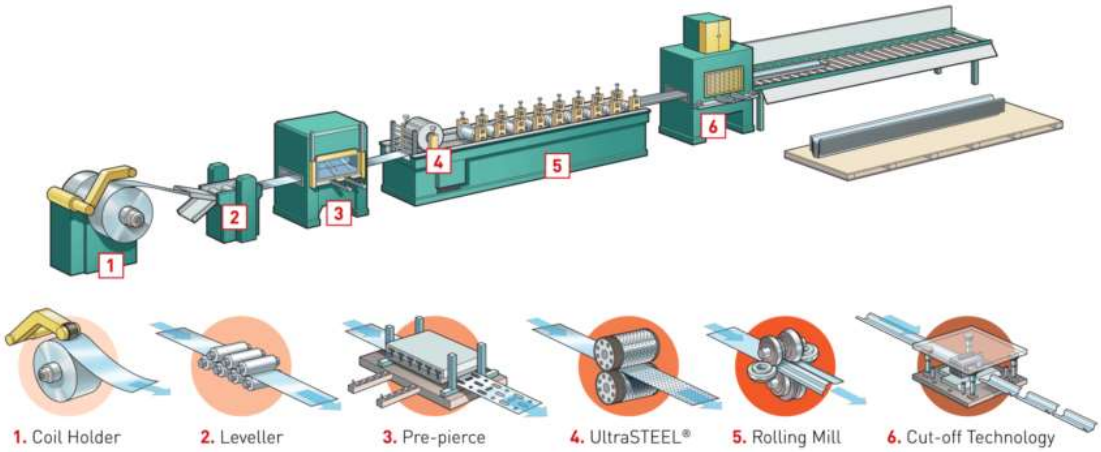

Figure 1.2 - Cold roll forming production line including UltraSTEEL® [6]

This UltraSTEEL® dimple texture is applied ahead of the rolling mill as shown in Figure 1.2 by two opposing rolls, illustrated in Figure 1.3, that are covered in the specially designed 'tooth' geometries to apply the appropriate plastic deformation to the coil.

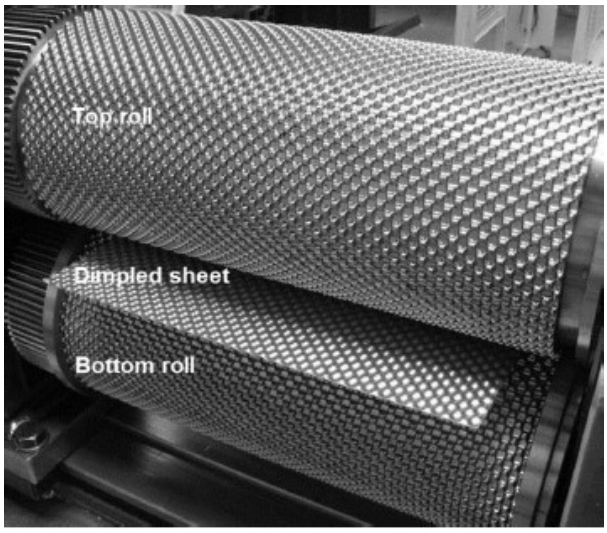

Figure 1.3 - The UltraSTEEL® dimpling process and dimpled steel sheet [2]

Though others have been considered, the UltraSTEEL® dimple texture has to-date been in production using three different dimple geometries, each producing greater increases to yield strength than those before. These are named simply UltraSTEEL 1® (US1), UltraSTEEL 2® (US2), and UltraSTEEL 3® (US3). The US1 dimple geometry is a square-based pyramid featuring 'sharp' edges and a pointed tip. US2 uses a

similar dimple geometry but with geometric radii to eliminate the 'sharp' edges and pointed tip of its predecessor. Taking this smoothing concept further, US3 features a spherical contact geometry for the dimple teeth. As the current production variant, UltraSTEEL 3® is discussed in greater detail in Chapter 7 .

1.3 Research Motivation

The previous research has shown that the strengthening effect is largely due to strain hardening [2, 4, 7, 8]. However, the mechanisms at work during forming are not currently well understood. Thus, the aim of this research is to further specific understanding of the mechanisms responsible for the observed strengthening of steel due to application of the dimpling process.

While the application of the dimpling process results in an increase in the tensile yield strength of processed steel, the magnitude of this increase cannot be predicted by existing models. Since the apparent unpredictability of this variation is largely attributed to the aforementioned limited understanding, this research incorporates the development of a predictive methodology. Intended for quick and easy application in an industrial context, this method enables a quantitative assessment of the strengthening potential of a given batch of plain steel, minimising waste due to the forming of steel that yields minimal strengthening.

1.4 Scope and Disambiguation

Accounting for approximately 90% [9] of UltraSTEEL® production, DX51D galvanised steel [10] is by far the most common material specification used by Hadley Industries [5, 9, 11]. Additionally, as noted previously, tensile yield strength is the most relevant measure in common applications of UltraSTEEL®. Therefore, any advances in understanding here while more widely applicable, focus on increases in tensile yield for material adhering to the DX51D specification.

Unless otherwise specified, the standard measures for yield strength are used [12]. The most notable upshot of this is that measures of increase in yield strength use the 'lower yield' for plain steel and the '0.2% offset yield' or 'proof stress' for UltraSTEEL®. The applicability and implications of the use of these measures are discussed in detail in Chapter 6 .

1.5 Aim and Objectives

The aim of this research is to identify and explain the main strengthening mechanisms at work in the application of the dimpling process to facilitate understanding in industry and illustrate how new understanding may be applied to benefit industrial efficiency and interests. The actualisation of this aim is split into the following interdependent objectives.

1. Explore the impact of the dimpling process on the overall stiffness of the resulting dimpled sheet as characterised by the elastic modulus in tension.
2. Develop for predictive purposes, an expression enabling quick and easy quantification of the potential increase in yield strength for a given batch of plain steel in the case that the UltraSTEEL® dimpling process is applied to it.

3. Explain from basic principles, the mechanisms responsible for the trends utilised in the development of the expression from objective 2 both to establish the correlation(s) as causative and to facilitate industry understanding of why the dimpling process is effective.
4. Illustrate why the standard yield criteria may not be appropriate for characterising the stress-strain curve of products incorporating macroscopic geometric non-uniformity such as dimple textures and propose a criterion overcoming this limitation of applicability.
5. Implement existing Finite Element models alongside new understanding of the relevant strengthening mechanisms to propose novel dimple geometries capable of effecting greater yield strength increases than UltraSTEEL®.

1.6 Structure of this Thesis

Chapter 1 presents the subject, motivations, and scope of the work herein and outlines the structure of this thesis.

Chapter 2 presents a summary overview of the relevant literature. The areas covered include: the cold roll metal forming process; the effects of non-uniform macrostructures and the dimpling process on the strength and stiffness of metals; standard methods and criteria for the quantification of yield strength in tension; the finite element modelling of the cold roll forming dimpling process.

Chapter 3 details experimental investigation of the effect of the UltraSTEEL® dimpling process on criteria such as the tensile yield strength and ultimate tensile strength and explores established theory regarding the strengthening mechanisms in ductile metals. In this way, the strengthening mechanisms at work during dimpling are identified with the help of microstructural examinations by SEM.

Chapter 4 presents statistical analyses of the dataset from Chapter 3 with the goal of identifying correlations between plain steel properties and the increase in tensile yield strength due to dimpling. Through the application of established theory and the SEM examinations, the strongest correlation identified is explained as causative. This causative relationship is then exploited to develop an expression quantifying the potential increase to the tensile yield strength of plain steel should the UltraSTEEL® dimpling process be applied.

Chapter 5 experimentally explores the response of the dimpled sheet to cyclic tensile loading with incremental increases to the maximum strain with each cycle, thereby investigating geometric contributions to stiffness as characterised by the 'effective' elastic modulus. Additionally, 2-dimensional beam bending finite element simulations are completed, validated using beam theory, to explicitly illustrate the effects of the macroscopic dimple texture on the response of beams to bending loads.

Chapter 6 summarises the standardised methods for the quantification of the tensile yield strength of ductile metals, detailing the assumptions made in the formulation of these standards and thus, the limitations of their applicability. Expanding on this, it is illustrated that these standards are not appropriate for samples exhibiting substantially continuous yield such as those incorporating macroscopic geometric non-uniformities (e.g. UltraSTEEL® products). A novel yield criterion that exhibits similar accuracy in conventional test cases and a wider applicability than existing standards is presented. This is then applied to the tensile results from Chapter 3 to explore the impact of the new criterion on the outcomes of Chapter 4 .

Chapter 7 explores and applies existing Finite Element models to compare the potential for strengthening due to the application of previous and current production UltraSTEEL® dimple geometries. This is followed by an assessment of previously considered geometries along with the presentation of novel geometries and patterns exploiting a more complete understanding of the mechanisms at work during the dimpling process.

Chapter 8 summarises the conclusions of the previous chapters and discusses possibilities for future work and recommendations for further investigation.

1.7 Original Contributions to Knowledge

This research encompasses several original contributions ranging in relevance from specific industry applications through to international standard practices. Centred around the effects of surface dimple textures on the mechanical properties of steel sheet, many of the outcomes may be relevant to other metals and to products incorporating macroscopic geometric non-uniformities such as porous metals.

- An extensive series of standard tensile tests was completed to investigate the industry-standard mechanical characteristics of both plain steel and dimpled steel in the form most produced by Hadley Industries. Additionally, microstructural examinations of the dimpled cross-section were conducted. Together, these tests enabled the development of specific understanding of the mechanisms responsible for the strengthening effects of the UltraSTEEL® dimpling process.
- This new understanding was then applied through the development of a quantitative expression with which to predict the magnitude of

strengthening to a given batch of plain steel should the UltraSTEEL® dimpling process be applied. The upshot of this expression is an industrially implementable capability to tailor the strength of UltraSTEEL® products to the given application by sourcing material offering the appropriate work hardening potential.

- Cyclic tensile loading tests incorporating incrementation of the peak strain with each cycle were completed. These served to explore the evolution of the elastic modulus through plastic deformation of a standard sample for both plain steel and dimpled steel. Referred to here as the 'effective' elastic modulus, this illustrated the variability of the geometric contributions to sample stiffness where macroscopic geometric non-uniformities are present. Illustrative finite element simulations were also completed for 'beam' cross-sections in both plain steel and dimpled steel to more clearly illustrate the effect of this geometric non-uniformity on the response to bending loads. These clearly showed how a reduction to sample stiffness is a necessity imposed by the geometric non-uniformity. However, comparison with results from the literature indicated that the material property changes due to the dimpling process largely negate any geometric stiffness reductions. It was also noted that this is likely the source of the observed variation in results regarding the post-dimpling stiffness.
- An analysis of methods for the quantification of tensile yield strength as defined by international standards organisations (BSI and ASTM) has been conducted for both plain steel and dimpled steel. As a result, it was determined that these standards are not suitable for the accurate

quantification of the tensile yield strength of dimpled steels. To address this observation, a novel approach based on the second derivative of stress with respect to strain in a standard stress-strain curve was developed. In addition to the reliable quantification of tensile yield in the case of severely continuous yield (such as that exhibited by dimpled steel), it was illustrated that this novel criterion correctly identifies the upper yield point in cases exhibiting discontinuous yield (such as plain steel). This elimination of the need to 'choose' a quantification method/criterion is perhaps the most significant strength of the proposed derivative yield criterion.

- New understanding developed through the present research was applied alongside a Collins-style finite element model to propose and assess the potential of existing and novel dimple tooth profiles and configurations.

Chapter 2 Literature Review

2.1 Mechanical Properties of Dimpled Steels

Some of the first investigations exploring the relationship between the topography of dimpled steel and the observed changes in the mechanical properties due to dimpling, conducted by Collins *et al*, found that there is a clear relationship between plastic strain and strain hardening [4, 13]. This was achieved through both experimental and simulated exploration of the topography of the dimpled surfaces alongside microhardness testing of the various regions of the cross-section thereof. This relationship can be explained, as discussed in section 3.2 , as the result of the motion of large numbers of dislocations through the material grains due to loading.

Knowledge of this relationship between plastic strain and strain hardening has since been used in numerous investigations [2, 8, 14–18] ranging from assessment of the dimple tooth geometries [13] through to investigation of the specific energy absorption of dimpled steel products in applications such as crash barriers [19].

Yet to be investigated however, is whether grain boundary strengthening may be an additional contributor to the strengthening effect observed in steel following the dimpling process. As Callister notes, one useful method to conduct the necessary examination of the material microstructure is scanning electron microscopy (SEM) [20]. In this way, it can be determined whether the dimpling process effects a reduction in the grain size (grain refinement) of the steel.

Numerous studies have explored the microstructure of various materials and how these evolve through the manufacture and testing methods commonly applied in industry [21–25]. It has been established that substantial plastic deformation

results in a refinement of the average grain size of the material. Substantially affecting the loading response thereof, this has led to the classification and development of processes for this particular purpose. Processes of this sort, equal-channel-angular-pressing (ECAP) for example, are sometimes referred to a severe plastic deformation (SPD) techniques [26–29].

2.2 Strengthening Mechanisms in Cold Roll Metal Forming

In 2004, Toribio [30] explored the mechanisms by which steel is macroscopically strengthened during continuous cold drawing. Through the combined microstructural evaluation and mechanical testing of samples with various degrees of cold drawing, it was determined that developments within the steel microstructure during drawing results in the observed macroscopic strengthening. Furthermore, it was noted that a Hall-Petch type relationship could not be fitted to the data, illustrating the need identified by Dieter [31] to apply the Hall-Petch equation with some caution.

In 2017 Wang *et al* [32] also explored the link between microstructural evolution and strengthening. In this study, it was observed that the GW102K alloy subjected to cyclic extrusion and compression for the purpose of grain size refinement does exhibit the Hall-Petch relationship. However, it was also noted that over-refinement of the grain structure results in decreasing strength for ultrafine grained materials.

2.3 The Effect of Dimpling on Sample Stiffness in Steel

In the 2011 study [14], Nguyen *et al* determined through tensile testing that dimpled steel dogbone samples, such as those defined in Chapter 3 , exhibit a stiffness that is lower than the plain steel equivalent by some undefined margin. At the time, this

was attributed to the 'unfolding' of the dimples in the early stages of loading for dimpled samples. This is illustrated in Figure 2.1 It was also noted that the apparent reduction in stiffness of the samples due to dimpling was rather small compared to the effect of the cold work.

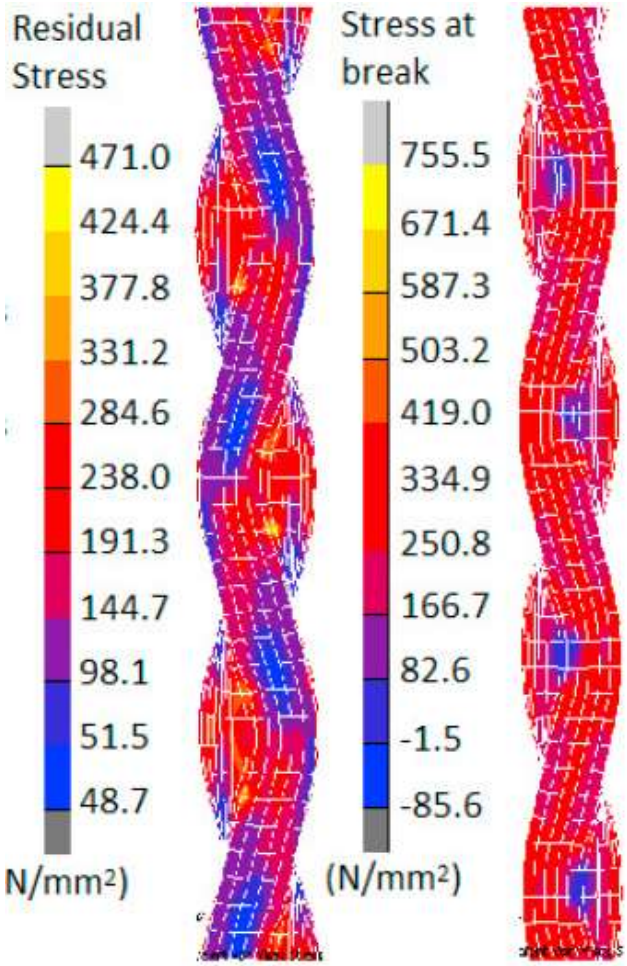

230

Figure 2.1 - FE tensile models showing the residual stresses before loading and the stress at failure (modified) [8]

These findings were reiterated in 2014 when Nguyen *et al* quantified this comparison in a study considering the results from both tensile and bending tests [2]. The work of fracture for the plain and dimpled samples was calculated by integration of the force-extension curve. The difference between these was taken as the cold work applied to the steel by the dimpling process. Measuring in, in this case, at less than 1% of this cold work, the stiffness reduction was indicated to be

negligible. This was further supported by bending tests completed as part of the same study and indicated similar stiffness for both plain and dimpled sheets. Figure 2.2 illustrates the tensile testing conducted as part of this study. This shows that there is no substantial difference between the elastic moduli of the experimental plain and dimpled specimens.

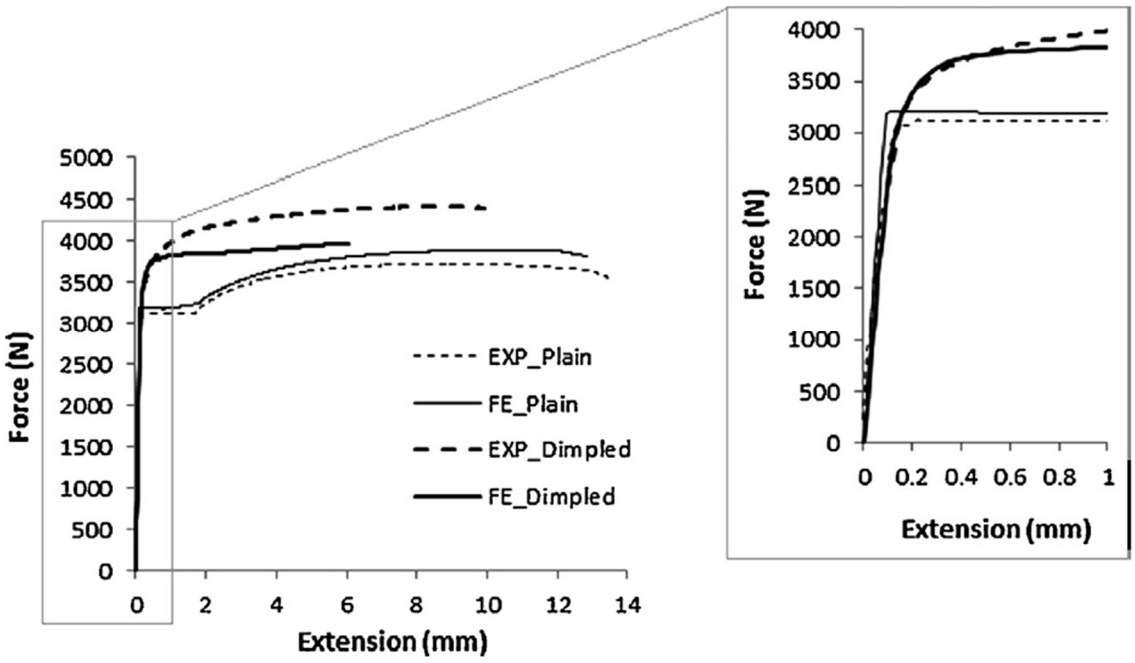

Figure 2.2 - FE and experimental force-extension curves of the plain and dimpled specimens [2]

In a later study in 2017 [8], looking again at the potential for stiffness reductions due to the UltraSTEEL® dimpling process, Nguyen *et al* explored these findings further. This study focused on the effects of including or excluding consideration of residual stresses in finite element simulation of the dimpling process. It was concluded, in this case, that the stiffness reduction observed, while still small, is a necessary result of the residual stresses within the dimpled steel samples.

In 2018, Liu *et al* explored the tensile and bending rigidities of a similar product referred to only as 'duplex embossed steel sheet' and produced using a punch and die setup [33] as opposed to the cold roll forming setup used to produce

UltraSTEEL® [34]. The effect on rigidity of several aspects of the dimpling specification were considered, forming depth for example, through tensile and bending tests in addition to some empirical analysis. Where the configurations considered match the current UltraSTEEL® standards, comparison of the load-deflection curves in bending for different forming depths and pre-strains show no substantial difference over a wide range of forming depths, as shown in Figure 2.3. This supports the assertion that any potential stiffness changes due to dimpling are small in magnitude.

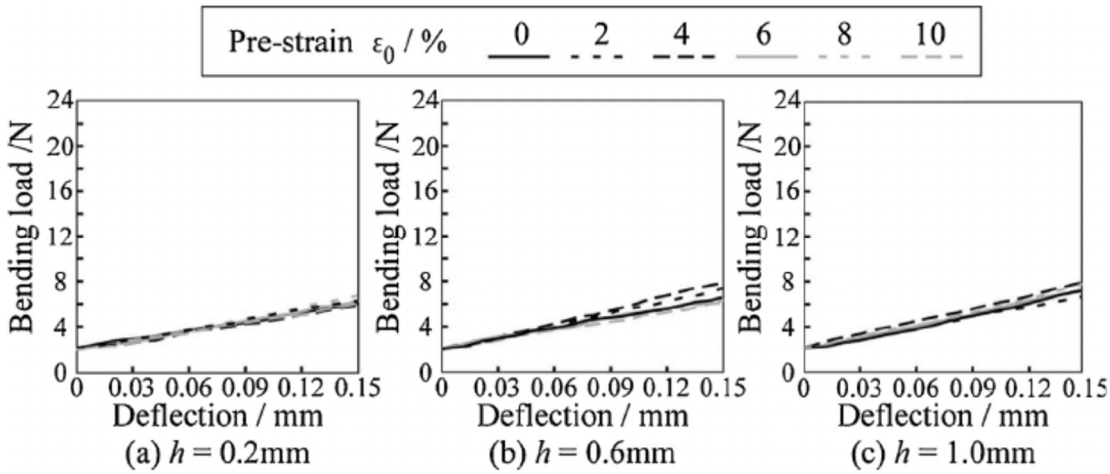

Figure 2.3 - Load deflection response of embossed steel sheets with different forming depths and pre-strains [33]

The plastic strain applied by the dimpling process, assuming a consistent tooth geometry, can be considered broadly in terms of the forming depth and distance between the forming teeth (tooth pitch): increased forming depth and decreased tooth pitch each effect an increase in the plastic strain applied. The effects that changes in these variables have on the mechanical properties of the dimpled sheet were investigated in 2018 by Wang *et al* through the application of finite element methods [35]. Regarding the elastic modulus, Wang *et al* observed that modification

of either of these variables to increase the plastic strain applied results in a decrease in the elastic modulus.

The above are all studies exploring the stiffness of dimpled steel versus plain steel in the form of a 'flat' sheet, be it rectangular (bending tests) or dogbone (tensile tests) samples. In 2012, Nguyen *et al* conducted a brief study exploring this question of stiffness in the context of UltraSTEEL® products [36]. Specifically, compression tests were conducted on the common C-stud beams [37]. In this study, again comparing the elastic regions of the load-displacement curves, it was found that the plain and dimpled columns exhibit substantially similar stiffnesses.

Nguyen *et al* have conducted a few studies exploring the stiffness implications of the UltraSTEEL® dimpling process where the elastic modulus was used as a measure representing the sample stiffness [2, 8, 14, 36]. The same measure will be adopted in Chapter 5 for the purposes of comparison.

2.4 Measurement of the Yield Strength of Materials

2.4.1 Standards for the Measurement of Yield Strength in Tension

The macroscopic yield of metallic materials in tension is usually defined as the point at which appreciable plastic flow begins [38–40]. However, application of this definition to identify said point is not straightforward which has resulted in the standardisation of multiple methods, selectively used based on the context. This currently amounts to 4 standard methods for the quantification of yield strength, defined by the ASTM [41] as follows.

The simplest case is that of discontinuous yield. This type of yield behaviour is easily identifiable based on the presence of the yield-point phenomenon which manifests

as a peak marking departure from linearity in the stress-strain curve, followed by a 'plateau'. The length of this plateau is measured in terms of strain from the highest point of the peak to the onset of strain hardening and is known as yield point elongation, YPE or Y_e. This is illustrated in Figure 2.4. Also illustrated in the same
300 figure are the related standard measures, the upper yield strength (UYS or σ_{UY}) and the lower yield strength (LYS or σ_{LY}).

The σ_{UY} is the measure most true to the as-defined yield and is based on the observation that discontinuous yield inherently incorporates a distinct point where the stress-strain behaviour departs from linearity. As such, σ_{UY} is simply measured as the maximum stress of the peak, marking the initiation of Y_e. It is worth noting that although this is a sound measure, it has been determined that the height of the peak is sensitive to testing conditions [42, 43]. As a result, the σ_{LY} is sometimes used instead in industry.

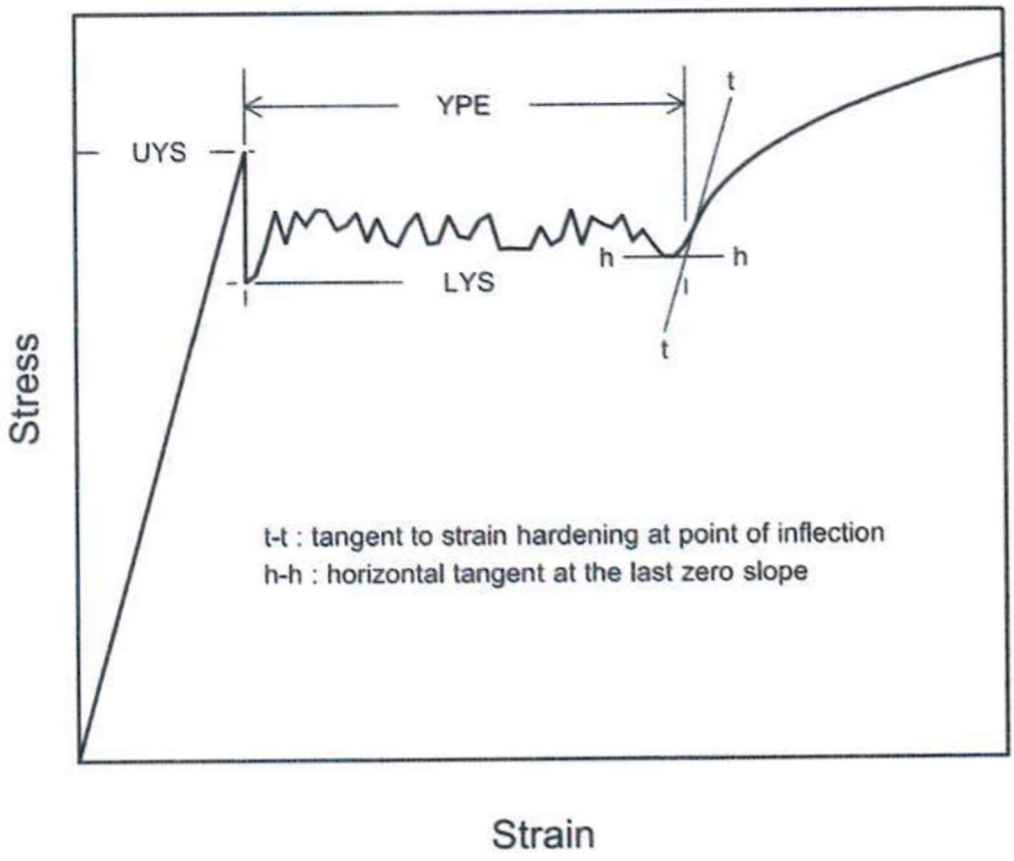

Figure 2.4 - Stress-Strain diagram showing Yield Point Elongation (YPE) and Upper (UYS) and Lower (LYS) Yield Strengths [44]

Rather than relying on the peak, the σ_{LY} is defined as the minimum stress observed during Y_e. Thus, effectively measuring the minimum tensile yield stress of the tested material, this measure incorporates a safety margin of sorts.

Both measures defined for the standard quantification of discontinuous yield are dependent on the presence of Y_e and are therefore limited in applicability to cases of clearly discontinuous yield only.

Identifiable based on a lack of Y_e, continuous yield is effectively considered as the alternative to discontinuous yield. This is illustrated in Figure 2.5 and, according to the standards, is quantified using either the proof strength, non-proportional extension (offset yield, σ_Y) or the proof strength, total extension (extension under load, σ_{EUL}).

The σ_Y is based on a strain-wise offset of a line representing the elastic modulus. This is illustrated in Figure 2.5 as line OA, offset to produce line mn. The point where line mn intersects the original stress-strain curve is then defined as the yield point. The offset used is not explicitly defined by the standards but is most commonly 0.2% strain [12, 44], producing the $\sigma_{Y,0.2}$. Note 33 of the ASTM specification also states that this measure is considered to be the default [44]. The 0.2% strain is a somewhat arbitrary figure used to approximate appreciable plastic strain and therefore implicitly assumes that offsetting the elastic modulus can be reliably used as an analogue to plastic strain. This results in three limitations to the applicability of the offset method. Firstly, the stress-strain curve must include a substantial linear-elastic region to enable reliable representation of the elastic modulus. Secondly, the elastic behaviour must not vary appreciably over the range of the offset employed. Finally, the microscopic and macroscopic yields must be similar to ensure that the stress-strain behaviour is predominantly plastic where the offset line is coincident with the stress-strain curve. The only remaining standard then, is the σ_{EUL}. This is represented by line qp in Figure 2.5 and is simply the stress at a pre-determined strain. As such, this measure is primarily applicable in applications where an allowable strain under a given load is more pertinent than the yield strength. Even so, this is explored further in the following sections.

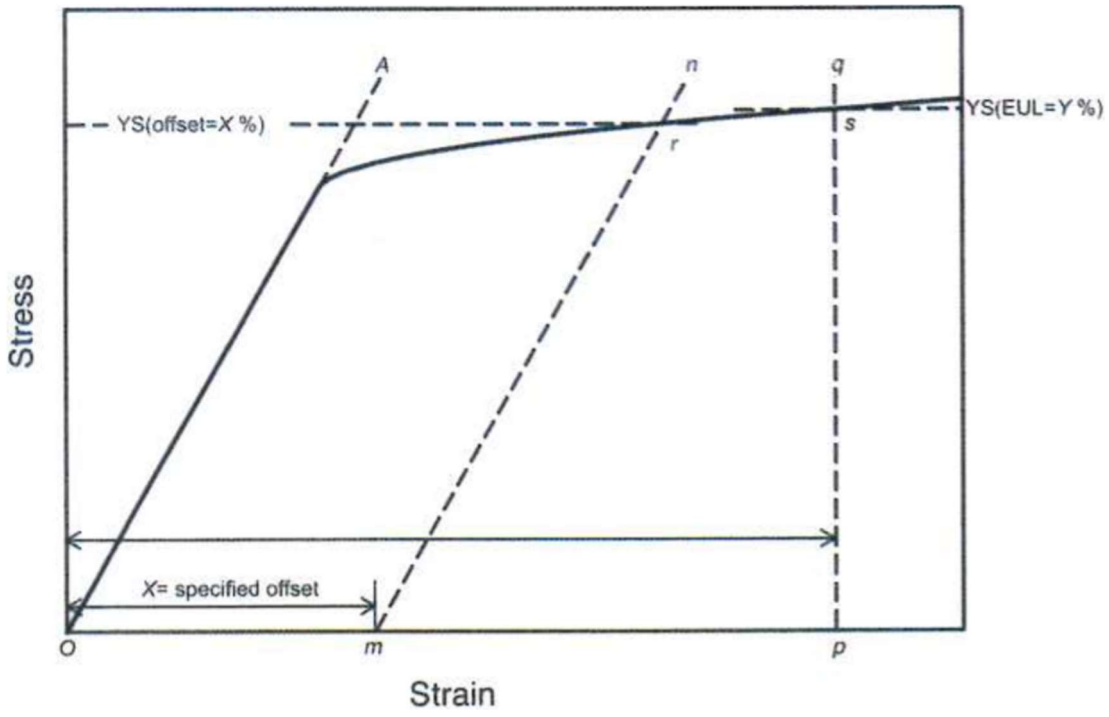

Figure 2.5 - Stress-Strain diagram illustrating the determination of both the Proof Strength, Non-Proportional Extension (a.k.a. Offset Yield) and the Proof Strength, Total Extension (a.k.a. Extension Under Load, EUL) [44]

2.4.2 Alternative Criteria for the Determination of Yield Strength

With numerous analytical yield criteria such as the Von Mises yield criterion [45] in regular use, there has been much debate regarding the applicability of the available criteria to various cases [46–54]. The associated investigations have produced many novel yield criteria for use in the cases where others either do not apply or provide inaccurate results. Of particular interest when considering macroscopic structures such as dimples, many of these investigations have explored the mechanical response of, and proposed yield criteria for, porous [55–67] and lattice [68–77] materials.

The distortion energy theorem [53, 78, 79] forms the basis for the common Von Mises yield criterion. This theorem asserts that the portion of specific strain energy contributing to isochoric shape change, the distortion energy, reaches some critical value associated with yield. Due to this basis purely on the isochoric shape change,

an assumption of plastic incompressibility is made. Thus, the Von Mises yield criterion states that yield is dependent on some function of the principal shear stresses only. Discounting the intermediate principal shear stress produces the simpler Tresca yield criterion. Despite its relative simplicity, use of the Tresca yield criterion, considering the maximum and minimum principal shear stresses, is less common due to the requirement of prior knowledge regarding which are the maximum and minimum principal shear stresses.

The question regarding the applicability of individual yield criteria goes back at least as far as 1989 when Donovan [46] conducted a study that determined that the Mohr-Coulomb criterion, not the usual Von-Mises criterion, is the more representative criterion in the case of $Pd_{40}Ni_{40}P_{20}$ metallic glass.

Subsequently, in 1993, Karafillis and Boyce [48] proposed a more general-form yield criterion in the form of an expression for the yield surface of polycrystalline materials. It was noted that this expression can also be reduced to the existing Tresca or Von-Mises criteria if appropriate.

Building on a criterion first proposed by Barlat and Lain [80] in 1989, Banabic *et al* [49] introduced in 2003, three additional coefficients to provide more accurate representation of the plastic behaviour of sheet metals. This was reported to exhibit increased flexibility compared with its predecessor due to the use of seven coefficients to describe the yield surface and performs well when applied to data collected by Kuwabara *et al* [81, 82].

Similar to the approach taken by Karafillis and Boyce [48], Cazacu and Barlat [50] proposed, in 2004, an expression describing the asymmetry in yielding of pressure insensitive metals. Reportedly exhibiting good agreement with both experimental

and theoretical yield loci, this expression, similarly to that proposed by Karafillis and Boyce, reduces to the Von Mises yield criterion in the case where the compressive and tensile yield stresses are equal. Continuing this investigation in 2006 and 2008, Plunkett, Cazacu, and Barlat [51, 52] produced multiple yield functions describing the anisotropic behaviour of textured metals. These functions are reported to accurately characterise different crystal structures and are based on the yield surfaces of aluminium and steel.

2.4.3 Alternative Criteria: Porous Materials

Instigating a series of investigations, the 1975 and 1976 publications by Gurson [62, 63] explored both the microscopic and macroscopic behaviour of porous materials. Gurson developed two different types of upper bound yield function that include consideration for rigid particle inclusions and void nucleation mechanisms, through application of a yield locus approach. These form the basis for what is now commonly referred to as Gurson type yield criteria [56, 58, 59, 61]. The distinction made between microscopic and macroscopic behaviour are now common [30, 57, 76, 77, 83, 84] with 'macroscopic' referring to the aggregate behaviour of the material as opposed to the pointwise 'microscopic' behaviour.

Sheet metal with through-thickness holes were used by Liao *et al* [57] as an analogue to represent the behaviour of porous materials. Employing this simplification, they produced a Gurson type closed-form upper bound macroscopic yield criterion for the case of in-plane uniaxial loading. Wang *et al* [61] validated this in 2004 through the finite element analysis of a cube containing a spherical void.

In 2001, Sevostianov and Kachanov [55] sought to eliminate the assumption of spherical porosity made in previous studies. To achieve this, a plastic yield condition

explicitly accounting for non-randomly oriented non-spherical pores was constructed. They also reported that the only significant effect of porosity on the mechanical behaviour of the material is a decrease in the yield strength, thereby determining that total strain at the onset of macroscopic plasticity is independent of the porosity.

More recently, McElwain *et al* [59] investigated the extension of the 1984 Gurson-Tvergaard-Needleman (GTN) yield criterion [85] to account for different arrangements of spherical voids. Featuring finite-element modelling to explore the yield behaviour of simple cubic, body-centred cubic, and face-centred cubic arrangements of spherical voids, this 2006 investigation effectively resulted in the development of different expressions tailored to each case. These proposed extensions to the GTN formula were reported to have achieved greater accuracy in the representation of general stress states without introducing additional parameters.

Taking a similar approach in 2008 to the original work by Gurson, Keralavarma and Benzerga [56] presented the derivation of analytical yield loci for anisotropic porous materials. In this way, they proposed a new yield criterion that includes consideration for spheroidal voids and Hill-type orthotropy.

In 2012, Madou and Leblond [58] conducted further work on the Gurson yield criterion to include consideration for arbitrary ellipsoidal porosity. They noted that this developed Gurson criterion approximately matches the original Gurson criterion when applied to the case of spherical voids.

2.4.4 Alternative Criteria: Lattice Materials

To date, studies regarding the applicability of various yield criteria to the mechanical behaviour of metallic lattices have produced somewhat mixed results. It seems likely that this is due to different investigations considering different specific lattice structures.

In 2001, Deshpande *et al* [70] used both analytical and finite element methods to explore the mechanical behaviour of the octet-truss lattice. Good agreement was reported between the FE predictions and the experimental results. However, Deshpande *et al* concluded that the considered extension to the anisotropic Hill yield criterion produces inaccurate characterisation of the collapse surfaces. Conversely, Khaderi *et al* [77] reported in 2014 that the anisotropic Hill criterion accurately represents the yield surface of the imperfect lattice for gyroid lattices.

Considering specifically stretching dominated lattices in 2006, Hualin and Wei [71] employed an equivalent continuum method to develop a more appropriate yield model. The resulting calculated yield surfaces reportedly showed good agreement with the experimental data.

Metal foam, metal hexagonal honeycomb, metal lattice, and lattice composite were investigated in 2008 by Zhang *et al* [69]. They established analytical elastic relations and failure criteria based on a unit cell assessment of the static equilibrium and deformation relations. These were then validated by FE simulation and it was reported that the out-of-plane constraint of these lattices significantly influences their in-plane strength during loading. The proposed analytical approach reportedly identifies this effect.

Chen *et al* [75] observed in 2012 that previous studies assume that the behaviour of lattice materials during loading is stretching dominated. To test the validity of this assumption, they investigated the bending resistance of the strut components of lattice truss sandwich panels. Based on their experimental results, Chen *et al* determined that stretching dominated models overestimate the strength of lattices and underestimate their stiffness. Chen *et al* go on to present a model reported to produce predictions that more closely match the experimental results.

It is evident from the above that the increasingly tailored approaches to the development of yield criteria have resulted in many methods for the quantification of yield that do not achieve broad applicability. The standard use of multiple, sometimes conflicting, methods for the quantification of yield strength also results in the necessary comparison of the results from yield criteria that are incompatible.

Considering the behaviour of dimpled steel under load, Liang *et al* [19] have shown that the curved nature of the stress-strain curve, the severely continuous yield, is a result of geometric non-uniformity. Additionally, Nguyen *et al* [8] and Wang *et al* [35] have determined that this geometric non-uniformity significantly impacts the stress-strain behaviour of the material. The stress concentrations lead to local microscopic yield occurring at lower stress levels and thus, departure from linearity in the stress-strain curve prior to macroscopic yield. This is similar to the deviation from the pre-macroscopic yield departure from the ideal elastic response observed by Máthis *et al* [84] in 2018.

2.5 Finite Element Modelling of the Dimpling Process

In 2003, Collins *et al* developed a reduced-geometry finite element model to simulate a minimum representative geometry (unit cell) for the UltraSTEEL® dimpling process [4]. Figure 2.6 shows that this consists of a block representing a portion of the steel sheet and four dimples, two above and two below the block.

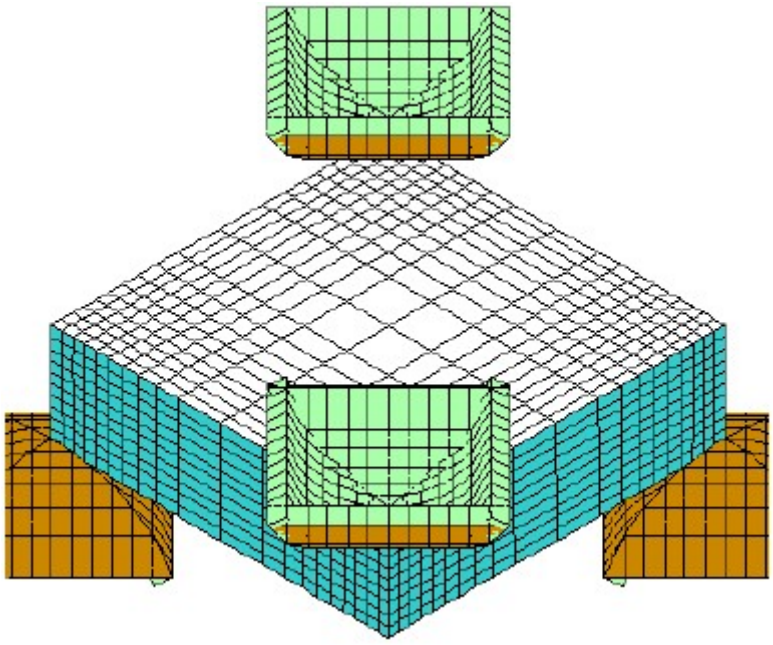

Figure 2.6 - Collins-style finite element model simulating the UltraSTEEL® dimpling process [4]

480 In this study, Collins *et al* explored the effects of forming depths from 1.25x to 2.2x the plain steel gauge – minimal dimpling through to a final overall thickness of more than twice that of the plain steel. By comparing the simulation results with experimental topographical scans, it was determined that this simulation methodology produces geometrically accurate computational specimens and therefore, accurate plastic strains. It was also noted that the plastic strain distribution bears some correlation with the strengthening due to dimpling.

Further evidence supporting the validity of this correlation was presented by the same authors in 2004 [13]. Through comparisons made between the simulated

plastic strains and experimental microhardness tests, it was determined that the plastic strain in simulation can be used as an analogue to the strengthening due to dimpling; this link is also explained in terms of microstructure in Chapter 3 . This was implemented in the same study to assess the potential strengthening effects of 4-, 8-, and 12-sided tooth profiles as well as spherical and ellipsoidal profiles as shown in Figure 2.7. This relationship between plastic strain and hardness was proven analytically in 2007 by Sonmez and Demir [86].

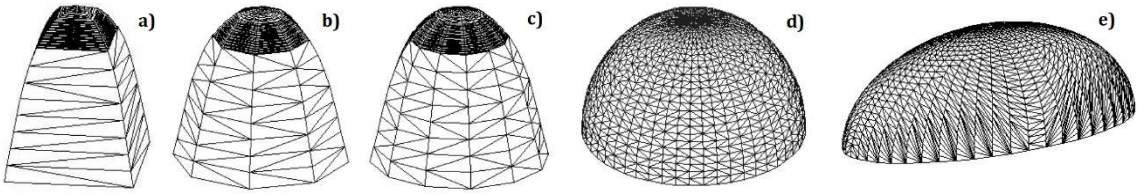

Figure 2.7 - Illustrations of the simulated tooth profiles considered by Collins et al: a) 4-sided (US1); b) 8-sided; c) 12-sided; d) spherical (multiple diameters); e) ellipsoidal (multiple aspect ratios) (modified) [13]

In 2009, Wang *et al* developed a more comprehensive model incorporating the rolling nature of the dimpling process as applied in practice [18]. This is illustrated in Figure 2.8. As shown, this consists of a thin section of two opposing rolls and a short sheet to model the, initially plain, steel. This model was used to explore the sensitivity of the effects of dimpling to the friction coefficient and forming depth as well as to assess the assumption made by Collins *et al* [4, 13] that shrinkage of the plate in the rolling direction is negligible.

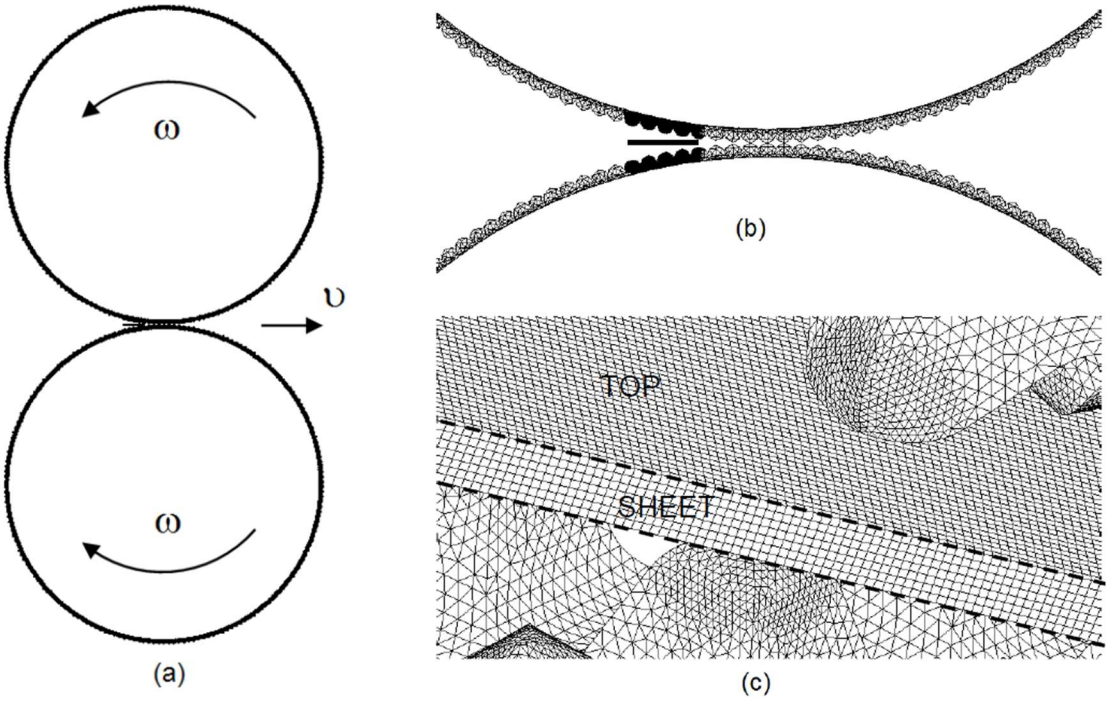

Figure 2.8 – Wang-style model simulating the rolling nature of the dimpling process. (a) complete finite element model, (b) the region of contact, (c)detailed view of the roll teeth and sheet steel meshes [18]

It was determined that the application of an increased forming depth and a higher friction coefficient results in increased plastic strain and thus, increased strengthening due to strain hardening. However, it is difficult to determine from these results how much of this increase can be attributed to each factor: the increased forming depth and the increased friction coefficient. Additionally, it was noted that increasing the forming depth and friction results in greater variation in thickness of the dimpled plate due to increased thinning in the tooth contact regions. Regarding the assumption made by Collins *et al* [4, 13], Wang *et al* [18] reported a maximum shrinkage in the rolling direction of 0.5%. This indicates that consideration of this effect may only be relevant for a small number of very specific cases where such small geometric margins are pertinent.

Later, in a study exploring the simulation of the load response for dimpled steel in 2011, Nguyen *et al* [14] developed a model similar to that used by Collins *et al* [4,

13] but with a dimple-centred unit cell that more clearly illustrates the effects of the dimpling process on a 'per tooth' basis. Both bending and tensile tests were conducted on plain and dimpled specimens and subsequently simulated. A comparison of these results was reported to show good agreement in the force-displacement curves produced.

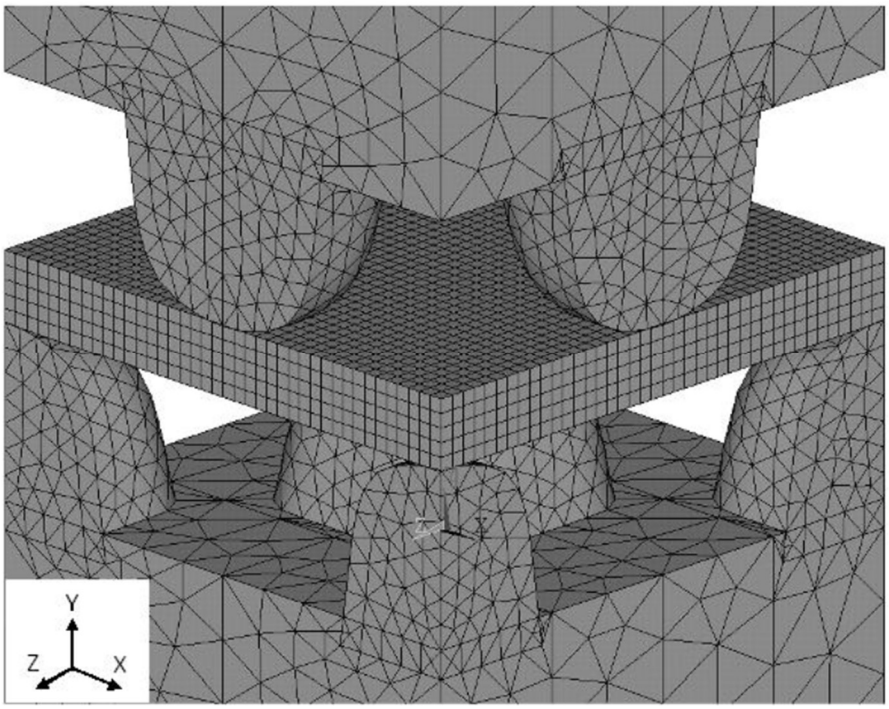

530 *Figure 2.9 - Nguyen-style model simulating the UltraSTEEL® dimpling process [14]*

Nguyen *et al* expanded on this simulation methodology in 2013 [15] and 2016 [17] by using the simulated unit cell as a basis for the construction of dimpled products such as a column of a 'C' cross-section for further simulated testing.

The Wang-style model illustrated in Figure 2.10 was developed in 2014 by Nguyen *et al* [2]. Effectively repeating the investigation from 2011 [14] with a more detailed simulation , this study investigated the effects of the anisotropy introduced into the material property changes by the rolling nature of the dimpling operations as applied in practice. As was the case in 2011, a good agreement was reported

between the experimental and simulated force-displacement curves in both tensile and bending load cases.

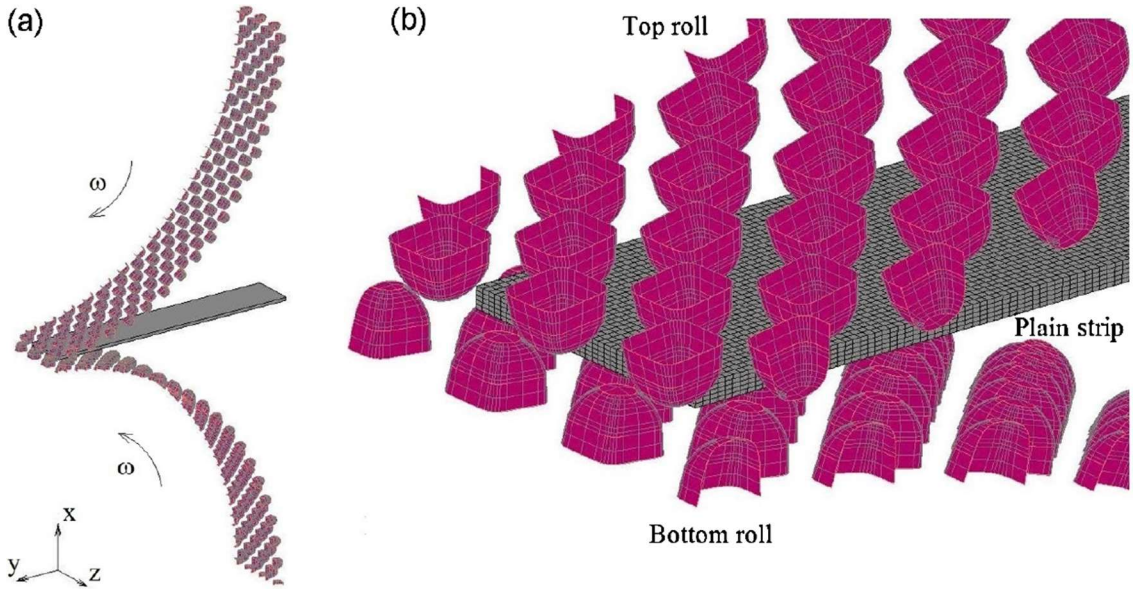

Figure 2.10 - Wang-style model as developed by Nguyen et al to simulate the rolling nature of the dimpling process for UltraSTEEL® [2]

Additionally, in assessing the sensitivity of the results to changes in the simulated friction coefficient, Nguyen *et al* [2] reported that there was no substantial effect on work hardening, thus indicating that the results reported by Wang *et al* [18] may be attributed largely to the change in forming depth.

Effectively combining the methods from their 2013 [15] and 2014 [2] investigations, Nguyen *et al* explored product simulation, testing, and development through the application of computational methods including the rolling model in Figure 2.10.

The most recent study, conducted by Liang [19], focused on assessing the relative crashworthiness of plain steel and dimpled steel products. This included various simulated methods, including a Nguyen-style model of the dimpling process. As shown in Figure 2.11 as compared with Figure 2.9, the geometry of this model is

identical to that used by Nguyen *et al* [14, 15, 17] however, Liang [19] took a different approach in the following steps to simulate tensile loading.

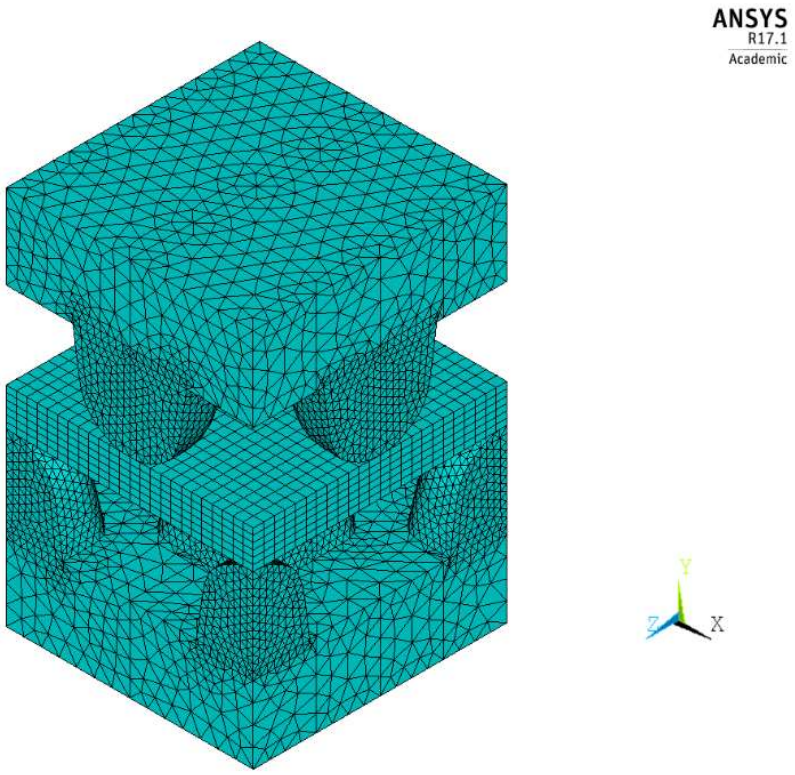

Figure 2.11 - Nguyen-style model as used by Liang to simulate the UltraSTEEL® dimpling process [19]

While Nguyen *et al* used the results of the dimpling simulation as a pre-stress state for the tensile simulation, Liang incorporated consideration of residual stresses through the application of modified material properties. Specifically, the constituent cells of the simulated plate were categorised based upon the level of plastic strain achieved. These categories were then used as the basis for application of otherwise identical material models with modified yield stress to match the average plastic strain for each category. In this way, the resultant dimpled geometry, combined with the modified material properties, represents dimpling by explicitly including the local yield strength increases due to residual stresses and plastic strains. The simulated stress-strain curves were reported to show good agreement with experimental results.

Chapter 3 The Effects of UltraSTEEL® on the Mechanical Properties of Mild Steel

3.1 Introduction

As noted in Chapter 1 , it has been well established that the application of surface textures such as dimples results in an increase in the tensile yield strength and ultimate tensile strength of the overall sample/product [2, 4, 7, 8, 13, 14, 16]. However, it has been observed in industry [87] that there is a substantial variation in these increases, particularly in the case of tensile yield strength. Since the mechanisms responsible for the strengthening effect of these dimples are not fully understood, these variations have thus far been considered largely unpredictable. Thus, the objective in this chapter is to provide a strong theoretical and experimental case explaining the mechanisms at work to form a basis for further conclusions drawn from the present research.

3.2 Background

According to dislocation theory, there are five mechanisms by which a metal may be strengthened. These are precipitation strengthening, phase transformation, solid-solution alloying, strain hardening, and grain size reduction [43, 88–90]. This research only considers the cold roll forming dimpling process. Since precipitation strengthening and phase transformation are both elements of heat treatment, these can be considered irrelevant in this context. Similarly, solid-solution alloying amounts to changing of the chemical composition of the metal. Since this research focuses on a single steel specification, this mechanism can also be discounted. This leaves strain hardening and grain size reduction (or grain boundary strengthening)

as two possible mechanisms by which dimpling effects an increase in tensile yield stress.

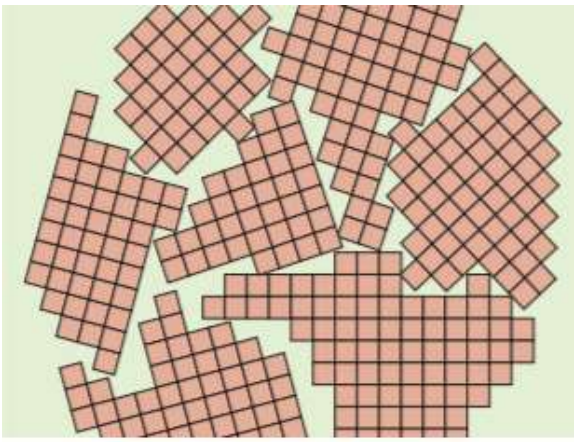

Figure 3.1 - Schematic illustration of interlocking crystallographic lattices in a polycrystalline material; the square grids represent regular atomic lattices [91]

It is well-known that the constituent atoms of metallic materials are arranged in regular crystal lattices. Due to various imperfections however, most metals are composed of many such crystal lattices and are therefore collectively termed polycrystalline [91]. Schematically illustrated in Figure 3.1, the individual crystal lattices in such materials are referred to as grains and they often contain imperfections of their own within the otherwise regular lattice, shown in Figure 3.2.

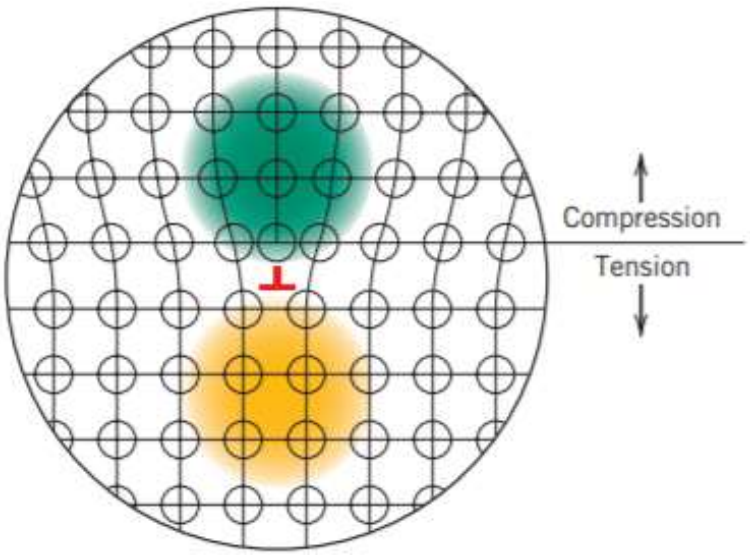

Figure 3.2 – Regions of compression (green) and tension (yellow) around an edge dislocation [90]

3.2.1 Strain Hardening

As shown in Figure 3.2, these intra-granular imperfections, known as dislocations, result in stresses imposed on the surrounding atomic bonds, impacting their response to loading. Figure 3.3 illustrates the process of strain hardening whereby plastic strain is produced through dislocation motion.

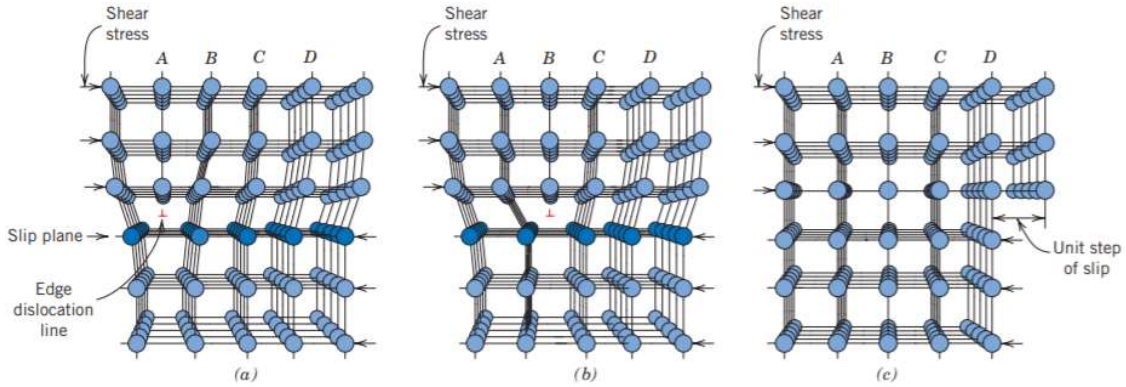

Figure 3.3 - Atomic rearrangement due to dislocation motion. (a) The dislocation before loading. (b) The dislocation effectively moves through the lattice due to loading. (c) The dislocation reaches the edge of the lattice, becoming part of the grain boundary [90]

Comparing (a) and (b) above, it is illustrated that the dislocation effectively moves through the crystal lattice by the repeated breaking and forming of inter-atomic bonds. In the same way, (c) illustrates the ledge formed when this dislocation reaches the edge of the crystal, or the grain boundary. This dislocation motion is accompanied by changes in the stress fields imposed by such dislocations, resulting in changes in the response of the material to external loading. This is known as strain hardening.

3.2.2 Grain Boundary Strengthening

During the process of dislocation motion, the material is undergoing plastic deformation. This ceases to be the case when the dislocation encounters some barrier preventing further motion. One common example of such a barrier to dislocation motion is the grain boundary.

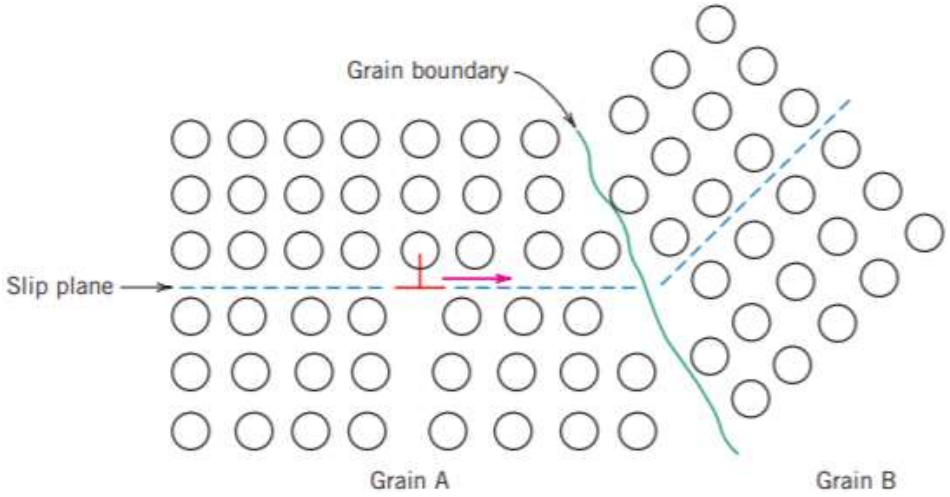

Figure 3.4 - Illustration of how misaligned slip planes across a grain boundary act as a barrier to dislocation motion [90]

630 As shown in Figure 3.4, once the dislocation reaches the grain boundary, it cannot move further. Therefore, plastic deformation due to the motion of this dislocation ceases. Thus, the abundance of grain boundaries directly influences the mechanical strength of the material: a fine-grained material (more grain boundaries) is stronger than the coarse-grained equivalent since there are more grain boundaries to impede dislocation motion [88]. This relationship is more explicitly defined by the Hall-Petch equation [90] in Eq. 3.1 below where σ_y is the yield strength, σ_0 and k_y are material constants, and d is the average grain diameter.

$$\sigma_y = \sigma_0 + k_y d^{-\frac{1}{2}} \qquad \textit{Eq. 3.1}$$

3.3 Experimental Setup

It was noted in Section 1.4 that the source material used for approximately 90% of the UltraSTEEL® production by Hadley Industries falls within the DX51D grade specification [10]. The vast majority of this is of a 0.5mm gauge [9]. Therefore, the samples used in the following tests are all DX51D galvanised steel with a nominal gauge thickness of 0.5mm.

3.3.1 Tensile Testing

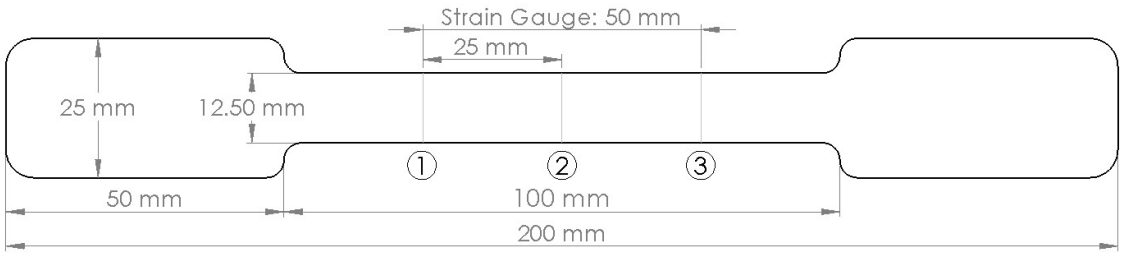

Figure 3.5 - Tensile dogbone sample with strain gauge markings

The 'dogbone' samples used, specified in Figure 3.5, are the same as those used by Nguyen *et al* [2, 8, 14, 15, 17, 36] and adhere to the British Standards for the quasi-static tensile testing of ductile metals [12]. Measurements of gauge and effective gauge were taken for each sample at the centres of the lines labelled 1, 2, and 3 in Figure 3.5 and the relevant average used. Effective gauge is the total thickness of the sample as is illustrated in Figure 3.6.

Due to the small variations observed within each dataset for the studies by Nguyen *et al* [14] and Collins *et al* [4], it is expected that a small number of samples are required to indicate consistency of results. To ensure consideration of the variation inherent within the DX51D specification, 20 separate batches (or coils) are included. From each coil, 3-5 plain steel samples were taken using a hydraulic punch. The remainder of the coil was then processed according to industry standards to apply

the UltraSTEEL® dimple texture after which 3-5 dimpled steel samples were taken using the same hydraulic punch. Thus, the total dataset consists of 80 plain steel and 80 dimpled steel samples grouped in matched sets based on the coil from which they were taken. The plain steel and dimpled steel samples used measured 0.54±0.03mm gauge and 1.22±0.08mm effective gauge, respectively. Note that all samples were cut with their major axis aligned to the rolling direction. This is a control for the potential relevance of directionality as this is beyond the scope of the present study.

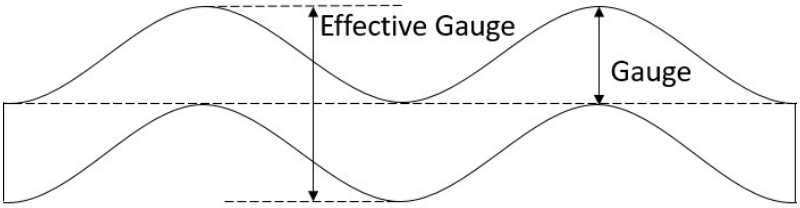

Figure 3.6 - Dimpled steel cross-section illustrating 'effective gauge'

The test rig [H50KS-0148], Figure 3.7, has a maximum load capacity of 50kN and consists of two opposing crosshead grips into which the samples were fixed, aligned with the grip axis to ensure loading through the length of the sample. As shown, a mechanical extensometer [Tinius Olsen Extensometer Epsilon SGSC-0432-FO8D4503 50mm GL 5-50%] of 50mm gauge length was also attached to each sample to enable accurate measurement of deformation along the loading axis. Each sample was tested to failure at a strain rate of 2.5mm/min with force readings taken from the test rig crossheads and elongation readings taken from the extensometer. Thus, the test procedure is as follows:

1. Fix the dogbone sample in the test rig grips with the sample major axis aligned to the loading direction.
2. Fit the extensometer aligned with markings 1 and 3 specified in Figure 3.5.
3. Load the sample to failure at a rate of 2.5mm/min

The data output for these measurements include 1,000 datapoints for each sample with an even distribution over the loading curve.

Figure 3.7 - Tensile test rig setup

3.3.2 Microstructural Examination

For the microstructural examinations, plain steel was again processed according to industry standards to apply the UltraSTEEL® dimple texture. Samples were then cut using wire electrical discharge machining (w-EDM) in the rolling direction as illustrated in Figure 3.8.

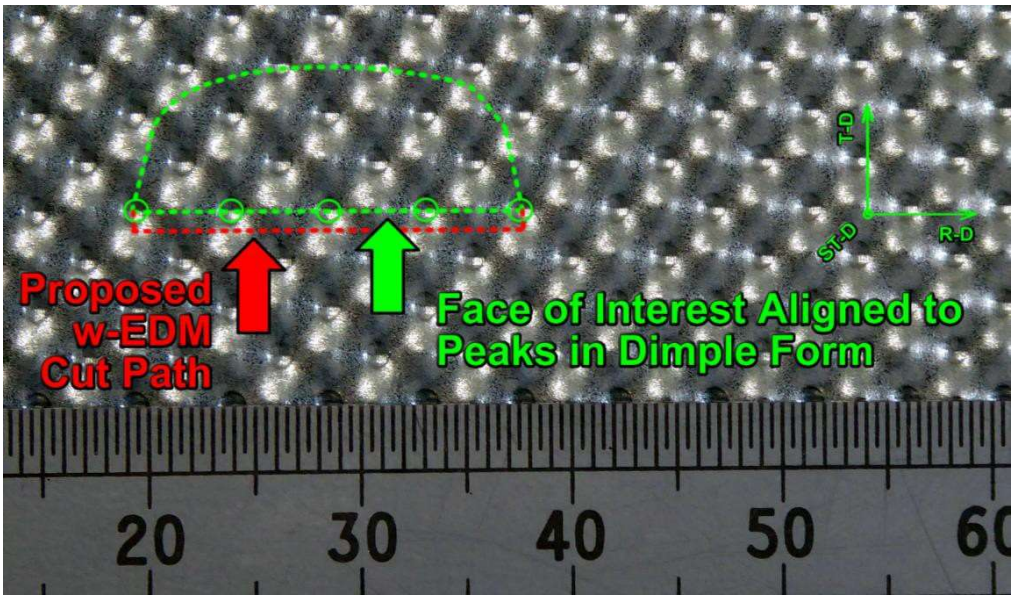

Figure 3.8 - Illustration of the w-EDM cut path and face of interest for the microstructural examinations (courtesy of Hadley Industries [5])

As shown, while the face of interest intersects the peaks and troughs at their maximum amplitude, the w-EDM cut path was offset from this. This offset serves to prevent the high temperatures involved in the cutting process from significantly impacting the crystallographic structure of the steel along the face of interest. The sample was then ground to remove material equivalent to the offset distance, revealing the face of interest, and polished to a mirror finish, as shown in Figure 3.9, to enable examination of the microstructural cross-section by SEM.

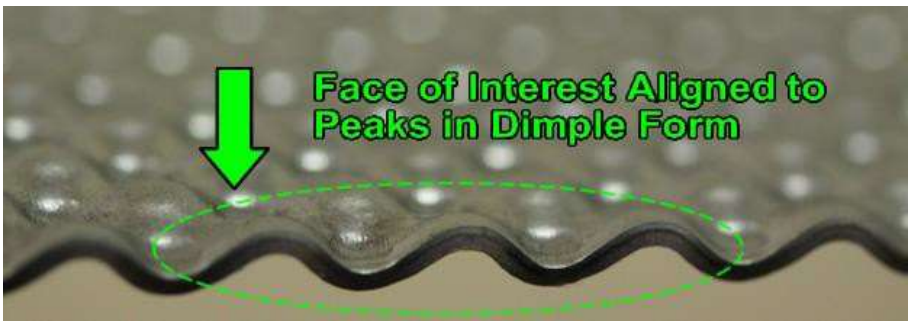

Figure 3.9 - Illustration of the UltraSTEEL® cross-section ready for microstructural examination (courtesy of Hadley Industries [5])

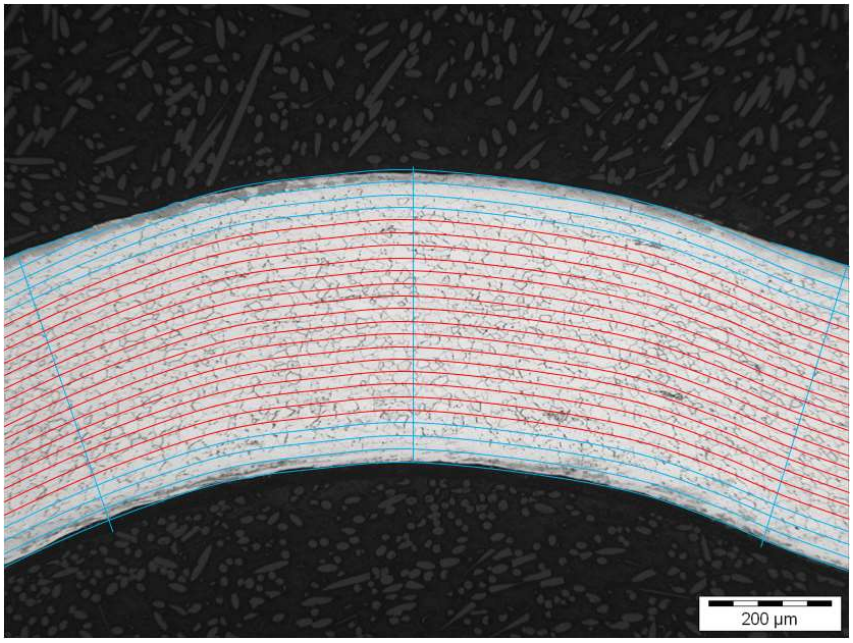

Figure 3.10 - Example of an 'axial' grid overlay to enable grain size quantification

The examination, and subsequent quantification, of the grain structure in the cross-section is completed using the intercept method [20]. A grid matched to the morphology of the cross-section is placed to overlay the sample as illustrated in Figure 3.10 and Figure 3.11. In this case, the lines are spaced at ~20µm intervals and the red lines are used to measure the average number of grain boundary intersects over a given span. Dividing the number of intersects by this span determines the average grain size over the same span. The blue lines serve the purpose of illustrating conformity to the sample morphology. Note that 'axial' and 'through-thickness' grain size are used to distinguish the direction of the lines used to measure the grain size being referred to. Thus, 'axial grain size' is measured as illustrated in Figure 3.10.

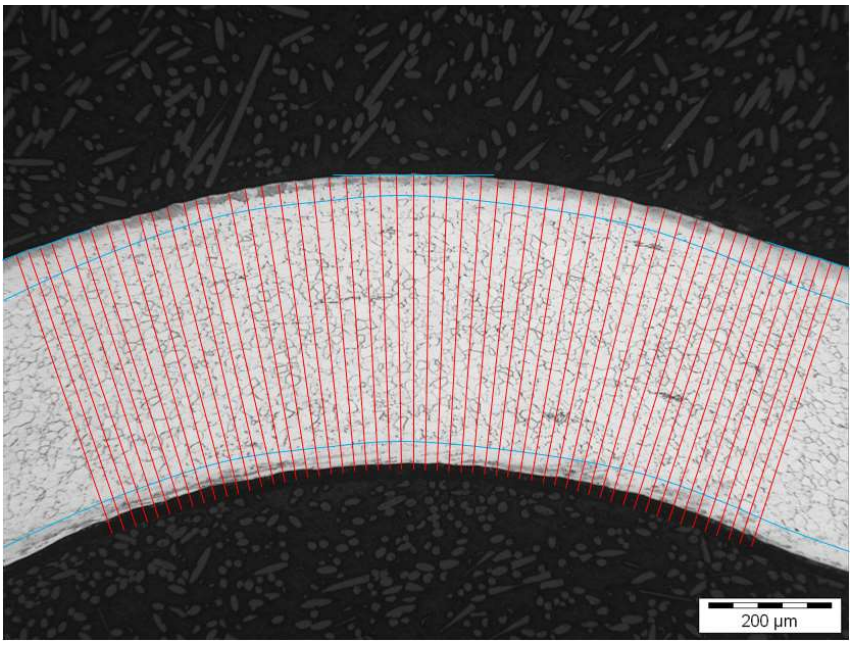

Figure 3.11 - Example of a 'through-thickness' grid overlay to enable grain size quantification

3.4 Results & Discussion

A summary of the tensile testing of 80 plain steel and 80 dimpled steel samples covering a total inclusion of 20 source coils is included in Table 1 below. See the Appendix for full per-coil listings of all measured variables. These tests were completed by the author in cooperation with the Hadley Group [5].

Table 1 - Summary of the mechanical properties of plain steel and dimpled steel when subjected to tensile loading

Mean ± SD	σ_{LY} / $\sigma_{Y,0.2}$ *(MPa)*	$\varepsilon_{y,0.2}$ *(%)*	*UTS (MPa)*	ε_{UTS} *(%)*
Plain Steel	317 ± 16.07	0.382 ± 0.028	381 ± 17.6	19.7 ± 2.08
Dimpled Steel	351 ± 21.14	0.375 ± 0.042	417 ± 18.8	8.93 ± 2.15

Exhibiting an average increase in both yield strength (9.9%) and ultimate tensile strength (9.3%), it is clear from this dataset that the UltraSTEEL® dimpling process applied according to current industry standards effects substantial improvements to the load response of mild steel. Reliability of these results is indicated by the low

values for standard deviation and supported by their agreement with the results produced in a similar test series conducted by Nguyen *et al* [14].

Figure 3.12 illustrates the ranges of the yield strengths present in this dataset for plain steel and dimpled steel. The black lines indicate the maximum and minimum values, the blue boxes contain the central 50% of readings bounded at the top and bottom by the upper and lower quartiles, and the red lines indicate the median values. The black crosses indicate the mean values. This makes evident the substantial increase in yield strength imparted by the dimpling process. Worth noting, is that the high outlier for the plain steel case corresponds with the highest value in the dimpled steel case. Similarly, the low outlier for the plain steel corresponds with a point in the lower quartile for the dimpled steel. This indicates that the strengthening effect imparted by the dimpling process may be relatively consistent.

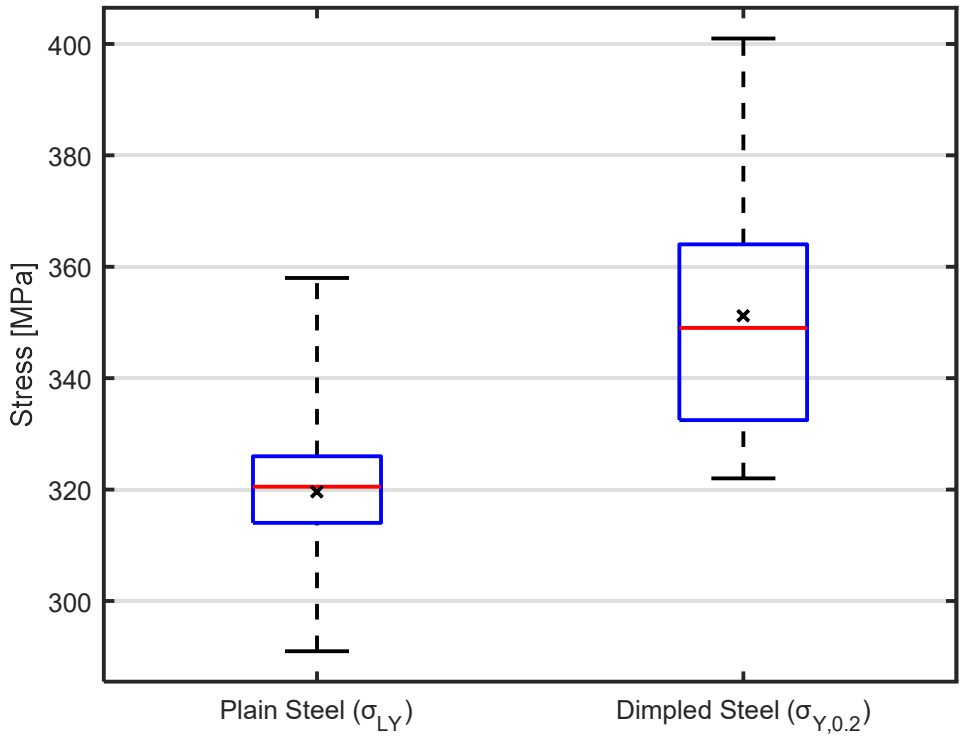

Figure 3.12 - Boxplots illustrating the effect of the UltraSTEEL® dimpling process on the yield strength of the steel samples using the standard measures for yield strength.

Figure 3.13 and Figure 3.14 present similar illustrations of the effect of the dimpling process on the UTS and the elastic modulus of steel. As with yield strength, the high and low values illustrated for plain steel and dimpled steel in Figure 3.13 represent corresponding samples. This, again, indicates consistency in the margin of increase in the UTS imparted by the dimpling process. The effect of dimpling on the elastic modulus is less clear. As shown in Figure 3.14, there is substantial overlap in the ranges exhibited by the plain steel and the dimpled steel samples so while an increase due to dimpling may be inferred, this data does not conclusively support such an assertion. Perhaps most notably here, is the observation that the elastic modulus of the dimpled steel samples is substantially more inconsistent than that of the plain steel samples. This may be a result of the measurement of the 'elastic modulus' from stress-strain curves of the aggregate behaviour of the samples but it could also be indicative of limited applicability of conventional measures for characterising the behaviour of dimpled steel. The elastic modulus, as it relates to sample stiffness, is investigated further in Chapter 5 .

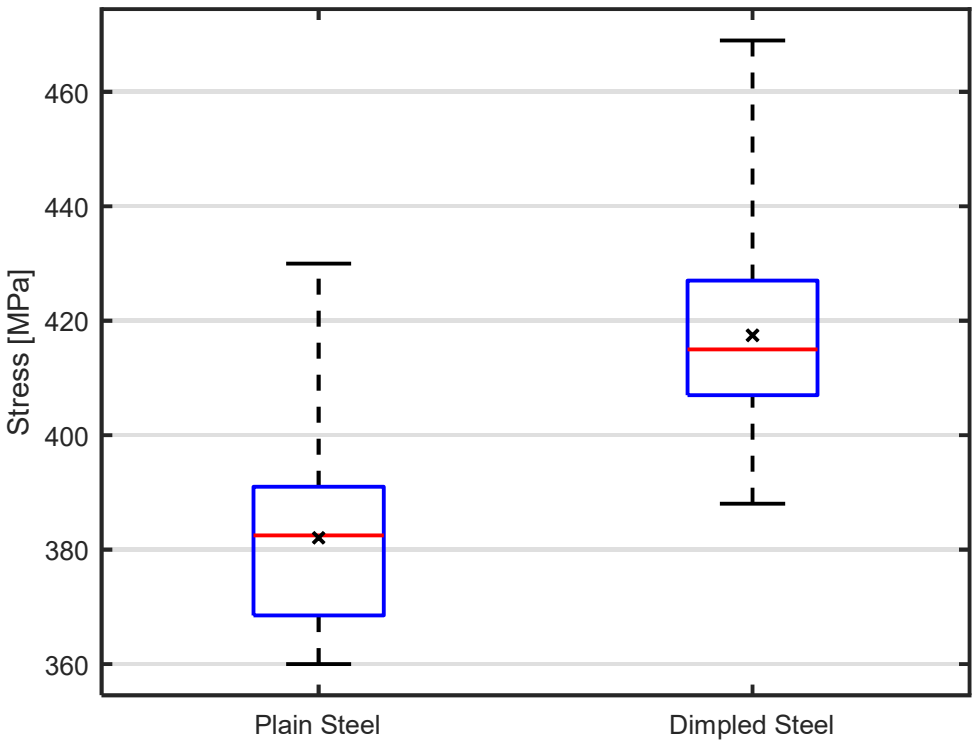

760

Figure 3.13 - Boxplots illustrating the effect of the UltraSTEEL® dimpling process on the ultimate tensile strength of the steel samples.

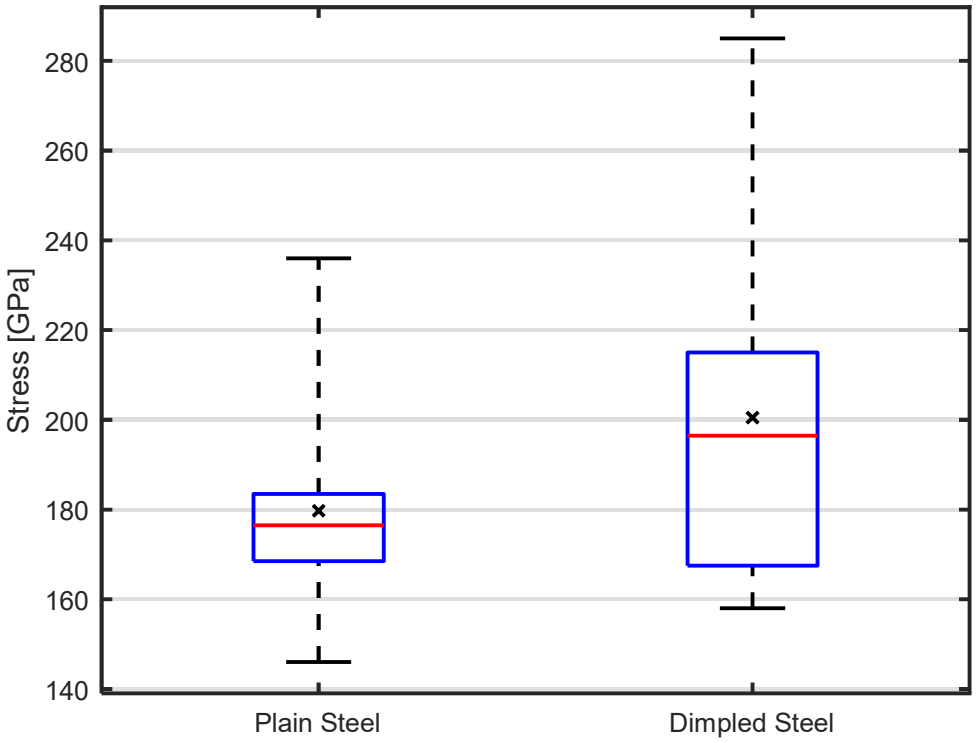

Figure 3.14 - Boxplots illustrating the effect of the UltraSTEEL® dimpling process on the elastic modulus of the steel samples.

It is interesting to note that although the expected decrease in ductility post-dimpling is evident when considering the total strain corresponding to the tensile strength, ε_{UTS}, a decrease of ~55%, there appears to be no substantial difference in the equivalent measure at yield ($\varepsilon_{y,0.2}$). This may, however, be somewhat due to the inappropriate assumption of substantial adherence to Hooke's Law inherent in the offset yield method when quantifying the loading response of materials such as dimpled steel that incorporate macroscopic geometric non-uniformities. This is explored in detail in Chapter 6 .

As noted in Section 2.1 , while the contribution of strain hardening to the strengthening due to dimpling has been explored previously, the possibility of some contribution by grain boundary strengthening has yet to be considered. Therefore, the following micrographs (two standard dimpled steel samples) have been produced using SEM, as described in Section 3.3.2 , to explore this possibility. Figure 3.15 and Figure 3.18 show the face of the cross-section cut through the dimple peaks and troughs for each sample at x25 magnification. Figure 3.16 and Figure 3.19, and Figure 3.17 and Figure 3.20 illustrate the peak-region and the inter-dimple region, respectively, for each sample at x100 magnification. These micrographs were provided by the Hadley Group [5].

The main assumption made in this analysis is that the inter-dimple region is more like the plain steel material than the peak-region is. This allows for a full analysis without needing to match plain and dimpled samples from corresponding source coils, substantially reducing the cost of the investigation.

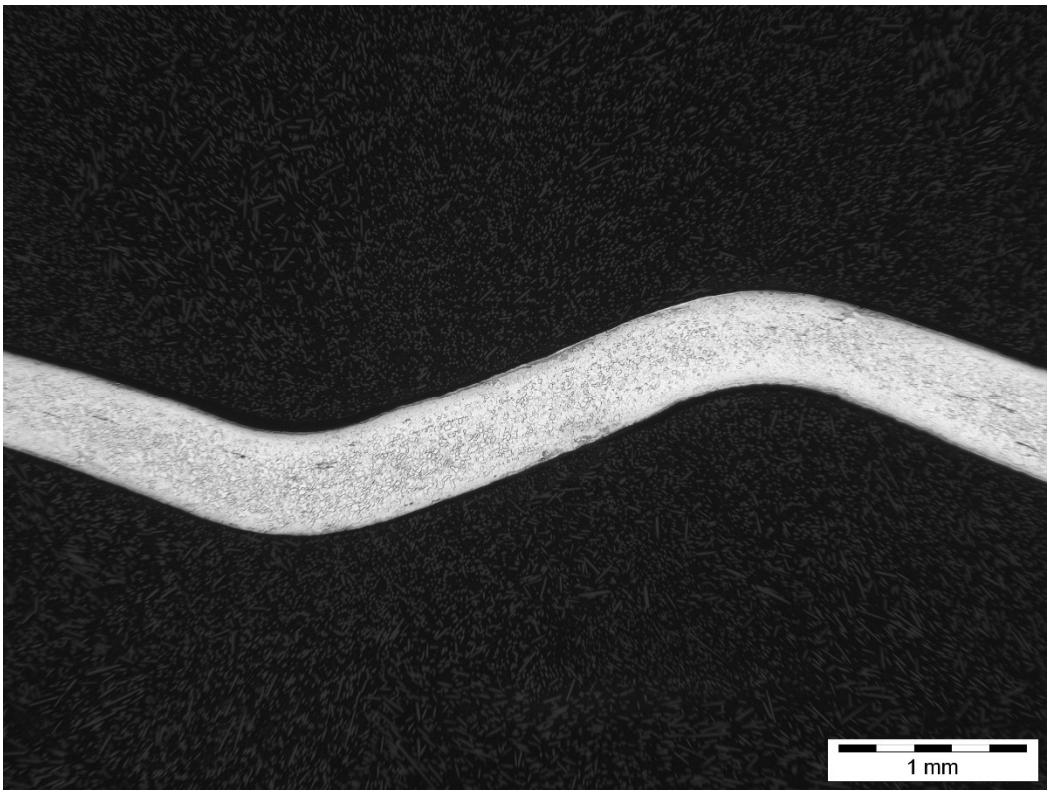

Figure 3.15 - Micrograph showing a 'through-peak' cross-section of dimpled steel – sample A (courtesy of Hadley Industries [5])

790

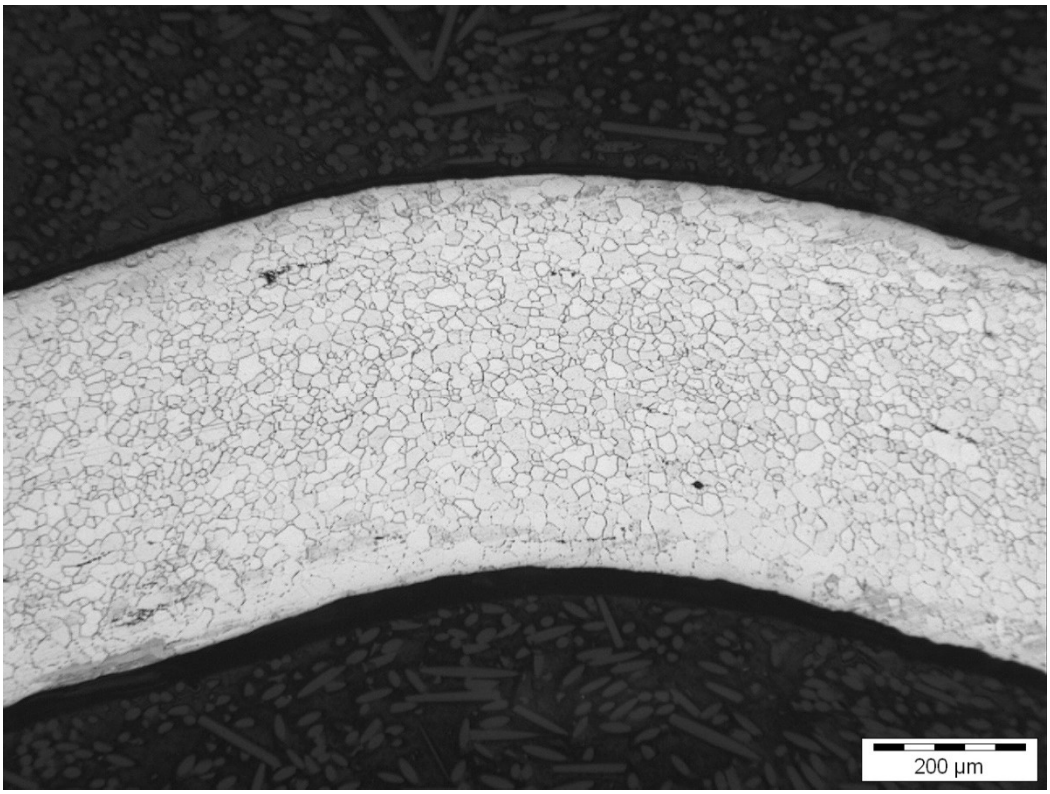

Figure 3.16 - Micrograph showing the dimple peak region of a 'through-peak' cross-section of dimpled steel – sample A (courtesy of Hadley Industries [5])

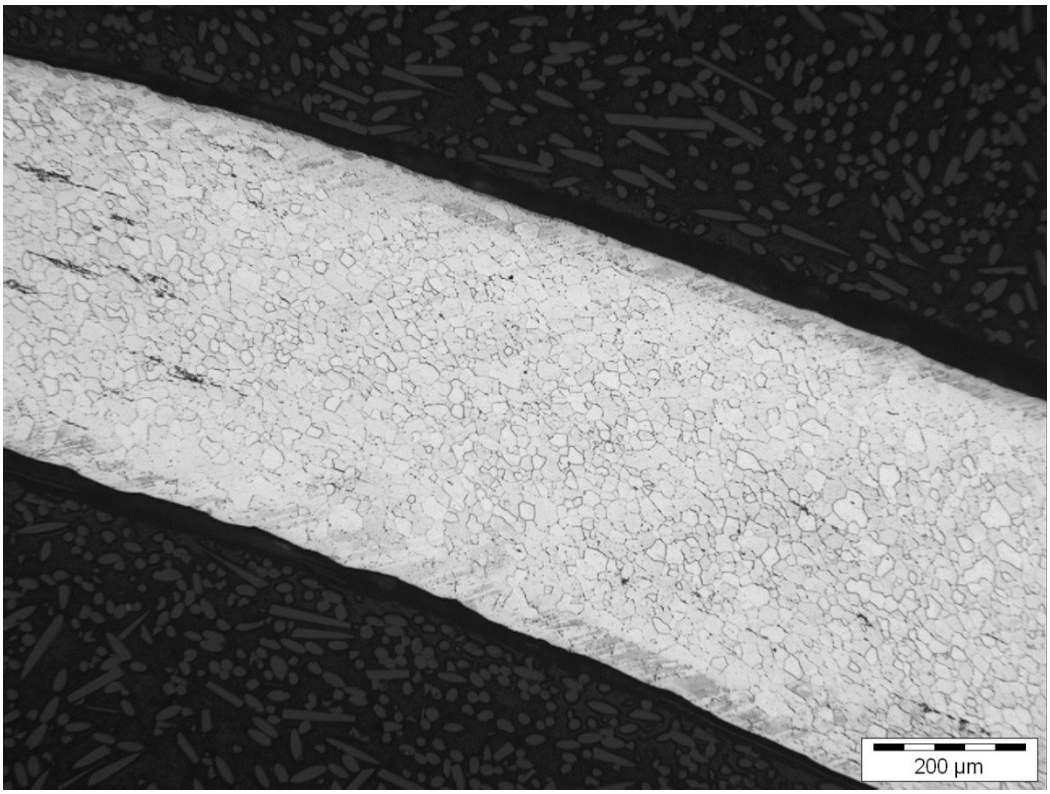

Figure 3.17 - Micrograph showing the 'inter-dimple' region of a 'through-peak' cross-section of dimpled steel – sample A (courtesy of Hadley Industries [5])

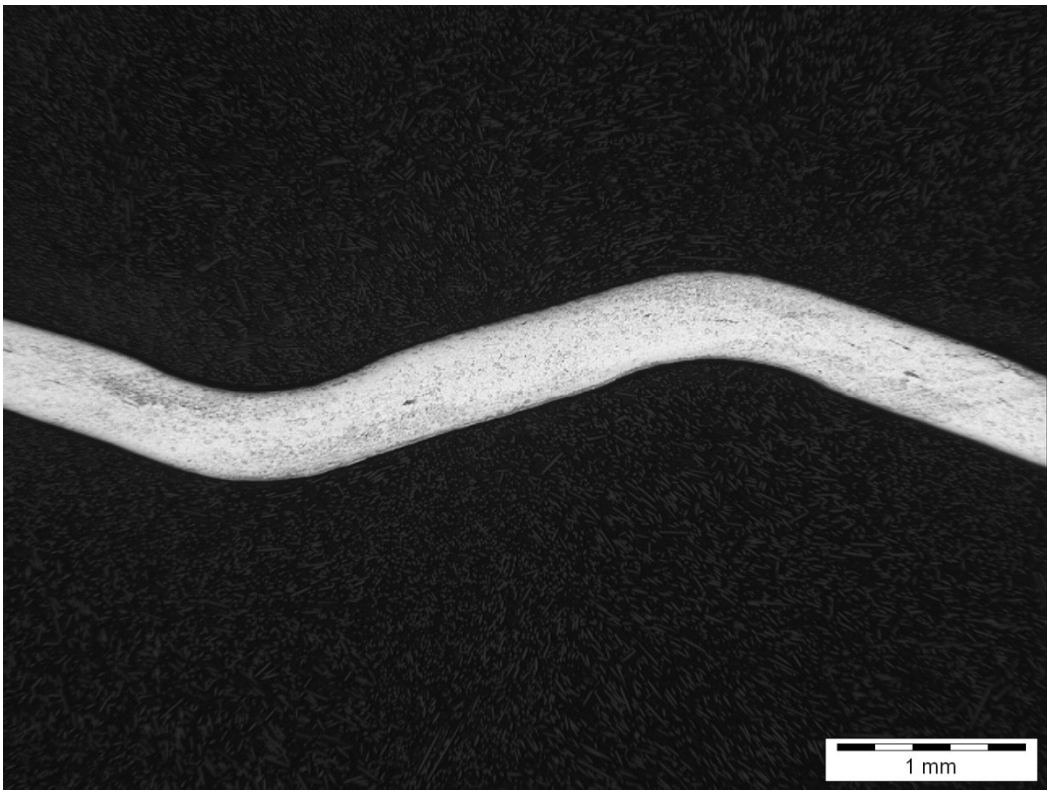

Figure 3.18 - Micrograph showing a 'through-peak' cross-section of dimpled steel – sample B (courtesy of Hadley Industries [5])

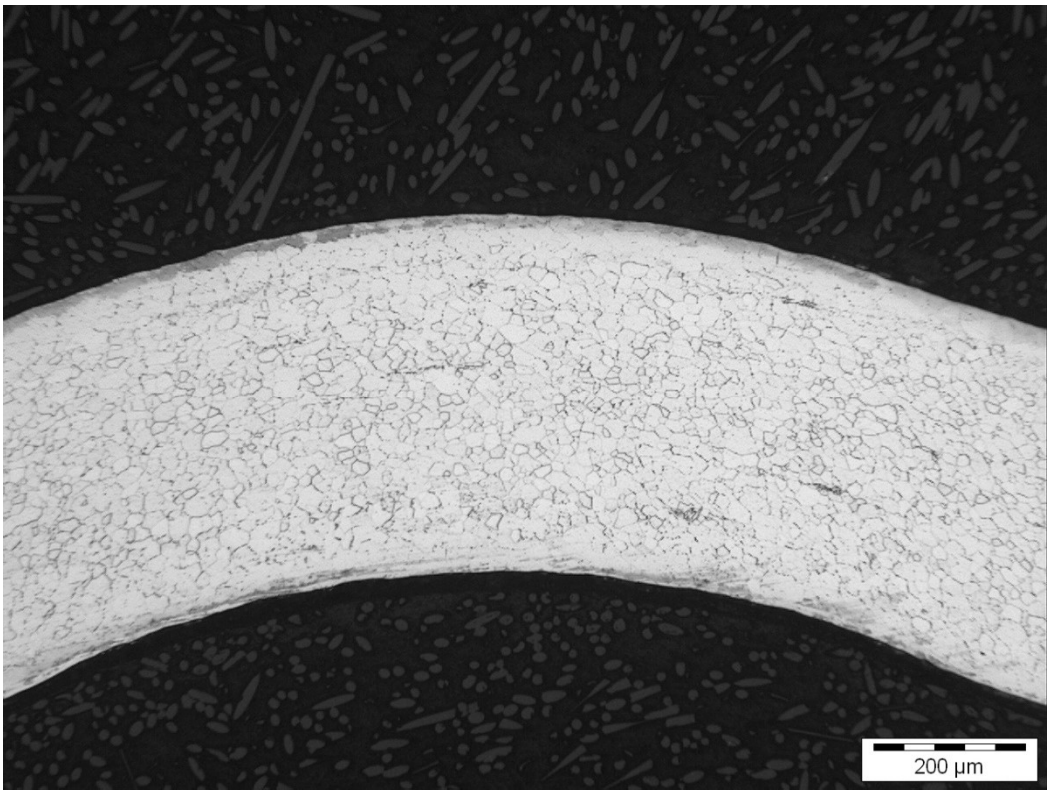

800

Figure 3.19 - Micrograph showing the dimple peak region of a 'through-peak' cross-section of dimpled steel – sample B (courtesy of Hadley Industries [5])

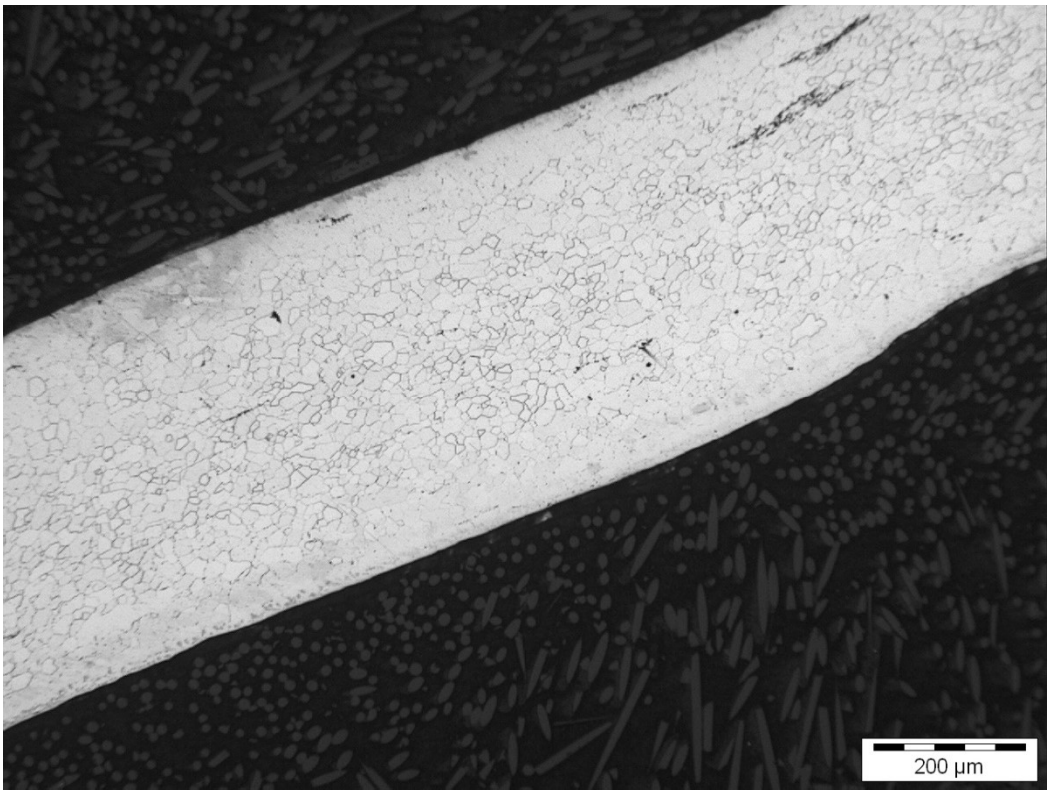

Figure 3.20 - Micrograph showing the 'inter-dimple' region of a 'through-peak' cross-section of dimpled steel – sample B (courtesy of Hadley Industries [5])

Therefore, the inter-dimple region is assumed to be somewhat representative of the plain steel source material while the peak region is considered representative of any grain size refinement due to the dimpling process. Figure 3.21 and Figure 3.22, then, indicate that there may be a small amount of grain size refinement taking place due to the dimpling process. In these figures, the black lines indicate the maximum and minimum values, the blue boxes contain the central 50% of readings bounded at the top and bottom by the upper and lower quartiles, and the red lines indicate the median values. The black crosses indicate the mean values.

Considering first the average grain size as measured in the axial direction, Figure 3.21, the overlap between the two datasets is substantial but the mean grain size in the peak region is smaller than that in the inter-dimple region by approximately 1.8% (16.6μm to 16.3μm). This trend is somewhat clearer for the through-thickness direction, measured perpendicular to the surface of the sample. Illustrated in Figure 3.22, this case shows the two regions producing similar boxplots, offset by grain size. This is indicative of a uniform (through-thickness) grain size refinement, in this case, of approximately 3.7% (13.5μm to 13.0μm).

While this data alone is not definitive enough to confirm that dimpling effects a grain size refinement, it does exhibit indications of this link as explained in Section 3.2 . Due to the assumption allowing consideration of the inter-dimple region as an analogue to the plain steel, it is expected that these results may underestimate any grain size refinement taking place. Further investigation is required to both confirm this and to quantify any such refinement as relating to the potential application of the Hall-Petch equation.

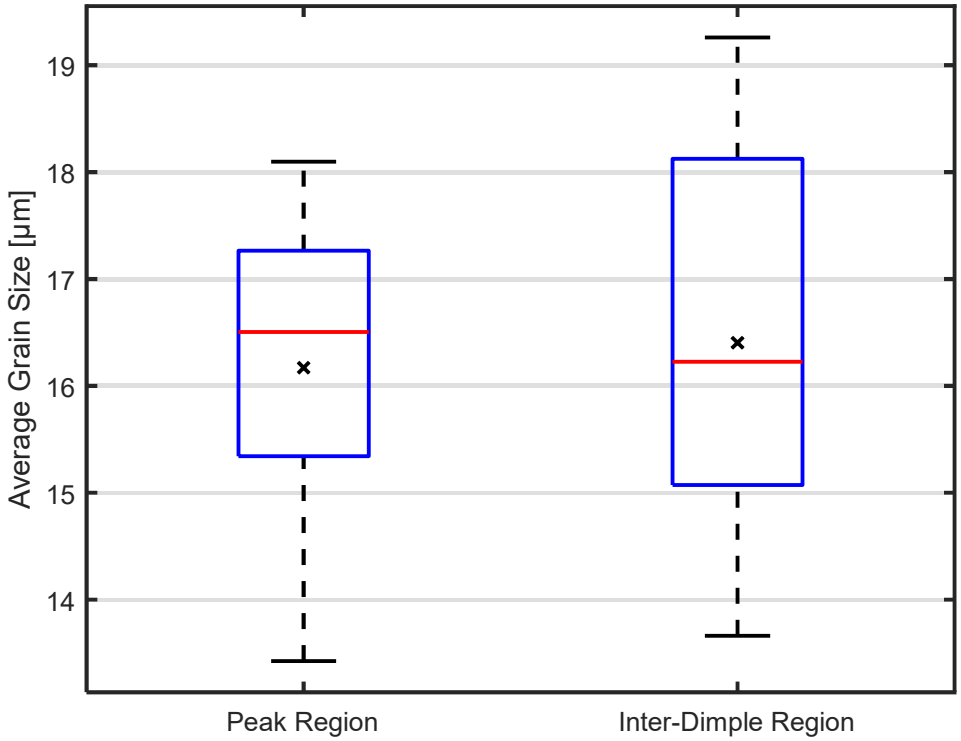

830 *Figure 3.21 - Box-plot comparison of the 'axial' grain sizes measured in the peak- and inter-dimple regions*

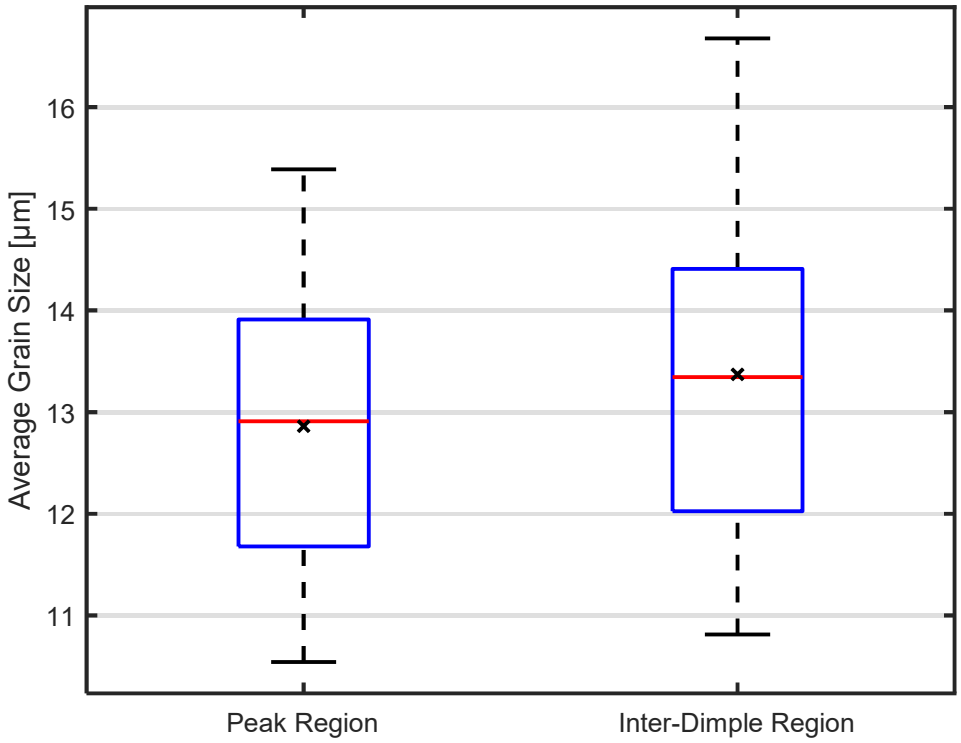

Figure 3.22 - Box-plot comparison of the through-thickness grain sizes measured in the peak- and inter-dimple regions

3.5 Summary

Corresponding steel samples (80 plain and 80 dimpled) covering a total inclusion of 20 DX51D source coils were tested in tension to failure. The results of these tests, in agreement with previous investigations, indicate an average increase in yield strength and ultimate tensile strength of 9.9% and 9.3%, respectively, due to the dimpling process.

Investigating the possibility that this strengthening may be, in part, due to grain size refinement resulting from the dimpling process, a brief SEM study was also conducted. This resulted in the production of micrographs focussed on both the peak region and the inter-dimple region of the cross-section that intersect the dimples at their maximum amplitude. Treating the inter-dimple region as a representation of the plain steel, the average grain sizes for the 2 regions were quantified using the intercept method. While the resulting grain size measurements are somewhat inconclusive, there are indications of a possible grain size refinement taking place.

Chapter 4 Predicting the Magnitude of the Strengthening Effect of UltraSTEEL® in Terms of Tensile Yield

4.1 Introduction

Although it is well documented that the dimpling process increases the yield strength of steel, there is industrially significant variation in the magnitude of this increase [92, 93]. In fact, the tensile dataset from Chapter 3 indicates that the strengthening due to the UltraSTEEL® dimpling process for 0.5mm gauge DX51D steel measured as a percentage increase in yield strength can range from 0.52% through to 17.32%. As such, the ability to predict the strengthening potential of a plain steel coil prior to dimpling has the potential to provide a substantial saving through avoidance of the processing of material that gains minimal benefit from dimpling.

It was determined in Chapter 3 that, of the 5 recognised strengthening mechanisms at work in ductile metals, the strengthening due to dimpling may be a combination of strain hardening and grain boundary strengthening. Statistical analysis of the tensile dataset also presented in Chapter 3 , in conjunction with this knowledge, should enable the identification and explanation of trends that make the desired predictions possible. This is the focus of the present chapter. It is worth reiterating that the dogbone samples used in the testing presented in Chapter 3 were all cut in an orientation such that the major axis of the sample is aligned with the rolling direction of the steel coil. Thus, anisotropy due to the rolling nature of the process is controlled for.

As discussed in Section 2.1 it has been determined previously that strain hardening is largely governed by plastic strain [13, 91]. Therefore, since the UltraSTEEL® process is specified based on plastic deformation (formed to an effective gauge equal to double that of the plain steel gauge, 'double-depth'), it is assumed here that the strain hardening effect is consistent enough to be considered constant and therefore not play a significant role in the variation in material properties being explored here. This means that mechanical properties relating to the potential grain boundary strengthening due to dimpling are most likely to exhibit the trends required to develop an effective predictive expression for yield strength increases.

Recall the Hall-Petch equation noted previously (Eq. 3.1). Taking the form of an inverse-power law, as illustrated in Figure 4.1, this asserts that an initially fine-grained material benefits more from grain boundary strengthening than an initially coarse-grained equivalent. This is illustrated by the pairs of lines (blue and magenta) showing that grain refinement by the same margin results in substantially different increases in yield strength.

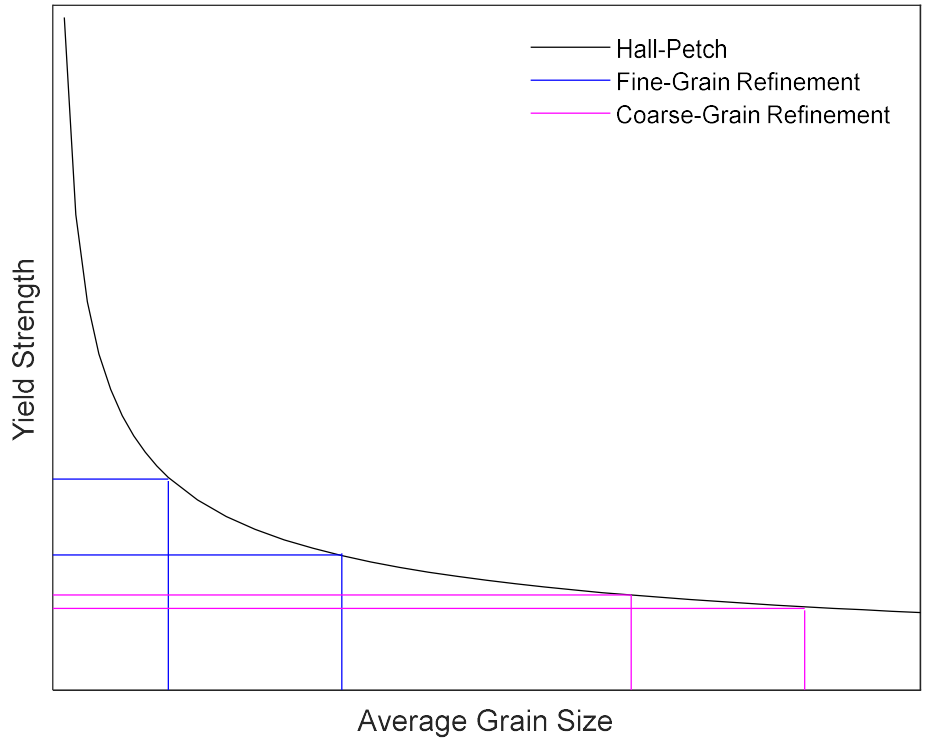

Figure 4.1 - Illustration of the relative effectiveness of grain boundary strengthening for initially coarse- and fine-grained materials according to the Hall-Petch relationship

890 Since there is no restriction on grain size in the DX51D material specification [10], this may be one source of the observed variation in strengthening due to dimpling. A statistical approach will be taken to investigate this possibility while also exploring other possible trends with strengthening.

4.2 Quantifying the Stress-Strain Curve

When assessing the response of a material to tensile loading, it is common practice to produce a stress-strain curve as this represents the force-elongation relationship independent from the scale of the sample being tested [38]. This is achieved through application of the following equations where σ_{eng} is engineering stress (MPa), ε_{eng} is engineering strain (mm/mm), F is force (N), A_0 is cross-sectional area (mm^2), L is

900 the length of the deformed sample in the direction of loading (mm), and L_0 is the original length of the sample in the direction of loading (mm).

Strain $$\varepsilon_{eng} = \frac{L - L_0}{L_0}$$ *Eq. 4.1*

Stress $$\sigma_{eng} = \frac{F}{A_0}$$ *Eq. 4.2*

While these provide accurate representation of the response of the sample to tensile loading for low-strain cases, the accuracy reduces with increasing strain. This is due to the inherent assumption of a constant cross-sectional area. Therefore, when considering high-strain cases, *true stress* and *true strain* are often used to account simply for a reducing cross-section through necking [94]. The conversion from engineering stress and strain to true stress and strain is as follows.

True Strain $$\varepsilon_{true} = \ln(1 + \varepsilon_{eng})$$ *Eq. 4.3*

True Stress $$\sigma_{true} = \sigma_{eng} \times (1 + \varepsilon_{eng})$$ *Eq. 4.4*

The effect of this conversion is illustrated in Figure 4.2 below for a typical plain steel response. Since the present work focuses largely on yield strength and industry

910 applications, engineering stress and strain are used unless otherwise specified.

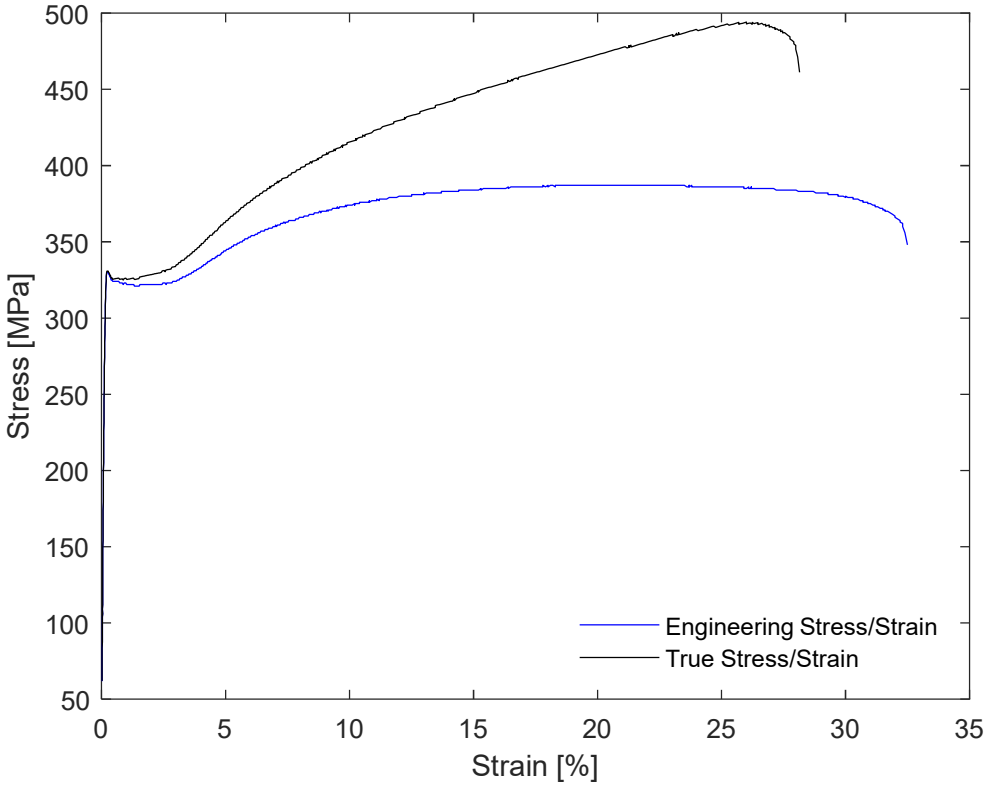

Figure 4.2 - Comparison of typical 'engineering' and 'true' stress-strain curves for plain steel subjected to quasi-static tensile loading

To assess various behaviours and points of interest, it is sometimes necessary to quantify the stress-strain curve. How this is achieved depends on the behaviour being quantified. Therefore, the variables considered in the present work are defined and categorised as follows.

4.2.1 Moduli

The tangent modulus, T_m, and its special case, the elastic modulus, E [12], are both common variables used to quantify the stress-strain curve. T_m is defined as the tangent to the curve at any given point and can therefore be used for various purposes. Possibly the most common is the special case where it is coincident with and parallel to the elastic region of the curve, illustrated as the black line in Figure 4.3. This is referred to as the elastic modulus, a constant gradient, and is used to represent the elastic behaviour of the material.

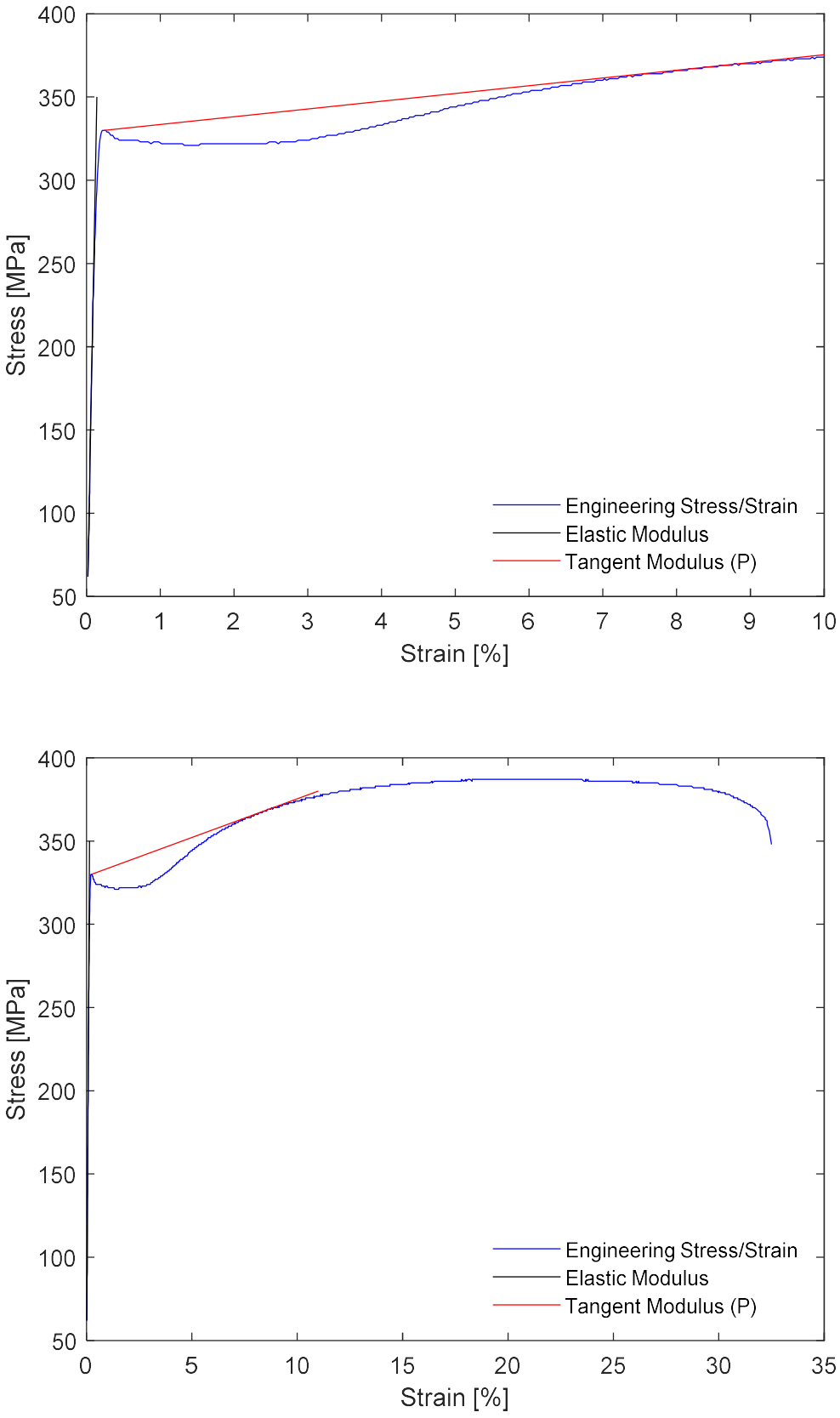

Figure 4.3 - Illustration of the elastic and tangent moduli for a typical plain steel response to quasi-static tensile loading. Top: low-strain region, bottom: full stress-strain curve

Another special case of the tangent modulus, applicable only to materials exhibiting discontinuous yield, is where the tangent at the yield peak is also tangential to the strain hardening portion of the curve. This is illustrated in red in Figure 4.3 and is commonly used as a basis for bilinear material models in finite element modelling [95–97]. Any further reference to the 'tangent modulus' in this chapter refers to this special case relating to the yield peak.

4.2.2 Yield Strength

The yield criterion for ductile materials subjected to quasi-static tension loading is defined most simply as the stress at which appreciable plastic flow begins [39, 45]. Where the yield-point phenomenon is present [39, 42], identifying this transition from elastic to plastic strain is trivial, however, some ambiguity in this definition arises in materials exhibiting continuous yielding. This has given rise to multiple methods for the identification of the yield point, as was discussed in Section 2.4 .

As noted in Section 2.4.1 , where the yield-point phenomenon is present, the definition of yield logically results in identification of the yield point as the upper yield stress, σ_{UY}, point 4 in Figure 4.4. However, the height of this peak is not an intrinsic property of the material and is highly dependent on the testing machine [42, 43]. Due to this and as an operational safety margin, the lower yield stress, σ_{LY}, is often used as the yield criterion for such materials [12]. Marked as 5 in Figure 4.4, this is the minimum stress exhibited during Lüders strain.

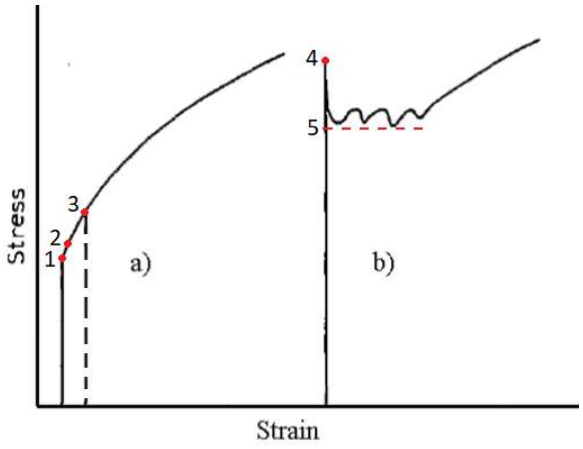

Figure 4.4 - Typical stress-strain curves for low-carbon steels (a) represents continuous yielding, (b) upper and lower yield points with Portevin-Le Chatelier effect during Lüders strain [98](modified)

Figure 4.4 shows the ambiguity introduced in the case of continuous yielding where a linear region is still present. In this case, the proportional limit (point 1) seems the most logical position for the yield point. However, this is often difficult to identify. Therefore, applying an offset along the strain axis to the line representing the elastic modulus is used to define an 'allowable strain' prior to an arbitrarily defined yield point. In this way, rather than using some undefined point beyond the proportional limit (point 2, for example), the point where this offset elastic modulus meets the curve is defined as the proof stress or offset yield stress, σ_Y. Due to its arbitrary definition, multiple offsets are commonly applied however, the British Standards Institution, BSI, illustration uses an offset of 0.2% strain (0.002 mm/mm) [12]. Therefore, a 0.2% offset is used in the present work. It is important to clarify that what is measured as 'yield strength' for the dimpled samples in present study is a practical average of the sample and not the conventional material property. This is due to the use of industry standard testing that measures the sample-wide response and therefore reports on the aggregate behaviour of the sample. The total strain at the onset of yield, ε_y, is also considered here.

4.2.3 Ultimate Strength

Defined by the BSI as the stress corresponding to the maximum force applied to the sample during tensile loading, the ultimate tensile strength, UTS, is considered in the present work [12]. Additionally, as with yield, the strain required to reach the UTS, ε_{UTS}, is also included.

4.2.4 Range Variables

Due to variations in the variables above, the ranges between these also varies. It is possible that these ranges may provide meaningful insights into the behaviour of the material. Therefore, the following 'range variables' are also considered in the present work.

Yield-point elongation or Lüders strain, Y_e, is a result of the yield-point phenomenon and corresponds to the 'plateau' region following the initial peak in discontinuous yield. This is defined by the BSI as the range between the start of yielding and the start of uniform work hardening, is expressed as a percentage strain [12], and is illustrated in Figure 2.4 as 'YPE'.

The yield drop, Y_d, is defined as the stress range between the upper and lower yield stresses.

The stress range between the yield point and UTS is used here as a simple characteristic to represent the strain hardening capacity of the sample. This is referred to in this work as the plastic stress range and denoted Δ_σ. Similarly, and for completeness, the equivalent plastic strain range is denoted Δ_ε.

4.2.5 Summary of Variables

Thus, the variables considered in the present work are detailed in Table 2.

Table 2 - Summary of test variables considered in the present work

Variable	*Units*	*Notation*
0.2% Offset Yield Stress	MPa	σ_Y
Elastic Modulus	GPa	E
Lower Yield Stress	MPa	σ_{LY}
Lüders Elongation	mm/mm	Y_e
Plastic Strain Range	mm/mm	$\Delta\varepsilon$
Plastic Stress Range	MPa	$\Delta\sigma$
Strain to UTS	mm/mm	ε_{UTS}
Strain to Yield	mm/mm	ε_y
Tangent Modulus (Peak)	MPa	T_m
Ultimate Tensile Stress	MPa	UTS
Upper Yield Stress	MPa	σ_{UY}
Yield Drop	MPa	Y_d

4.3 Statistical Methods

The primary goal of statistical analysis, as applied in the present work, is the development of an accurate description of behaviour with a less-than-exhaustive dataset. Due to practical limitations, this results in seeking maximum understanding of the manufacturing process from the minimum material usage. The analyses employed to achieve this are described below. It must be noted that statistical methods are based on correlations and do not address the presence or lack of a causative relationship between the considered factors. Additionally, interactions between variables are not statistically addressed in the present work and are instead accounted for through consideration of the investigation of material microstructure presented in Chapter 3 .

4.3.1 Factorial Design of Experiments

To achieve the most in-depth understanding of the relationships between control factors (independent variables) and measured outputs (dependant variables), it is necessary to measure all the variables in addition to all their possible combinations. This results in a dataset fully describing the effects of the independent variables on the dependant variables. Since it, by definition, accounts for all factors, this is sometimes called a ‘full-factorial’ approach [99, 100].

Such an exhaustive approach, however, is usually not feasible. This may be due to time and cost limitations. In such cases, it is then necessary to identify and remove less-promising factors. At the cost of details or ‘experimental resolution’, this effectively results in isolation of the fraction of the full factorial most likely to produce useful results. As such, this is sometimes referred to as a ‘fractional

factorial' approach. The present work uses varying degrees of fractional factorial approaches to account for limited time and materials.

4.3.2 Pearson's Correlation Coefficient

One simple way to assess the relative behaviour of two variables is through the calculation of a standardised bivariate correlation coefficient such as Pearson's correlation coefficient, *r*. This is calculated as shown below where S_x and S_y are the standard deviations of each x and y and cov_{xy} is the covariance of x and y [101].

$$r = \frac{\mathrm{cov_{xy}}}{\mathrm{S_x S_y}} = \frac{\Sigma_{\mathrm{i=1}}^{\mathrm{n}}(\mathrm{x_i} - \bar{\mathrm{x}})(\mathrm{y_i} - \bar{\mathrm{y}})}{(\mathrm{N} - 1)\mathrm{S_x S_y}} \qquad \textit{Eq. 4.5}$$

The possible values range from -1 to +1, indicating perfect negative and perfect positive correlations, respectively. A value of 0 indicates no correlation. Therefore, calculating *r* for each pair of variables may be used as an indication of which variables are least likely to provide useful insights. Data thinning based on this in the present work is paired with inspection of the scatter plot for each relationship. This is to ensure that the inherent assumption of a linear relationship in the calculation of *r* does not result in the erroneous elimination of variables.

4.3.3 Regression Analysis

Regression analysis is the logical extension of the Pearson's correlation coefficient, allowing for the elimination of the assumption of linearity inherent in the calculation of *r*. Additionally, regression can be extended to more than 2 sets of data. Thus, unlike Pearson's coefficient which is a linear bivariate assessment, regression can assess bivariate, multivariate, linear, or nonlinear correlations. The main features of

regression analysis when assessing model fit are the p-value, the *F*-statistic, and the coefficient of determination (R^2).

The *F*-statistic and p-value are used in conjunction to determine model significance [100, 102, 103]. The coefficient of determination, R^2, is an indication of the adequacy of the model. With possible values for R^2 ranging from 0 to 1, this is a representation of what proportion of the variation in the outcome is accounted for by the model, as a percentage [102].

When calculating a regression, one calculated value is referred to as the test statistic. While this can take many forms, the *F*-statistic for example, what is important to note is the probability of this test statistic taking the value that it has. According to Fisher's criterion, when this probability, the p-value, falls below 0.05 or 5%, the test result may be considered statistically significant [104].

To summarise, Pearson's *r* will be used in conjunction with inspection of the relevant scatter plots as an initial data thinning procedure for all the variables detailed in the previous section. The thinned dataset will then be subject to bivariate and multivariate, linear and nonlinear regression using a combination of Microsoft Excel (and its descriptive statistics plugin) [105, 106] and the statistical analysis software, SPSS [107]. An iterative process will be employed whereby each independent variable will be considered with respect to the dependent variable, yield increase, before including consideration for a second independent variable alongside the first. In this way, the optimum combination of independent variables may be identified for a strong correlation with the dependent variable.

4.4 Results and Discussion

An extensive series of regression analyses was completed for the tensile test data presented in Chapter 3 . The purpose of this was to identify which mechanical properties exhibit strong correlations with the strengthening effect due to dimpling, the percentage increase in yield strength, Y_{inc}. Once explained, such correlations could then be used as a basis to develop an expression for use to predict the strengthening potential of plain steel coil. Having explored linear bivariate, linear multivariate, nonlinear bivariate, and nonlinear multivariate cases for the mechanical properties considered, two possibilities were found for the desired predictive capability:

- Polynomial (2^{nd} order), bivariate relationship between the tangent modulus and Y_{inc} (R^2=0.64), illustrated in Figure 4.5.
- Linear bivariate relationship between the Lüders elongation and Y_{inc} (R^2=0.64), illustrated in Figure 4.7.

It is interesting to note that both possibilities are bivariate correlations. This shows that the iterative procedure described in the previous section has determined that considering Y_{inc} as a function of more than one mechanical property provides no substantial increase in the coefficient of determination, R^2, compared to any function of a single mechanical property.

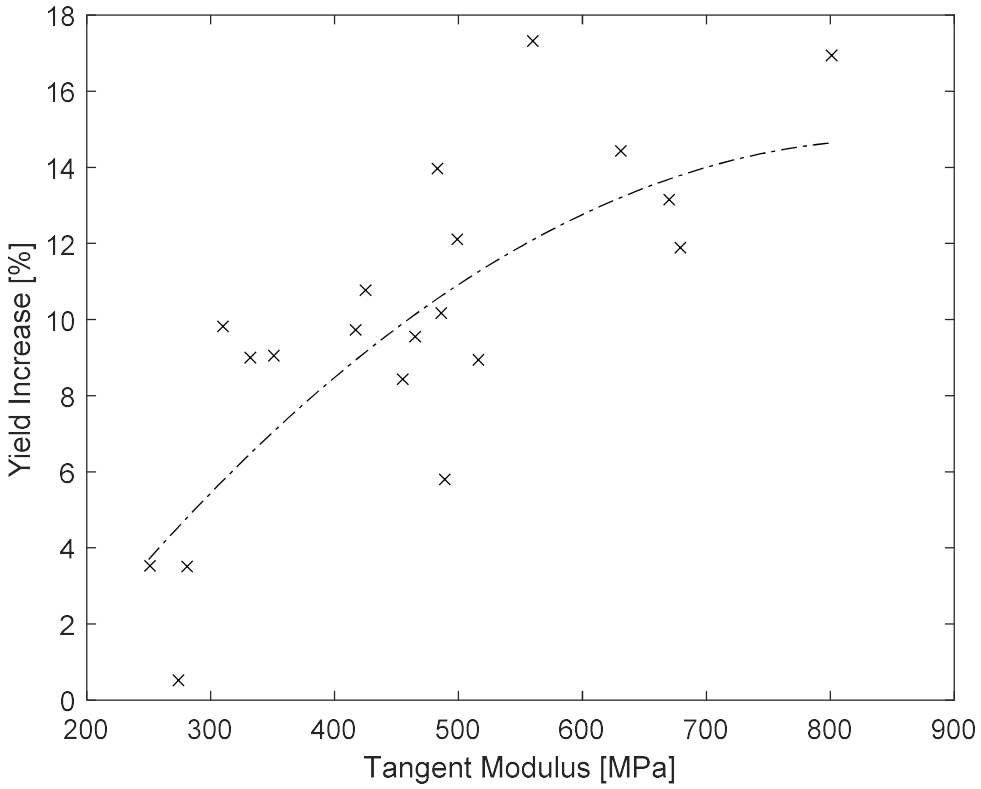

Figure 4.5 - Plot of points, each representing a material coil, indicating a polynomial correlation between the yield strength increase and the tangent modulus of the plain steel

Although the statistical analysis indicates that the tangent modulus of the plain steel may be a good predictor for the magnitude of the strengthening due to dimpling, this may be limited to this specification of UltraSTEEL® only. This is because, if the stress-strain curve of an UltraSTEEL® sample is offset along the strain axis from that of a corresponding plain steel sample to simplistically represent the plastic strain applied by dimpling, it is evident that the tangent modulus occurs near the point where the two curves meet. This is illustrated in Figure 4.6. However, if a greater or lesser plastic strain were to be applied to the same plain steel, for example through the application of a greater or lesser forming depth, this point of curve intersection would change without any change in the tangent modulus. Therefore, this correlation is considered unusable since any changes in the dimple geometry or method of application would render predictive capability based on it obsolete.

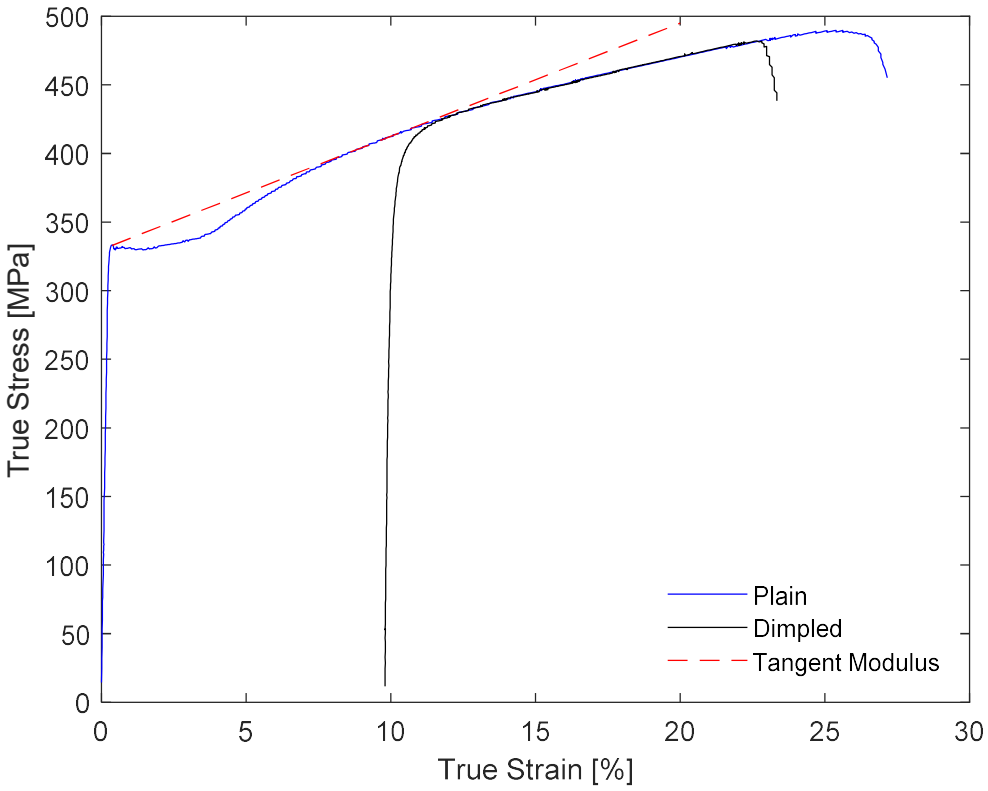

Figure 4.6 - Illustration showing the reason for the coincidental correlation between the tangent modulus of plain steel and the yield strength increase due to the UltraSTEEL® dimpling process

Exhibiting a similarly promising result in the statistical analyses, the linear bivariate correlation between Lüders elongation and strengthening due to dimpling, see Figure 4.7, can be explained based on material microstructure. Specifically, Lüders elongation is an indication of dislocation mobility within the crystal lattice of the material [88]. As discussed in Chapter 3 , grain boundaries impede dislocation motion, Lüders elongation then, is functionally indicative of the initial grain structure in the material: coarser grain structures produce longer Lüders elongation since there are fewer grain boundaries to inhibit dislocation motion.

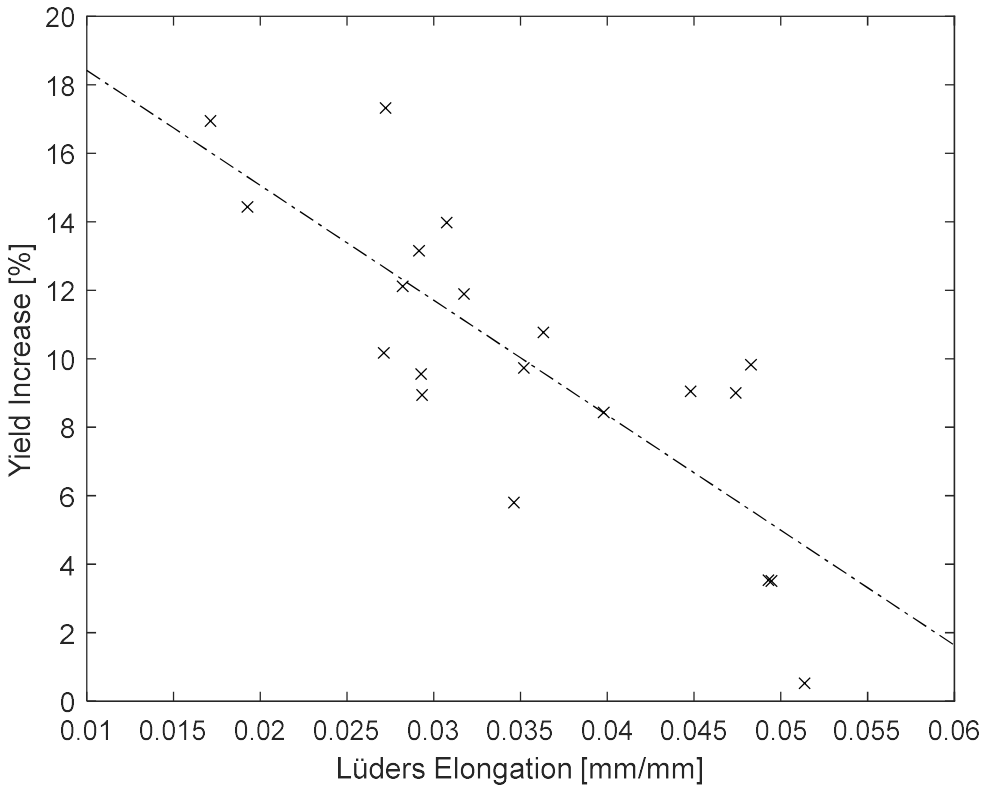

Figure 4.7 - Plot of points, each representing a material coil, indicating a linear correlation between the yield strength increase and the Lüders elongation exhibited in the plain steel

It was determined in Chapter 3 that there are two strengthening mechanisms at work when producing dimpled steel: strain hardening and grain boundary strengthening. Since the plastic strain due to dimpling is considered constant for any specific dimple geometry and method of application, the strain hardening due to dimpling can be considered similarly constant. Since the yield strength increase and Lüders elongation can both be considered symptoms of the same cause, average grain size, this correlation can be considered representative of any grain boundary strengthening resulting from the dimpling operation.

Therefore, the expression in Eq. 4.6 below can be used to predict the strengthening potential for a given source coil prior to forming including the UltraSTEEL® dimpling process. Similarly, the relationship can be used to define an assessment criterion

whereby source coils may be accepted or rejected from dimpling based upon their predicted potential for strengthening due to dimpling.

$$Y_{inc} = -336Y_e + 21.8 \qquad \textit{Eq. 4.6}$$

This expression would need to be adjusted in the event of the introduction of a new dimple geometry/layout or changes to the method of application (e.g. forming depth) to account for differences in the plastic strain applied. This can be easily achieved in the same way as detailed above and would amount to changes in the coefficients. Any trends in such coefficient changes are beyond the scope of this investigation and would therefore require further investigation.

4.5 Summary

The tensile test results presented in Chapter 3 were analysed through the application of statistical methods. These identified two correlations with the potential to form the basis of an expression capable of predicting the potential strengthening of a steel source coil prior to dimpling.

The first, a correlation between the tangent modulus and yield strength increase, was dismissed as a potential predictor due to the coincidental and inflexible nature of this trend.

The second, a correlation between the Lüders elongation and yield strength increase, was explained as these variables being separate results of a common cause: the initial average grain size of the material. Established as a causative relationship, this link between Lüders elongation and yield strength increase was then used to produce the expression in Eq. 4.7 below.

$$Y_{inc} = -336Y_e + 21.8 \qquad \textit{Eq. 4.7}$$

Although this is only applicable to UltraSTEEL® as applied according to current industry standards [5, 108], it is expected that modifications to dimple geometry or application methods may be accounted for through modification of the coefficients based on the relevant tensile testing.

Chapter 5 Study of the Stiffness of Dimpled Steels Using FE and Experimental Methods

5.1 Introduction

There is some debate over the effect of the dimpling process on the stiffness of steel – some studies suggest that the dimpling process results in a decrease in sample stiffness while others suggest an increase. However, since many applications require a focus on other properties (yield in structural columns [15–17, 36] and specific energy absorption in crash barriers [7, 19, 109], for example), there has been little work towards investigating this. It is, however, important to understand the stiffness of dimpled products in common applications such as structural beams. Furthermore, in applications where mechanical failure is the purpose of the product such as is the case for crash barriers [7, 19, 109], the evolution of the material stiffness through loading is also of interest.

Regarding structural applications where the product stiffness is relevant, as discussed in Section 2.3 , the current literature is unclear regarding whether the dimpling process meaningfully changes the stiffness of processed material. It seems if a change due to dimpling is present, that it is small and may therefore be negligible irrespective of whether it constitutes an increase or decrease. Furthermore, it has been hypothesised that there may be some stiffness reduction necessitated by the geometry of the dimpled steel [9, 87, 110] where the external product profile geometry remains unchanged. However, this may be offset by changes to the material properties resulting from the dimpling process [8]. Purely illustrative FE models will be constructed here to show the stress-concentrating effects of non-

uniform geometry such as dimples and how this results in a geometrically necessary reduction in stiffness. The results of these simulations will then be considered alongside the literature to show the counterbalancing effect of the material property changes due to the dimpling process.

Addressing applications where the evolution of stiffness through loading is relevant or where substantial pre-strains are likely, incremental cyclic tensile testing will be conducted to directly test the evolution of stiffness through loading. In this way, the evolution of the effective elastic modulus may be used as an analogy for the evolution of the aggregate stiffness of the sample. The term 'effective elastic modulus' is used here to distinguish between the conventional elastic modulus and the average elastic modulus measured after a pre-strain is applied, representing the aggregate response of the sample to pre-strains.

Together, these are expected to provide a more complete understanding of how the stiffness of dimpled steel might impact the design and application of UltraSTEEL® products.

5.2 Finite Element Modelling

Serving the purpose of illustrating the stress-concentrating effects of non-uniform geometry and how this impacts the aggregate elastic behaviour of the sample, 2D finite element models were constructed for both plain and dimpled steel cross-sections in the form of cantilever beams using the ANSYS finite element software [111]. These are implemented using the Dimpled-Geometry-Plain-Material (DGPM) approach used by Liang et al [19] where both the plain and dimpled geometries are simulated as having uniform plain steel material properties. In this way, any

material property changes due to the dimpling process are omitted such that, at the onset of loading, only geometric effects have been considered.

Since these simulations are merely illustrative and their focus is on the elastic behaviour, a bilinear isotropic hardening material model based on the data presented in Chapter 3 is used. This model is characterised as follows: elastic modulus, 205 GPa; Poisson ratio, 0.3; density, 7810 kgm^{-3}; coefficient of friction, 0.1; yield stress, 335 MPa; tangent modulus, 500 MPa.

The geometries used for these models include a 0.5mm x 13.95mm plate for the plain steel cross-section and a waved plate with a length of 13.95mm, a gauge of 0.5mm, and an effective gauge of 1.0mm for the dimpled cross-section. Thus, the dimpled cross-section conforms with the double-depth standard for forming depth, is assumed to feature negligible thinning due to the dimpling process, and represents the dimpled steel cross-section along a plane that cuts through the maximum amplitude of the dimples. In both cases, a sheet thickness of 0.2mm is applied in simulation. These geometries are illustrated in Figure 5.1 which also shows that the dimple pitch is such that 3 periods of the cross-section wave form are present over the length of the plate. Furthermore, with an edge length of 0.5mm, the computational meshes used are sufficiently fine to ensure reliable simulation of the shear characteristics and prevent shear locking during loading. Composed entirely of plane183 elements, these meshes consist of 2,790 and 2,968 elements for the plain and dimpled geometries, respectively.

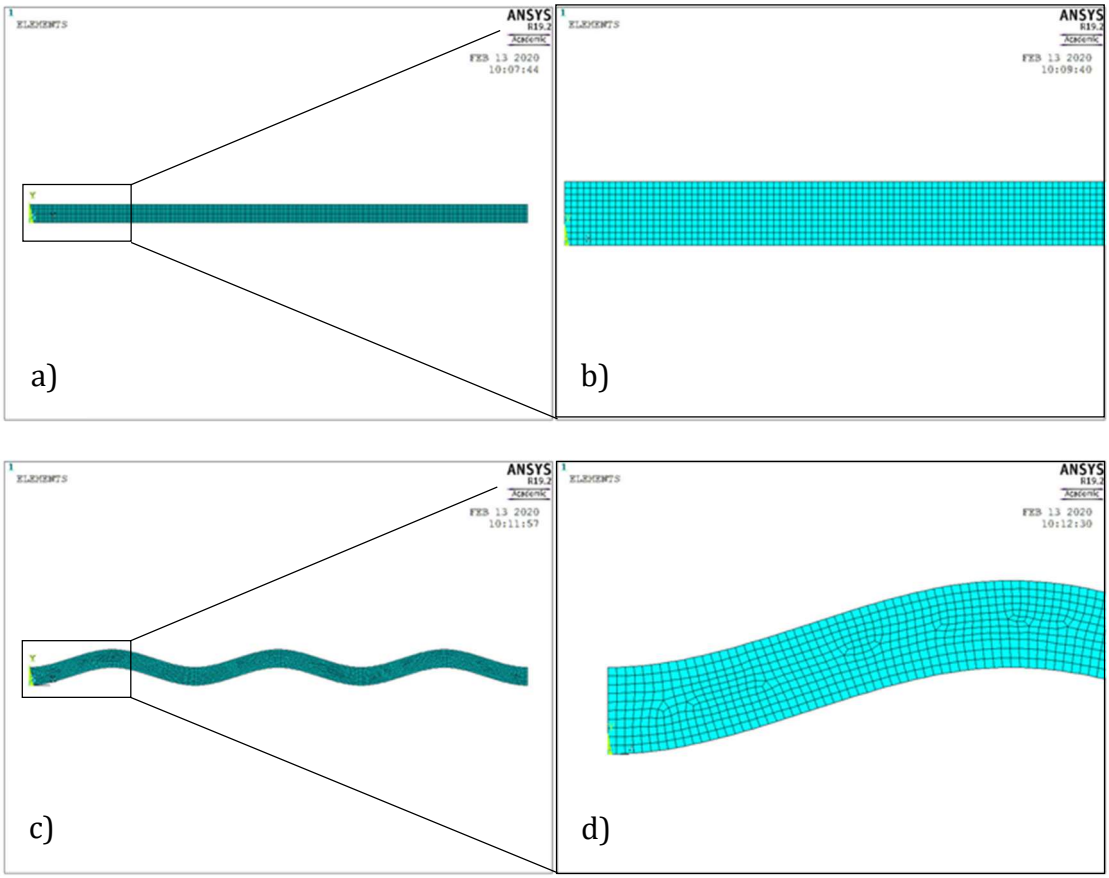

Figure 5.1 - Meshed plain steel and dimpled steel cross-sections as used in beam bending simulations. a) plain steel geometry; b) close-up view of the mesh used for the plain cross-section; c) dimpled steel geometry; d) close-up view of the mesh used for the dimpled steel cross-section

As illustrated in Figure 5.2, these plates are fully fixed along the left-side edge and loaded by a force perpendicular to the major axis of the beam at the right-side edge. For the purposes of this illustration, the loading force is defined in terms of displacement to a maximum of -5.35mm.

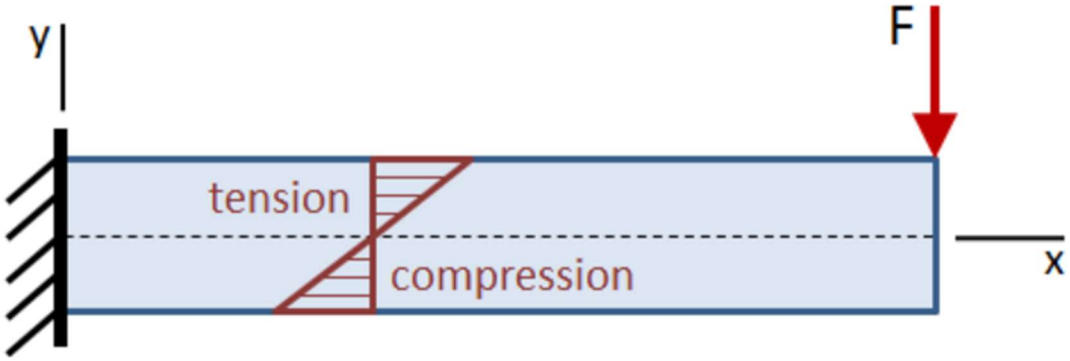

Figure 5.2 - Illustration of cantilever beam boundary conditions and the resulting tension/compression distributions [112]

5.3 Analytical Assessment of Beam Cross-Sections in Bending

The well-established 'beam theory' [113] is an analytical tool enabling the quick assessment of the response of a beam subjected to pure-bending loads. To apply here, for the plain steel, it is assumed that the beam has a uniform cross-section, is straight prior to loading, and exhibits homogeneous and isotropic material properties. These assumptions enable the derivation of the 'differential equation of the elastic curve' (Eq. 5.1) and thus, the beam deflection equations (Eq. 5.2 and Eq. 5.3) below [113]. 'y' is the linear deflection normal to the major axis of the beam, 'x' is the distance from the point of loading, 'M' is the bending moment, 'E' is the elastic modulus, 'L' is the length of the beam, 'F' is the load applied, and 'I' is the moment of inertia (defined for a rectangular cross-section in Eq. 5.4 where 'b' is the length of the base and 'h' is the height of the rectangle).

$$\frac{d^2y}{dx^2} = \frac{M}{EI} \qquad \textit{Eq. 5.1}$$

$$\frac{dy}{dx} = \frac{FL^2}{2EI} \qquad \textit{Eq. 5.2}$$

$$y = -\frac{FL^3}{3EI} \qquad \textit{Eq. 5.3}$$

$$I = \frac{bh^3}{12} \qquad \textit{Eq. 5.4}$$

This can be applied to the plain steel cross-section to show whether the present simulation methodology produces the expected result for the elastic response. Applying Eq. 5.3 to the beam bending of plain steel as described in Section 5.2 then provides a method by which to support the pre-yield results of the simulations. This

is achieved by substituting in a force below the simulated yield along with the values listed in Table 3 to calculate the related deflection and thus, a point that should lie along the simulated force-deflection curve.

Table 3 - Summary of the beam theory properties of the plain steel beam

Variable	*L (mm)*	*E (MPa)*	*b (mm)*	*h (mm)*
Value	13.95	205 000	0.2	0.5

5.4 Experimental Procedure

Using the elastic modulus in tension as an analogy for sample stiffness, incremental cyclic tensile testing is applied to measure the sample aggregate response to pre-strains. The experimental setup used to achieve this is largely the same as that presented in Chapter 3 and illustrated in Figure 3.7. The only difference here is in the test procedure. Previously, the sample being tested was simply loaded to failure. During these tests, the rig will instead load the sample to a pre-defined peak total strain before executing a controlled return to zero load. The sample will then be loaded again to a higher pre-defined peak total strain before being returned, again, to zero load. In this way, an incremental cyclic loading will be completed covering peak total strains at 0.1% increments up to 1.5% with additional peaks at 2, 5, and 10% prior to loading to failure. Thus, the procedure is as follows:

1. Fix the dogbone sample in the test rig grips with the sample major axis aligned to the loading direction.
2. Fit the extensometer aligned with markings 1 and 3 specified in Figure 3.5.
3. Load the sample to 0.1% total strain.
4. Execute a controlled return to zero load.

5. Load the sample to the next peak total strain (e.g. 0.2%)
6. If the sample has yet to fail and the previous peak total strain is not the final pre-define peak (e.g. 10%), then go to step 3. Otherwise, load the sample to failure.

As before, the tests will again be arranged in corresponding pairs of plain steel and dimpled steel samples. Note that the definition of the 'return to zero load' will result in a non-zero strain at zero stress once the peak total strain exceeds the proportional limit of the material.

The resulting stress-strain plots can then be assessed for the elastic modulus relating to the elastic strain region of each peak, referred to here as the 'effective elastic modulus' for clarity. This is simply measured as a linear estimate of the elastic portion of the unloading/reloading curve after each defined peak strain. It is expected that this will provide some understanding of the evolution through loading of the stiffness of both plain and dimpled samples, thereby providing indications of the extent of the relevance of macroscopic departure from plain steel geometry such as dimpled textures.

5.5 Results and Discussion

5.5.1 Stiffness as Resistance to Bending in FE Modelling with Analytical Support

Figure 5.3 illustrates the simulated force deflection curves for the plain and dimpled cross-sections in response to a pure bending load case. A reduction in the stiffness resulting purely from the non-uniform distribution of stresses and strains due to the dimpled geometry is evident with a comparison of the initial slopes of these curves

suggesting a difference of ~10%. Similarly, there is a reduction in the indicated yield stress of approximately 5%.

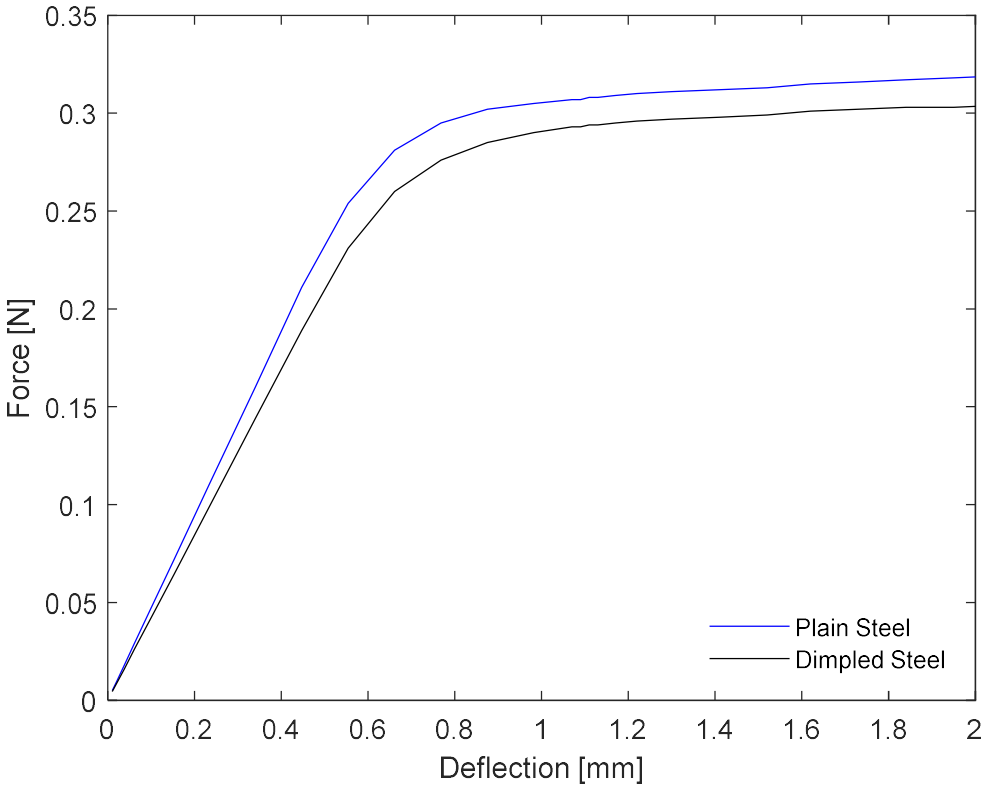

Figure 5.3 - FE force-deflection curves for plain steel and dimpled steel cross-sections subjected to pure bending loads

This stiffness reduction due to the changing geometry is due to the stress-concentrating effects inherent in these changes. As shown in Figure 5.2, the tension and compression developed in a cantilever beam are, for plain steel, distributed across the top and bottom surfaces, respectively. This is also illustrated in Figure 5.4. In the case of a dimpled steel cross-section however, these stresses are instead concentrated by the peaks and troughs of the dimpled geometry. This is illustrated by the stress concentrations between the dimples in Figure 5.5. Furthermore, in considering a 3-dimensional dimpled sheet, it is intuitively deducible that this inter-dimple region exhibiting the stress concentrations is the weakest point in bending.

This is because the alternating nature of the dimples along their maximum amplitude, in the normal direction, effectively acts as a stiffener to resist in-plane bending forces. Contrarily, the inter-dimple region is effectively a plain steel mean-line within the dimpled geometry offering no resistance to bending loads orthogonal to this mean-line.

Applying the analytical assessment presented in Section 5.3 predicts a deflection of
1300 0.53 mm when the applied load is 0.25 N. The plain steel simulation presented in Figure 5.3 indicates a deflection of 0.55 mm for the same load. Due to this close agreement, the simulation methodology is considered in agreement with established analytical results.

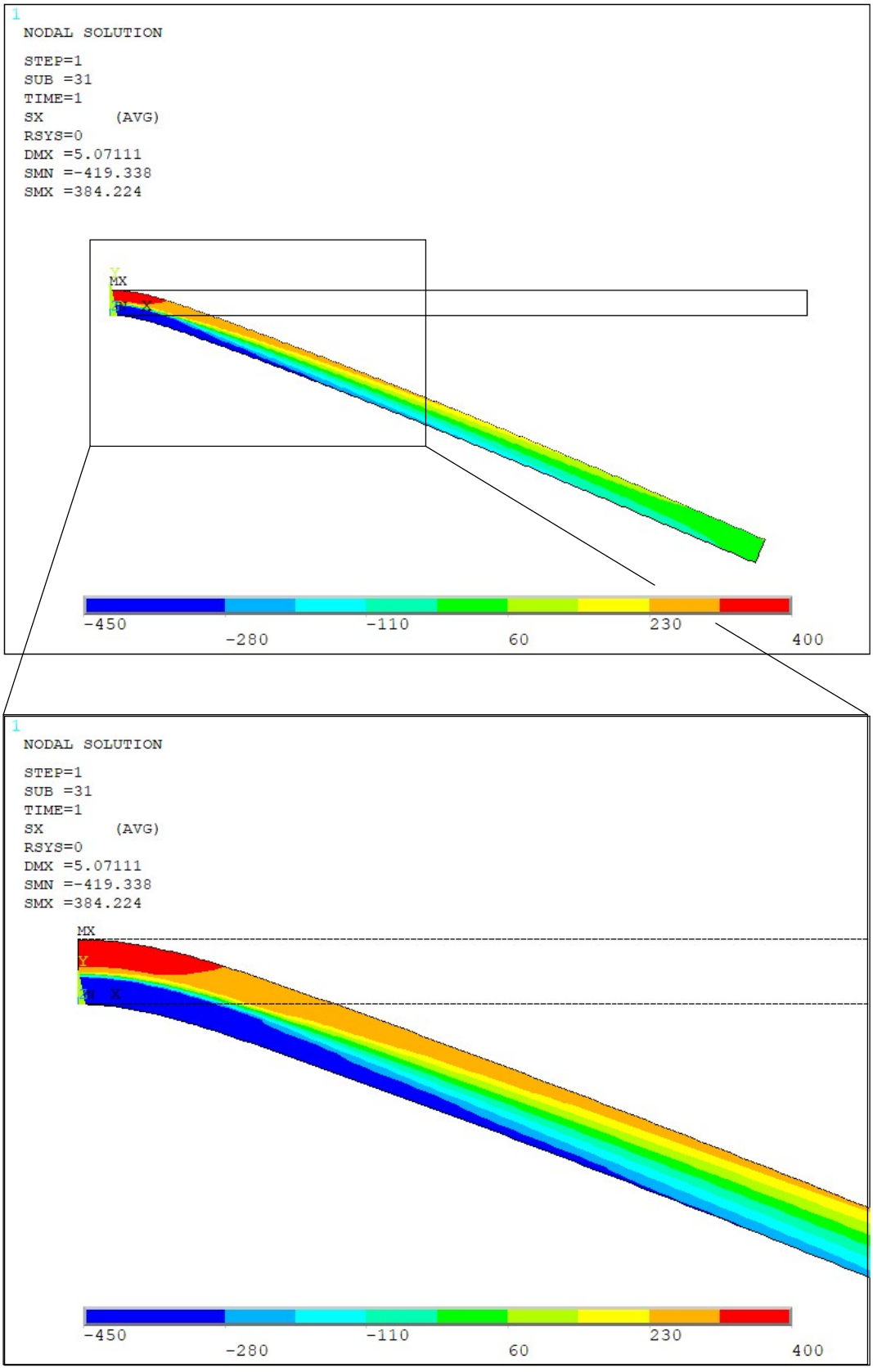

Figure 5.4 - Plots of the principal stress in the x-direction for the plain steel cross-section subject to beam bending loads. Top: overview. Bottom: detailed view

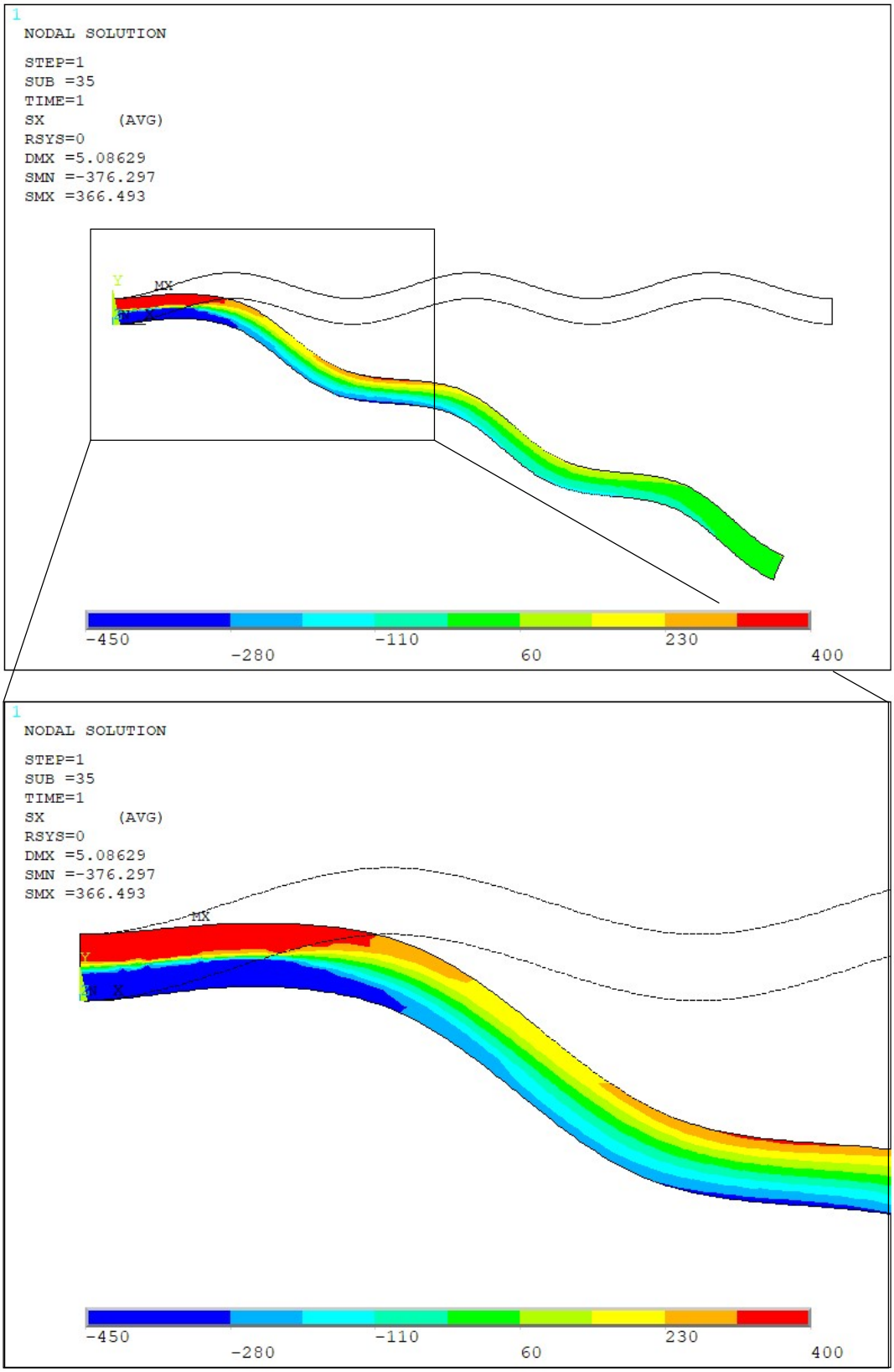

1310 *Figure 5.5 - Plots of the principal stress in the x-direction for the dimpled steel cross-section subject to beam bending loads. Top: overview. Bottom: detailed view*

A DGPM simulation such as this does not account for changes in the material properties due to plastic strains and residual stress and therefore, while useful in exploring the geometric implications of dimpled geometry, cannot be used to predict the true loading response of dimpled steel. However, Nguyen *et al* illustrated in 2014 [2] that including consideration for plastic strains and residual stresses in the form of pre-stress formulation can achieve accurate prediction of the elastic loading response. This is illustrated in Figure 2.2 by the close agreement of the FE and experimental dimpled curves for extensions less than 0.5mm. and suggests that while geometric changes due to dimpling necessitate a reduction in the elastic modulus, this reduction is largely negated by changes to the material properties that would otherwise result in an increase to the elastic modulus by a similar magnitude.

5.5.2 Experimental Evolution of the Elastic Modulus Through Loading

It was noted in Section 5.1 that it is necessary in applications such as crash barriers to understand the nature of the failure of dimpled steel when subjected to loads exceeding the capacity of the product. Therefore, the evolution of the elastic modulus through loading has also been explored. Enabling the direct assessment of the effect of pre-strains on the aggregate behaviour of the samples, the stress-strain plots produced by incremental cyclic loading as described in Section 5.4 are shown in Figure 5.6 and Figure 5.7. These tests were completed by the author in cooperation with the Hadley Group [5].

As expected, the most noticeable trend is that increasing pre-strains generally result in increasing yield strengths with the magnitude of this change in yield being dependant on the shape of the relevant stress-strain curve.

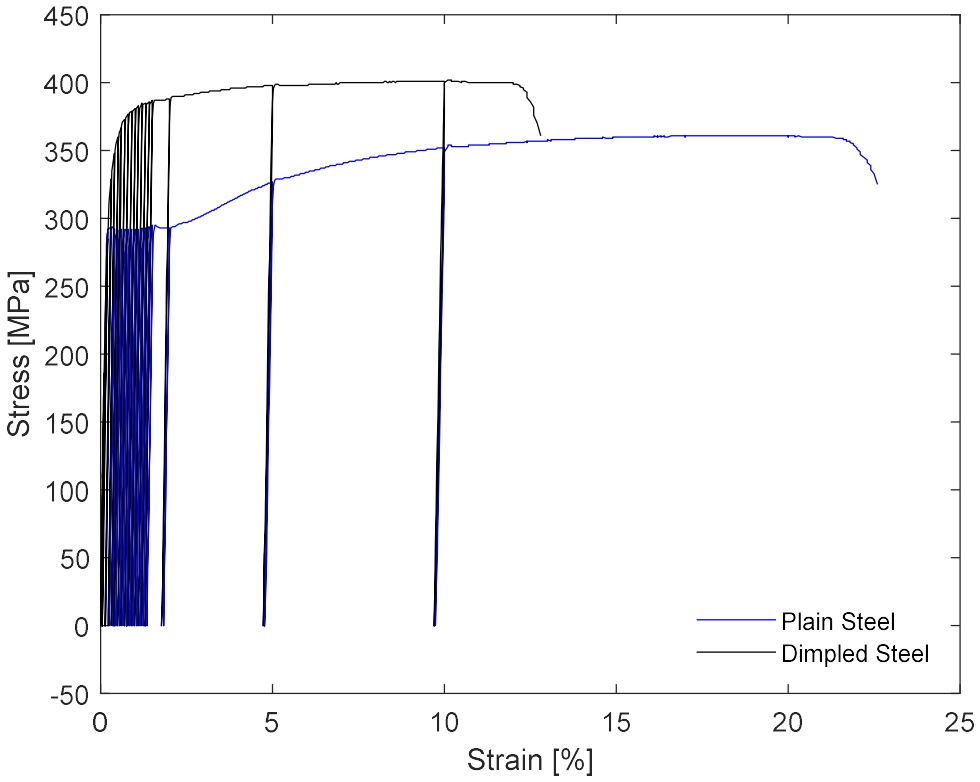

Figure 5.6 - Comparison of the evolution of the elastic properties of plain and dimpled steel through incremental cyclic tensile loading

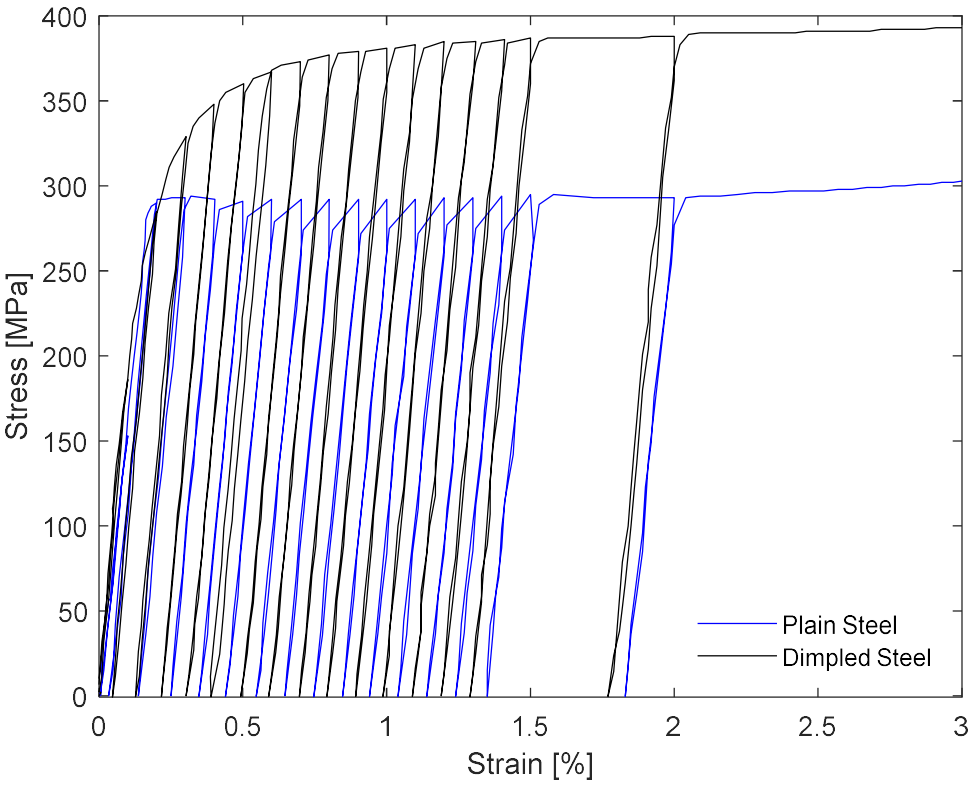

Figure 5.7 - Comparison of the evolution of the elastic properties of plain and dimpled steel through incremental cyclic tensile loading (up to 3.0% total strain)

1340

The data from Figure 5.6 and Figure 5.7 was used to assess, for each increment, the effective elastic modulus of plain and dimpled steels. Specifically, a linear approximation of the elastic portion of the unloading/reloading curve following each peak strain increment was measured. The result, illustrated in Figure 5.8, clearly indicates that pre-strain results in a decrease in the stiffness of the sample regardless of whether it is plain or dimpled steel. While the nature of this decrease appears to vary, the common trend is that the effective elastic moduli for corresponding plain and dimpled samples converge with increasing strain. It is also important to note, as shown, that there is some variation in whether the effective elastic modulus of the plain steel or the dimpled steel is initially higher. However, with $p < 0.05$, a one-tailed paired t-test indicates that the pairwise difference between the elastic moduli of the plain and dimpled samples is significantly lower at 2, 5, and 10% strain than it is at 0% strain for the present dataset irrespective of which is initially stiffer.

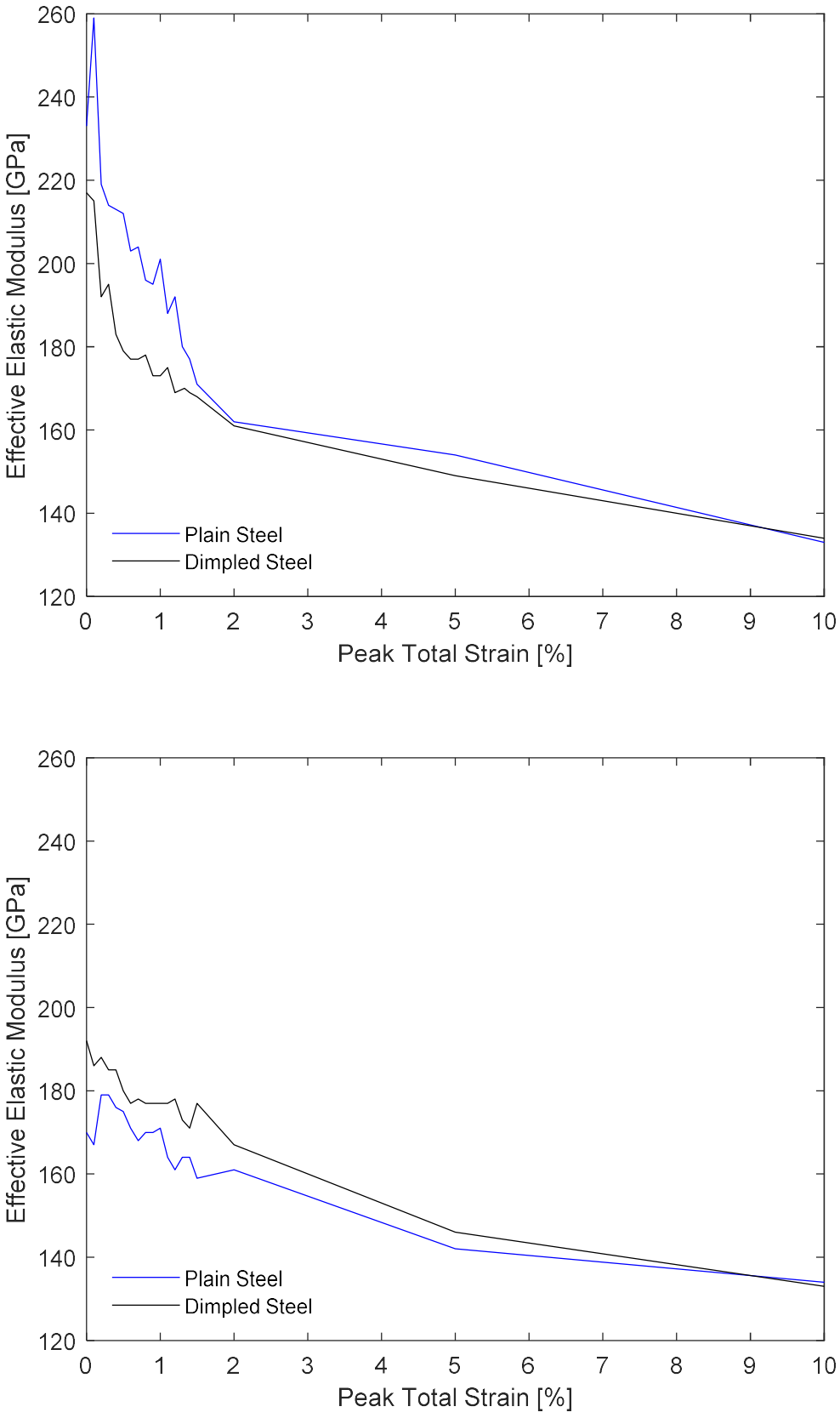

Figure 5.8 - Evolution of the elastic moduli of plain and dimpled steels through tensile loading (top: plain steel is initially stiffer; bottom: dimpled steel is initially stiffer)

This convergence of effective elastic moduli is indicative of a phenomenon noted in Section 2.3 and introduced into the literature in 2011 by Nguyen *et al* [14]. Specifically, as the dimpled sample is loaded in tension, the dimples 'unfold'. This geometric deterioration is illustrated in Figure 2.1. The decreasing amplitude of the dimples results in diminished geometric contributions to sample strength and stiffness. Similarly, the stress concentrations due to the dimpled geometry, also illustrated in Figure 2.1, result in local material failures that negate the effects of the material property contributions to sample strength and stiffness. Thus, the overall stiffness of the samples in large-strain cases are substantially similar for plain and dimpled steel.

5.6 Summary

A plane strain, DGPM approach was applied in Finite Element simulation of a plain steel cross-section. Taking the standard case of a cantilever beam, the FE model produced results in agreement with standard beam theory. This FE approach was then applied to a dimpled steel cross-section taken through the dimples at their maximum amplitude. Applying the same material properties, taken from the experimental tensile testing of plain steel, this approach showed that the dimpling of steel results in a necessary reduction in the elastic modulus due to the non-uniform distribution of stresses and strains that is symptomatic of the geometry.

Considering this result as compared with simulations by Nguyen *et al* [2], it was determined that the plastic strains and residual stresses resulting from the dimpling process cause an increase in the elastic modulus of a similar magnitude. Thus, simulations accounting for these changes show, as in experiment, that the elastic moduli of plain and dimpled steel do not differ substantially.

Following this, to evaluate the evolution of the sample stiffness through loading, incremental cyclic tensile tests were completed. In this way, the effect of pre-strains on the loading response of plain and dimpled steel was assessed. It was found that while there is some variation regarding which, plain or dimpled steel, exhibits a higher elastic modulus, their effective elastic moduli converge with increasing axial strain. This was attributed to a combination of two changes through loading. Firstly, the previously noted unfolding of dimples resulting in diminishing geometric
1390 contributions to the strength and stiffness of the samples. Secondly, local material failure due to stress concentrations resulting from the dimpled geometry. These local failures effectively negate the overall contributions to sample strength and stiffness of material property changes due to the dimpling process.

Chapter 6 Definitions and Standard Methods for the Quantification of Yield Strength in Ductile Metals

6.1 Introduction

Many organisations responsible for standardisation of measurement (the International Organization for Standardization, ISO [114]; the European Committee for Standardization, CEN [115]; the British Standards Institution, BSI [116]; the American Society for Testing and Materials, ASTM [41], Standards Australia, AS [117]) have addressed the question of measurement of the strength of materials. Regarding yield strength, this has been standardised in much the same way for all the organisations considered.

Despite this, the measurement of yield strength in tension is not necessarily straightforward. First the type of yield must be categorised as either continuous or discontinuous. Even this can be less than clear in some cases. Only after this categorisation can a measure of yield be selected. Currently, there are 4 distinct, widely recognised, standard measures of yield strength in tension:

- Proof Strength, Non-Proportional Extension (or Offset Yield, σ_Y)
- Proof Strength, Total Extension (or Extension-Under-Load, σ_{EUL})
- Upper Yield Strength, (σ_{UY})
- Lower Yield Strength (σ_{LY})

Even with these measures being distinct from one-another, there are still cases where none of these are appropriate due to limitations inherent within the assumptions made in their formulation. Furthermore, the availability of multiple

standardised measures results in substantial potential for confusion and miscommunication in industries where changes in yield strength are important since this may result in the comparison of incompatible measures of yield strength.

The standard methods are addressed here with consideration for the limitations to the applicability of each. The studies by Sevostianov and Kachanov [55] and Clausen *et. al* [68] were noted in Section 2.4.2 in the discussion of alternative yield criteria. The data from these studies (Figure 6.2 and Figure 6.3) is used here alongside the data from Chapter 3 to illustrate the application and limitations of the standard methods. Thus, cases exhibiting discontinuous (plain steel), continuous (steel lattice [68] and porous Ti_6Al_4V [55]), and severely continuous (dimpled steel) yield are considered. 'Severely' is used here to distinguish cases of continuous yield that exhibit substantial departure from linearity in the stress-strain curve prior to macroscopic yield. Furthermore, cases where the necessary comparison of mutually incompatible yield measures produces misleading results are illustrated.

Addressing the need for a more appropriate and widely applicable yield measure arising from the limitations identified, a novel yield criterion based on the second derivative of stress with respect to strain is presented. Applied to each example case, this criterion is shown to be independent of the type of yield behaviour and the presence or lack of macroscopic structures such as dimples while maintaining a level of simplicity in application not easily achieved by analytical means. The implications of this novel criterion regarding the outcomes of previous chapters are also addressed alongside illustration of the compatibility of measurement enabling the representative comparison of yield strengths for different types of yield.

6.2 Applicability of Standard Tensile Yield Criteria in Application

First consider discontinuous yield. As illustrated in Figure 6.1, this is the behaviour exhibited by the plain steel tested in tension in the present work and clearly the standard σ_{UY} and σ_{LY} apply. Since it more closely matches the as-defined yield, σ_{UY} is used for the purposes of this chapter.

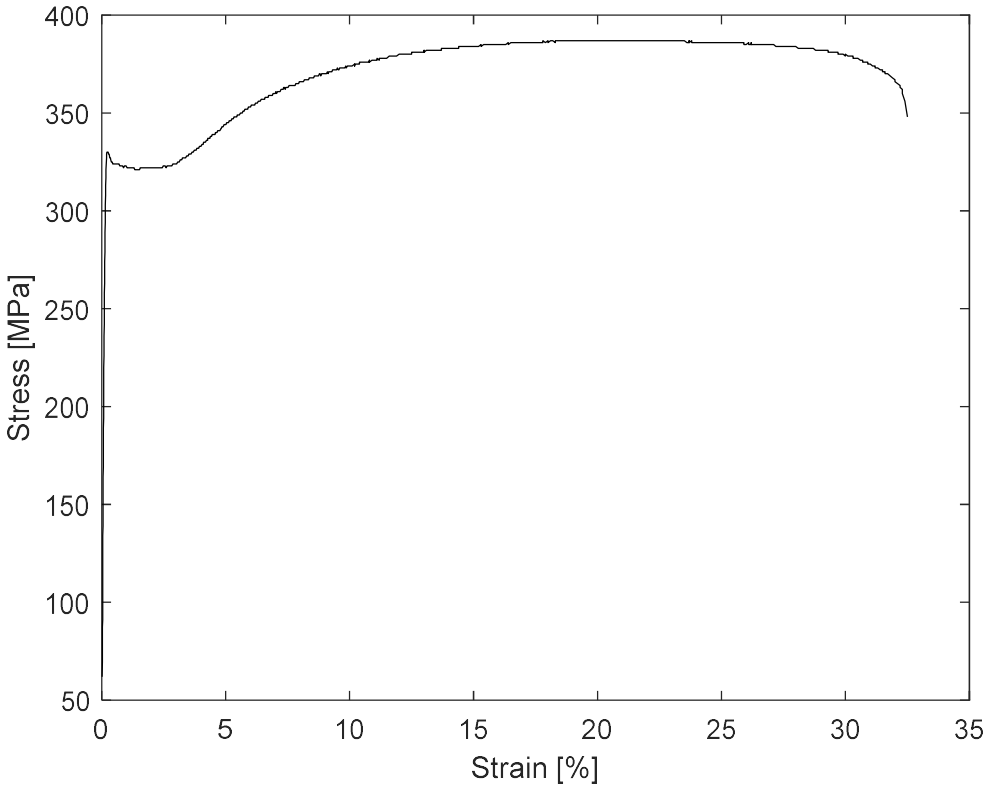

Figure 6.1 – Experimentally measured stress-strain curve for plain steel subjected to tensile loading

Figure 6.2 and Figure 6.3 clearly indicate that σ_Y applies to the stainless steel lattice and the 7.6% porosity Ti_6Al_4V, respectively. Conversely, inspection of Figure 6.4 and Figure 6.5 reveals a substantial departure from linearity prior to macroscopic yield. This is typical of the tensile load response of dimpled steel and makes σ_Y inapplicable.

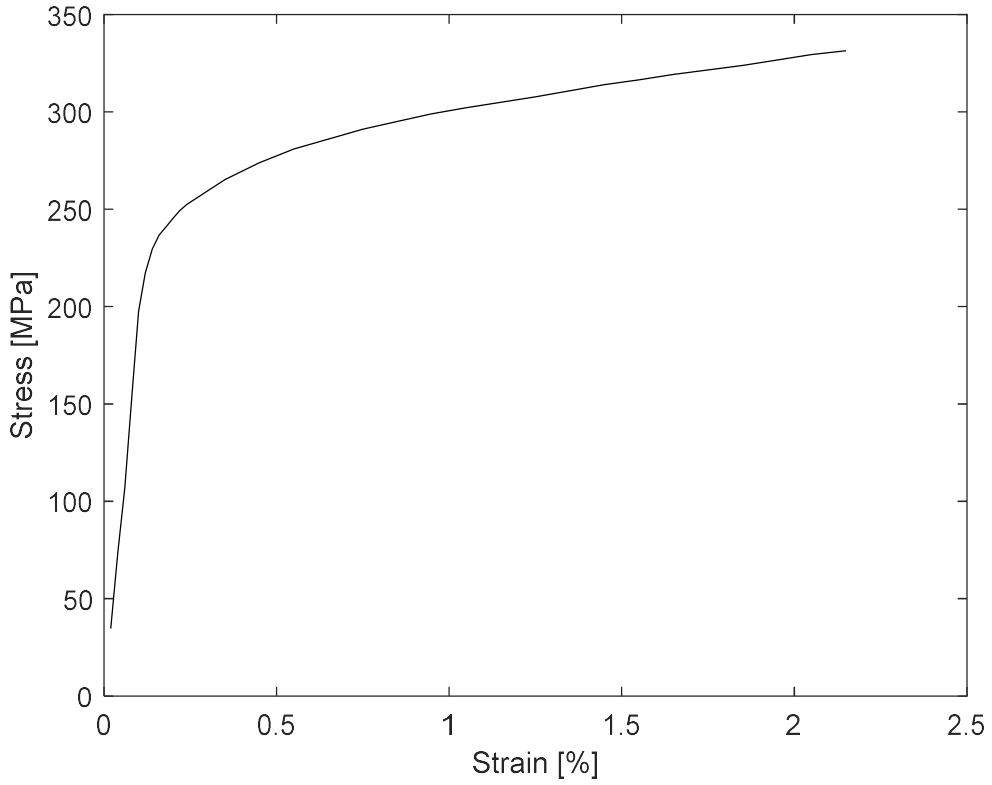

Figure 6.2 – Experimentally measured stress-strain curve for a stainless steel lattice subjected to tensile loading [68](reconstructed data)

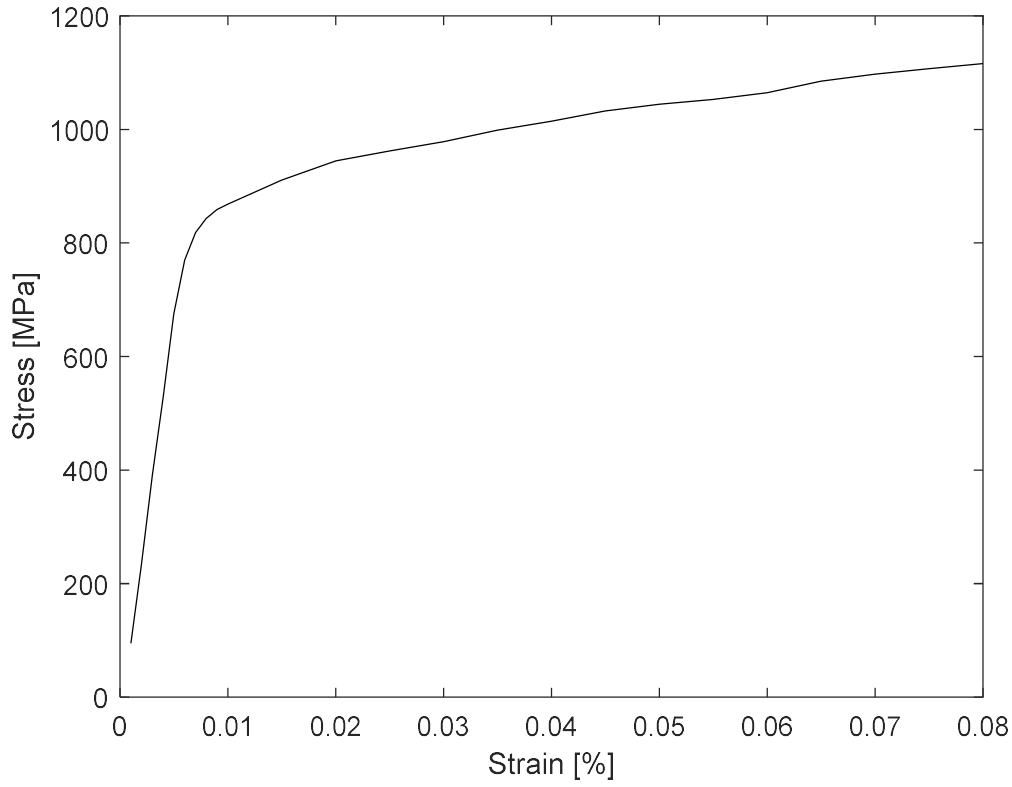

Figure 6.3 - Experimentally measured stress-strain curve for porous Ti_6AL_4V (porosity 7.6%) subjected to tensile loading [55](reconstructed data)

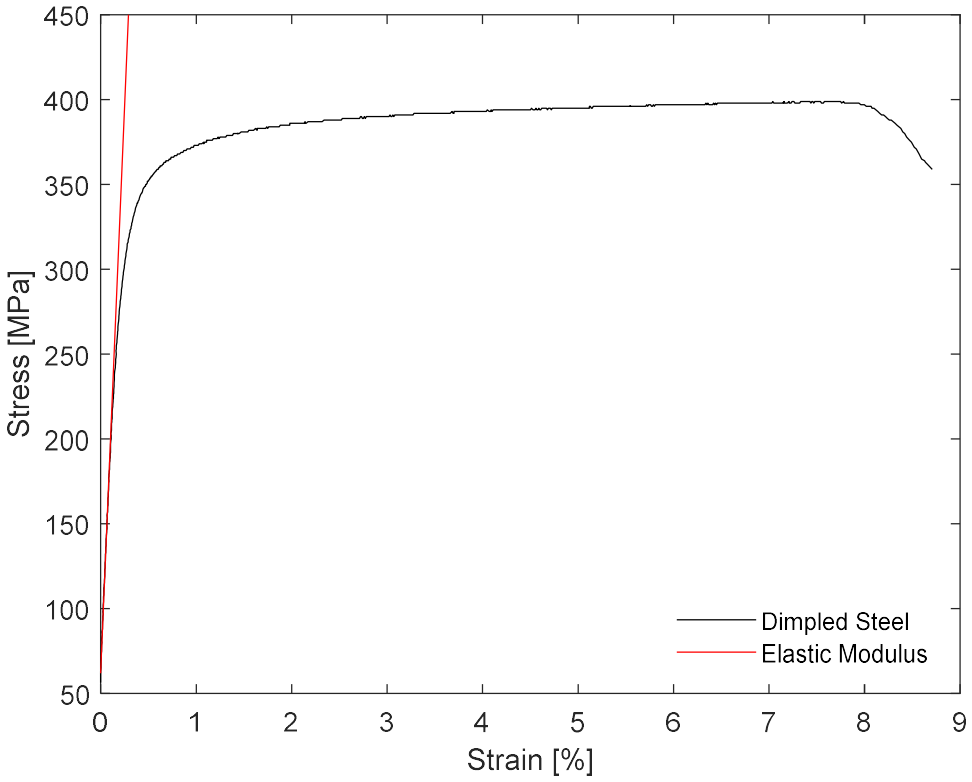

Figure 6.4 - Typical stress-strain curve for dimpled steel subjected to tensile loading with the elastic modulus illustrated

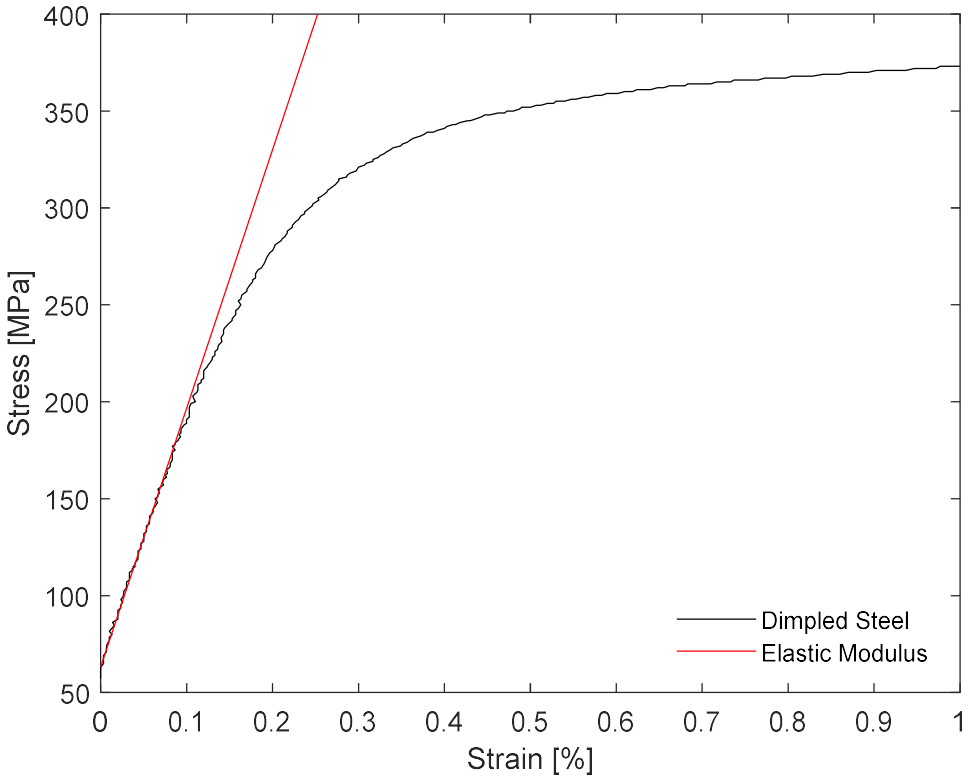

1460

Figure 6.5 - Low-strain region of a typical stress-strain curve for dimpled steel exhibiting 'severely continuous yielding'

Furthermore, it has been shown that the offset yield method, despite being defined as the default, is not applicable to cases where the yield behaviour is severely continuous. For these reasons, a novel criterion to quantify yield strength independent of yield behaviour is sought here.

6.3 The Novel Derivative Yield Criterion

Considering Figure 6.5, it is clear that the microscopic yield leads to small deviations from linearity while the macroscopic yield produces a relatively localised change in the instantaneous tangent to the stress-strain curve, the tangent modulus. Marking the transfer from predominantly global to predominantly local strain that underlies macroscopic yield. It is important to note that this localised change in the tangent modulus at yield is also evident in discontinuous and continuous yield types (Figure 6.1, Figure 6.2 and Figure 6.3). It is proposed then that this commonality irrespective of yield type may provide a basis for the non-arbitrary determination of yield strength independent of the type of yield behaviour of the material.

The tangent modulus is the first derivative of stress with respect to strain. A substantial, localised change in the tangent modulus effectively amounts to a pronounced peak in the derivative thereof, i.e. a turning point in the second derivative of stress with respect to strain. A turning point in the second derivative is more clearly characterised by a corresponding value of zero for the third derivative. Thus, the novel 'derivative yield' is proposed. This new criterion asserts that $\frac{d^3\sigma}{d\varepsilon^3} = 0 \; when \; \varepsilon = \varepsilon_{yield}$. This can be applied one of 2 ways.

1. A 4th order polynomial fit can be applied to the yield portion of the stress-strain curve. The third derivative of this polynomial is then equal to zero when $\varepsilon = \varepsilon_{yield}$, allowing the determination of the yield stress by identifying the stress reading at ε_{yield} in the original stress-strain curve. The result of this is illustrated graphically using the turning point of the second derivative in Figure 6.12.
2. Using the stress-strain data, a pointwise differential of stress with respect to strain can be calculated using the finite difference method. Applying this method in succession determines the second and third differential of stress which can be used in the same way as with the polynomial. The result of this is illustrated graphically using the turning point of the second differential in Figure 6.6

Clearly the polynomial fit method requires more work in application. This is because it requires prior knowledge of the approximate location of the yield point. Furthermore, to obtain a good polynomial fit, a region containing the yield point must first be isolated, for example, by eliminating data below 100 MPa and above 1% strain. This eliminates low-stress readings to minimise the impact of related uncertainty as well as much of the plastic region to ensure goodness of fit. This method is also not applicable to cases of discontinuous yield since a polynomial cannot be adequately fitted to this curve shape.

Conversely, the finite difference method is applicable irrespective of curve shape and does not require any prior knowledge relating to the yield stress. However, this method may be sensitive to noise in the data. Therefore, calibration of the step size used in the finite difference calculations is necessary to ensure an accurate result.

The novel criterion is applied for all the example cases along with the appropriate standard in the following section.

6.4 Tensile Yield Criteria in Application

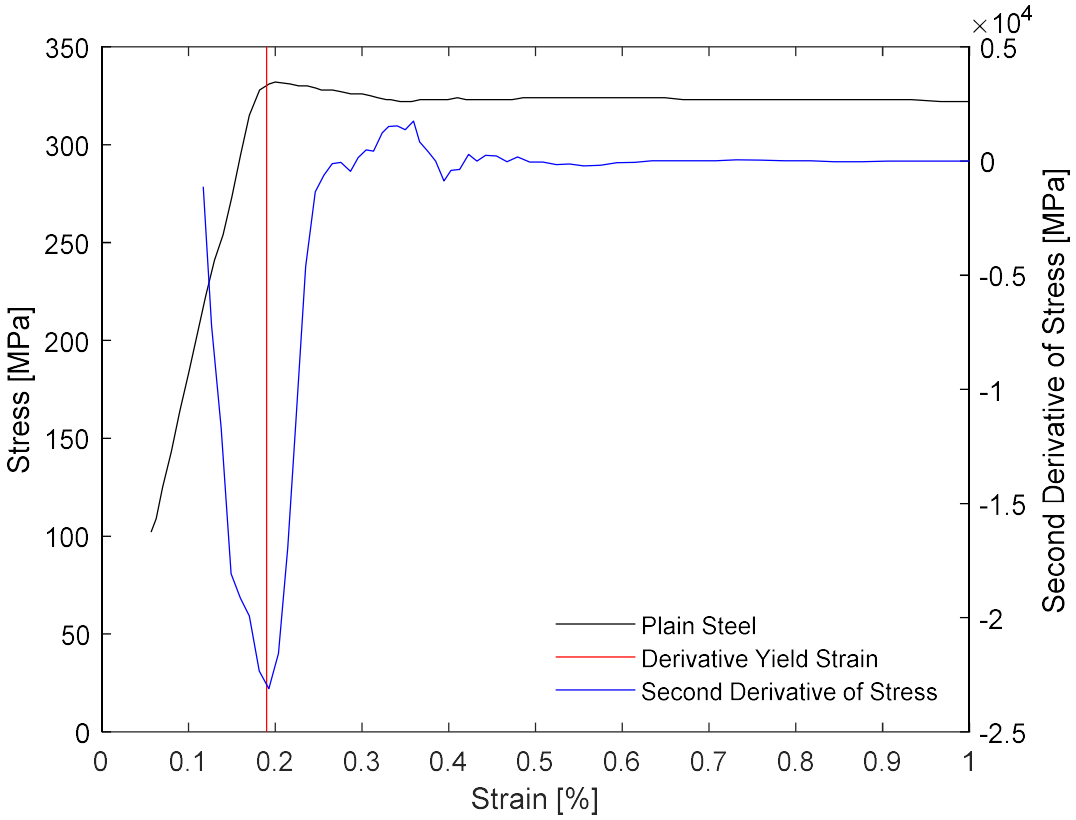

Figure 6.6 – Derivative yield as applied to a an experimentally measured stress-strain curve for plain steel subjected to tensile loading

Illustrating application of the novel derivative yield, $\sigma_{\Delta Y}$, to discontinuous yield, Figure 6.6 features a clear turning point in the second derivative of stress with respect to strain as plotted against strain. This is taken to indicate the strain at yield which, as shown by the red dashes, is then used with respect to the experimental stress-strain curve to determine the yield strength of the tested material. Figure 6.6 also shows the good agreement between the novel $\sigma_{\Delta Y}$ and the standard σ_{UY}.

Next, conventional continuous yield such as that exhibited by the literature data from lattice (Figure 6.2) and porous (Figure 6.3) samples. In the same way as with discontinuous yield, Figure 6.7 and Figure 6.9 feature clear turning points in the second derivative which are used to identify the yield point as shown. Since the

default standard, σ_Y, is applicable for these cases, this is compared with the $\sigma_{\Delta Y}$ in Figure 6.8 and Figure 6.10. These comparisons make evident the non-arbitrary way in which the derivative yield criterion makes it possible to identify the first significant departure from elastic strain. Furthermore, it is evident that this is more representative of the loading response of the materials than the standard offset approximation.

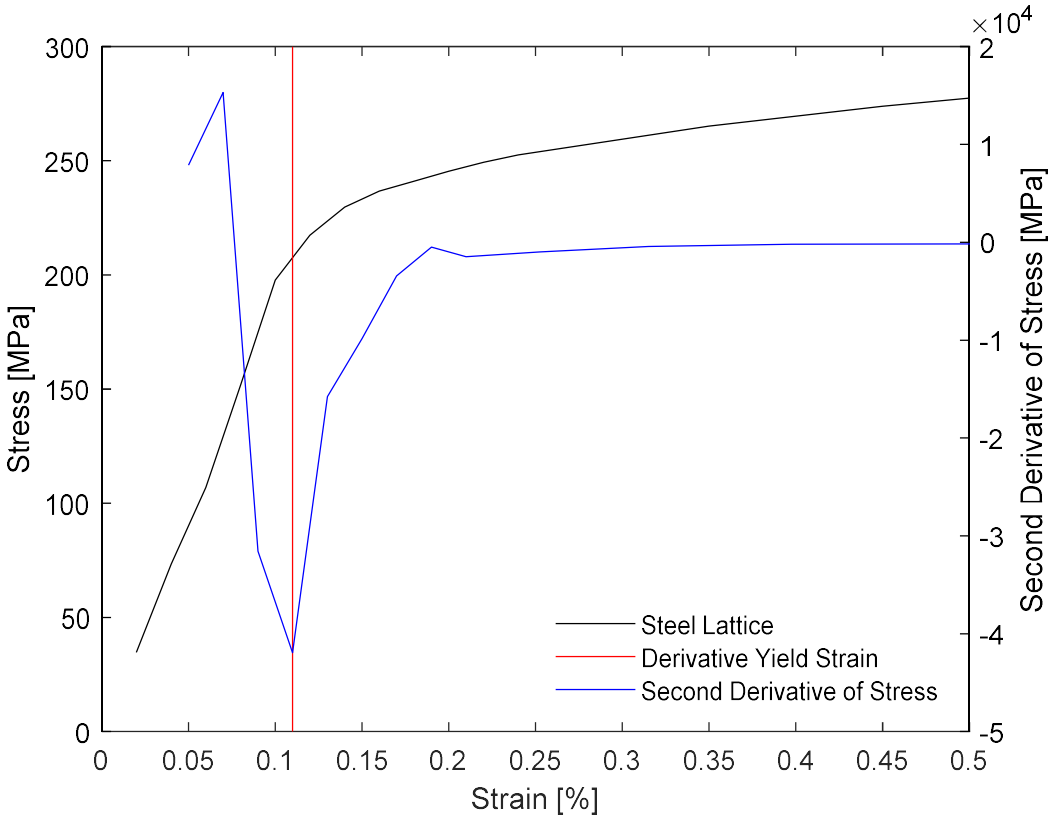

Figure 6.7 - Derivative yield as applied to the experimentally measured stress-strain curve for a steel lattice subjected to tensile loading

1530

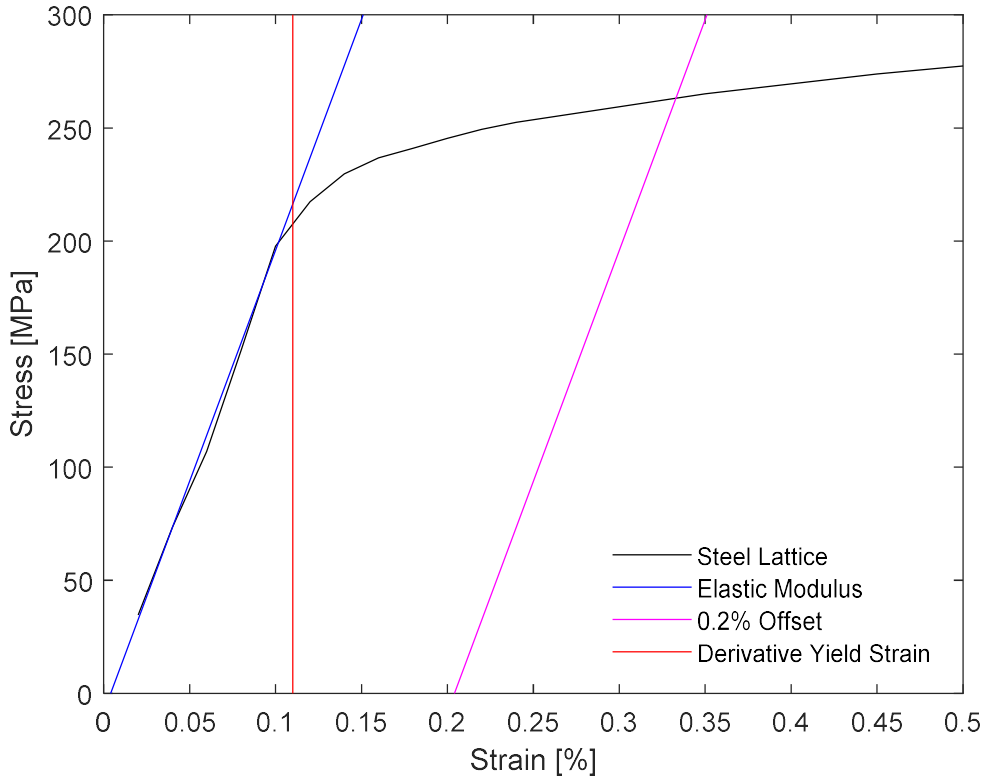

Figure 6.8 - Comparison of the results from the offset yield and the derivative yield as applied to the experimentally measured stress-strain curve for a steel lattice subjected to tensile loading

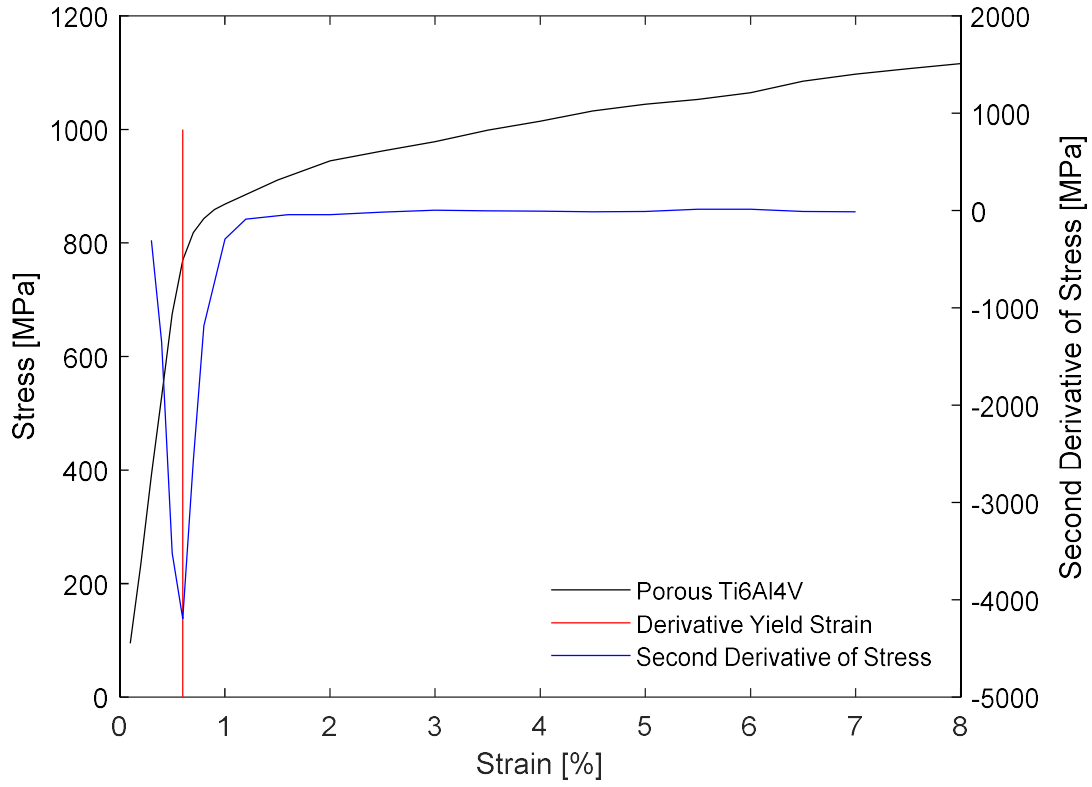

Figure 6.9 – Derivative yield as applied to the experimentally measured stress-strain curve for porous Ti_6AL_4V (porosity 7.6%) subjected to tensile loading

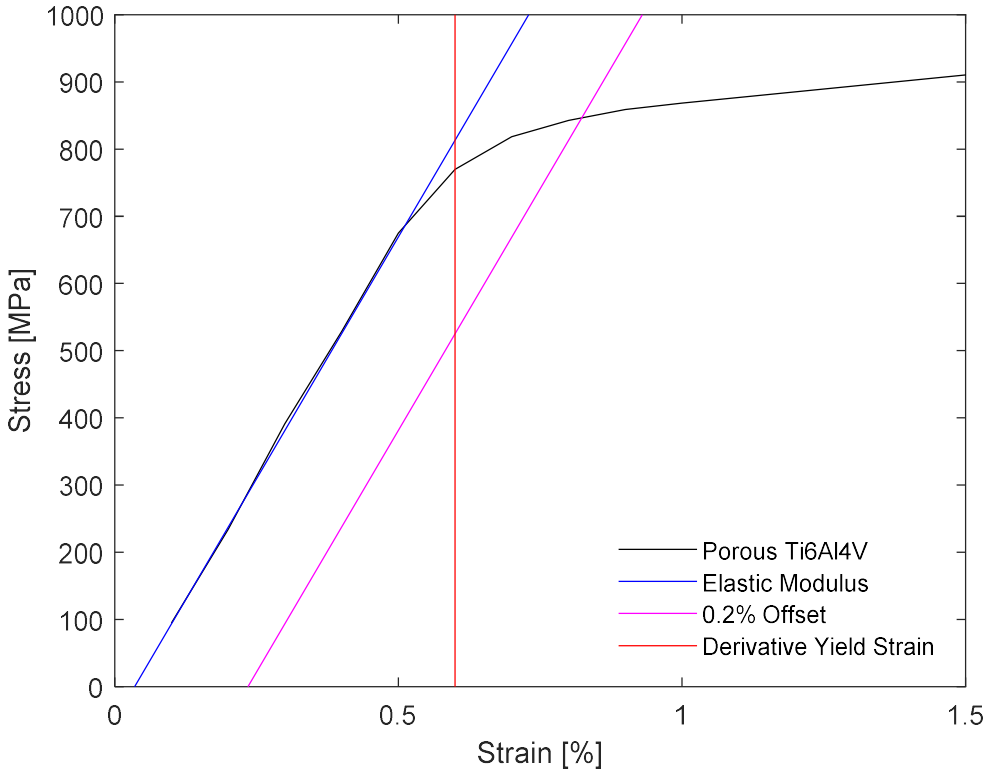

Figure 6.10 – Comparison of the results from the offset yield and the derivative yield as applied to the experimentally measured stress-strain curve for porous Ti_6AL_4V (porosity 7.6%) subjected to tensile loading

1540

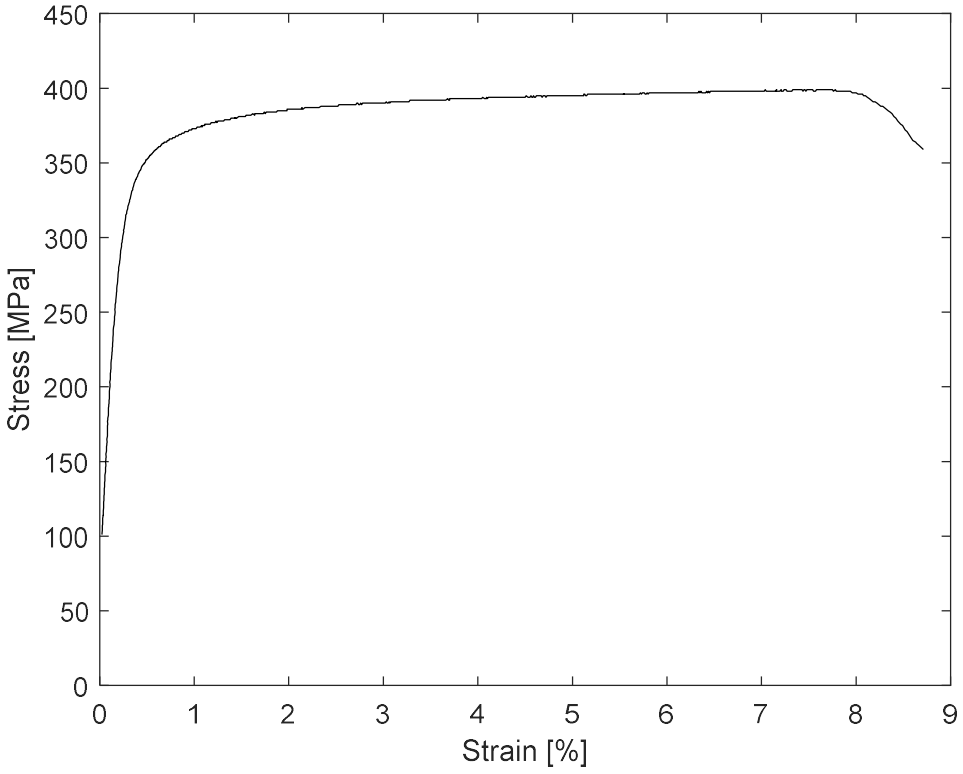

Figure 6.11 – Experimentally measured stress-strain curve for dimpled steel subjected to tensile loading

Finally, identified as a case where none of the standards strictly apply, severely continuous yield such as that exhibited by the dimpled steel tested in the present work is illustrated in Figure 6.11. The standard offset method is inapplicable due to the substantial departure from linearity prior to macroscopic yield that is characteristic of severely continuous yielding. Even so, since this is defined as the default method for the determination of yield strength, it is used here as an indicator for whether the alternative standard, σ_{EUL}, may be applicable. According to the standard offset method with an offset of 0.2%, the average strain at yield for the dimpled steel is 0.4%. However, the substantial variability (range = 0.13%) in this measure may be indicative that the σ_{EUL} is not appropriate for this case either.

Applying $\sigma_{\Delta Y}$ as shown in Figure 6.12 clearly and non-arbitrarily identifies the point of most pronounced yielding in the dimpled steel unhindered by the limitations of the σ_{EUL} and σ_Y. Furthermore, as is illustrated in Figure 6.13, the result of application of the $\sigma_{\Delta Y}$ criterion is clearly more representative of the behaviour of dimpled steel than the standard σ_Y method.

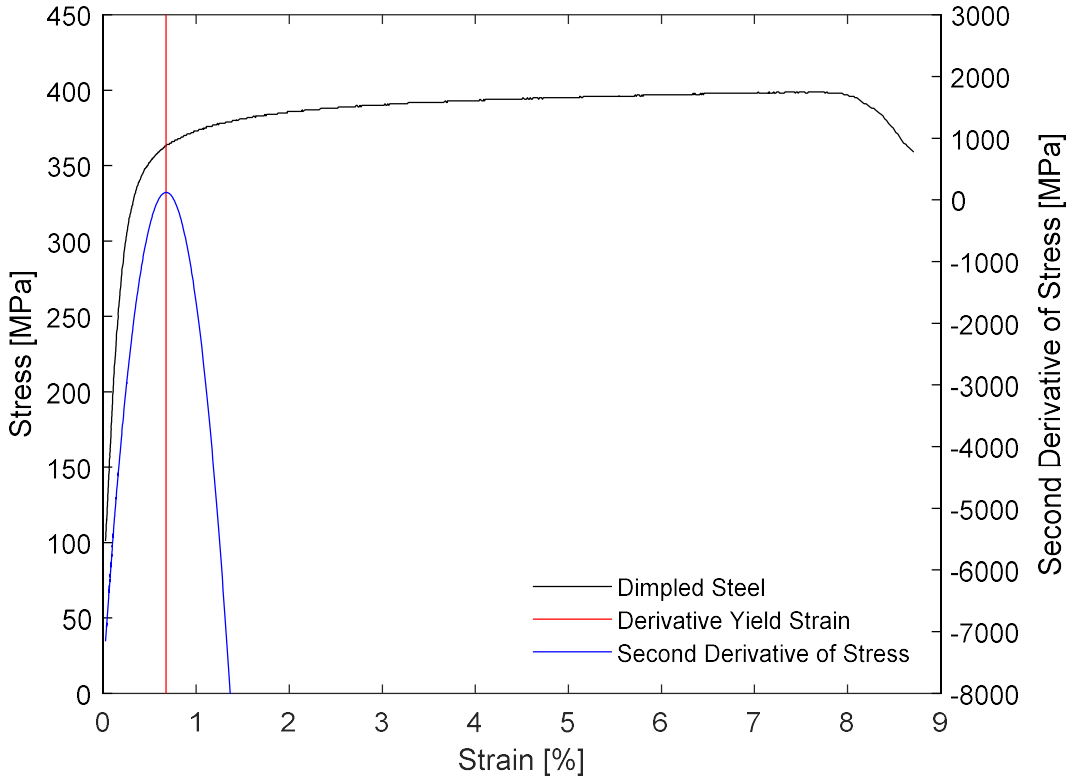

1560 *Figure 6.12 – Derivative yield as applied to a an experimentally measured stress-strain curve for dimpled steel subjected to tensile loading*

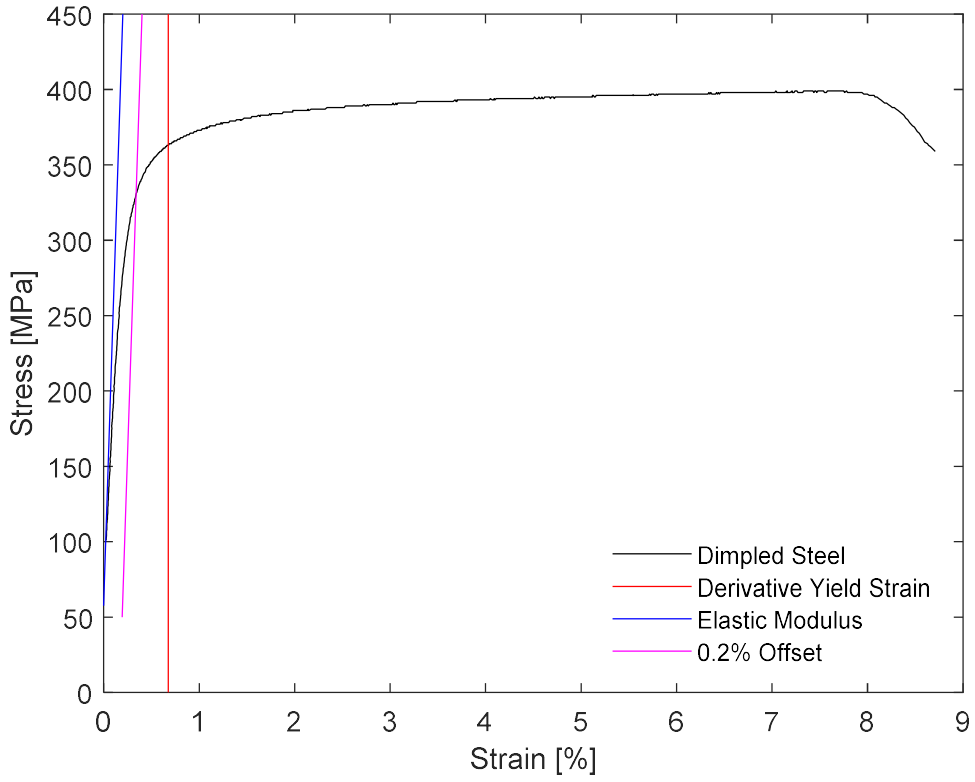

Figure 6.13 - Comparison of the results from the offset yield and the derivative yield as applied to an experimentally measures stress-strain curve for dimpled steel subjected to tensile loading

6.5 Quantification of Differences in Yield Strength

Another clear illustration of the inadequacy of current standard yield criteria when considering materials with macroscopic geometric non-uniformities arises from the need to compare the yield strength of materials exhibiting different types of yield. Measurement of the margin by which dimpled steel is stronger than the plain steel equivalent, for example, represents a comparison between discontinuous yielding and severely continuous yielding behaviours. Figure 6.14illustrates the case from the data set presented in Chapter 3 where the use of the standard measures (lower yield and 0.2% offset yield for plain and dimpled steels, respectively) indicates that the application of the UltraSTEEL® dimpling process has resulted in a negligible change to yield strength (+0.52%). It is clear from the figure however, that the material has been strengthened by a substantial margin. The red line shows that the novel derivative yield criterion also overcomes this problem. As shown, the derivative yield for the dimpled steel is substantially greater than the yield strength of the plain steel. In this case the indicated increase in yield strength due to dimpling is 12.81% according to the derivative yield as opposed to the 0.52% indicated by the standard 0.2% offset yield. Consequently, the derivative yield can be applied irrespective of yield type to produce a representative measurement of yield strength. In this way, accurate comparison of yield strengths is made relatively trivial even when the materials being compared exhibit different types of yield behaviour.

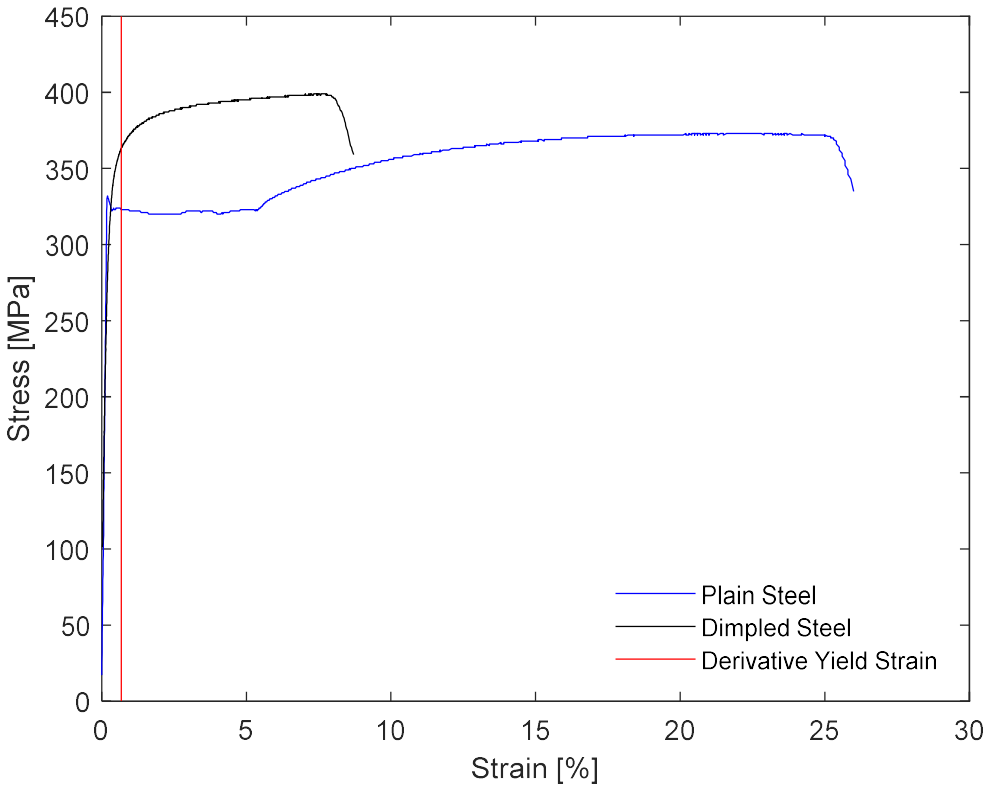

Figure 6.14 – Illustration of the derivative yield as applied to dimpled steel where standard measures indicate negligible strengthening due to the UltraSTEEL® dimpling process

6.6 Implications of Derivative Yield for Previous Results

1590 Recall, from Chapter 2 and Chapter 4 , the tensile tests conducted on plain and dimpled steel samples and the subsequent development of an expression to predict the potential strengthening of plain steel due to the application of the UltraSTEEL® dimpling process. These results were all based on the standard lower yield for plain steel and the standard 0.2% offset for dimpled steel. Therefore, the outcomes must be addressed in the context of the proposed derivative yield criterion. Note that since the predictive expression is intended for use in industry, the lower yield is still used for plain steel samples.

Table 4 - Comparison of the yield strengths and strengthening magnitudes/predictions indicated by the standard measures with the proposed derivative yield. Figures are reported in the form Mean ± SD

Dimpled Steel Yield Measure	*Standard 0.2% Offset*	*Derivative Yield*
Dimpled Yield Strength (MPa)	351 ± 21.14	374 ±22.8
Increase in Yield Strength (%)	9.93 ±4.31	17.84 ±4.27
Lüders Elongation Prediction	$Y_{inc} = -336Y_e + 21.8$	$Y_{inc} = -363Y_e + 30.7$

1600 The notable differences from the results reported in Chapter 2 and Chapter 4 are summarised in Table 4. It is evident from this that use of the derivative yield indicates a substantially greater yield strength in dimpled steel (increased by approximately 6.6%) than the 0.2% offset yield as is expected upon inspection of Figure 6.14. As a result, the indicated strengthening due to the UltraSTEEL® dimpling process is also substantially greater than with the 0.2% offset method, now with an average increase of 17.8% as opposed to 9.9%. Despite this, the two measures of strengthening exhibit approximately equal levels of variation as measured by standard deviation. The upshot of these changes is illustrated more clearly in Figure 6.15 and Figure 6.16.

1610 As an expanded version of the plot presented in Chapter 3 , Figure 6.15 shows the additional increase in the yield strength of the steel samples accounted for by the novel derivative yield criterion. Furthermore, the similarity of the spread in results for dimpled steel using the standard measure and the novel criterion indicated by the standard deviations is clear in this plot.

It is clear in Figure 6.16 that the nature of the predictive model remains largely unchanged, featuring a marginal change to the coefficient and an increased constant

to account for the increased yield values. Notably, the coefficient of determination, R^2, for the predictive model based on the derivative yield ($R^2 = 0.76$) is greater than that based on the standard 0.2% offset yield ($R^2 = 0.64$). The relationship between strengthening and Lüders elongation was determined in Chapter 4 to be a result of the initial microstructure of the material and the changes thereto. Therefore, this increased value for R^2 may serve to further support the validity of the derivative yield criterion as a measure that is more representative of the behaviour of materials incorporating macroscopic geometric non-uniformities.

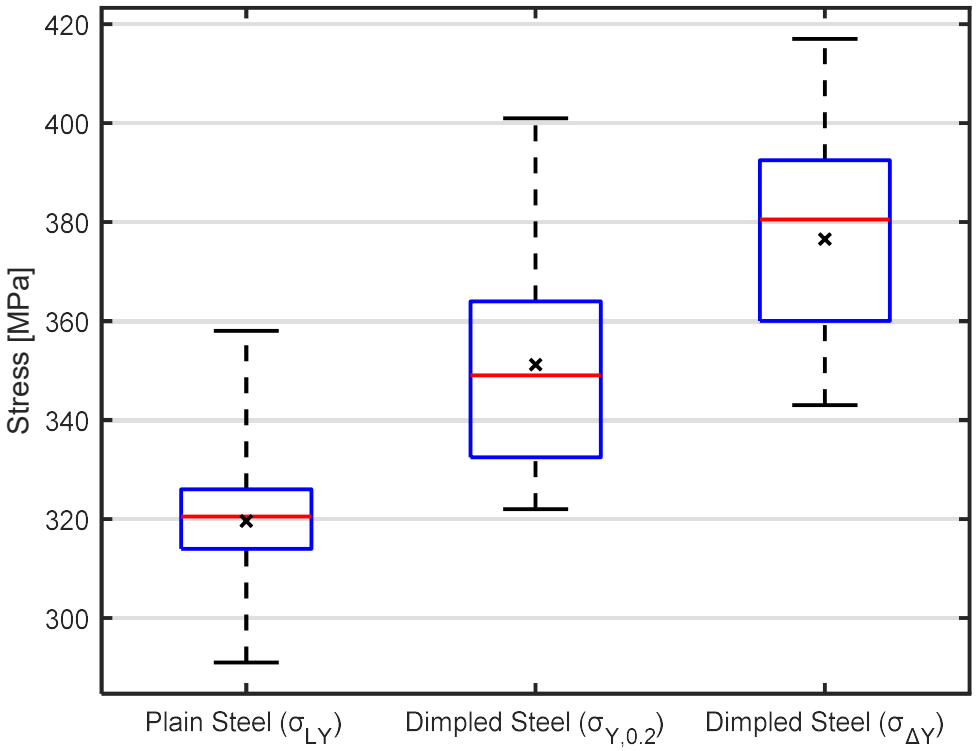

Figure 6.15 - Boxplots illustrating the effect of the UltraSTEEL® dimpling process on the yield strength of the steel samples using the novel derivative yield criterion for dimpled steel alongside the standard measures for yield strength.

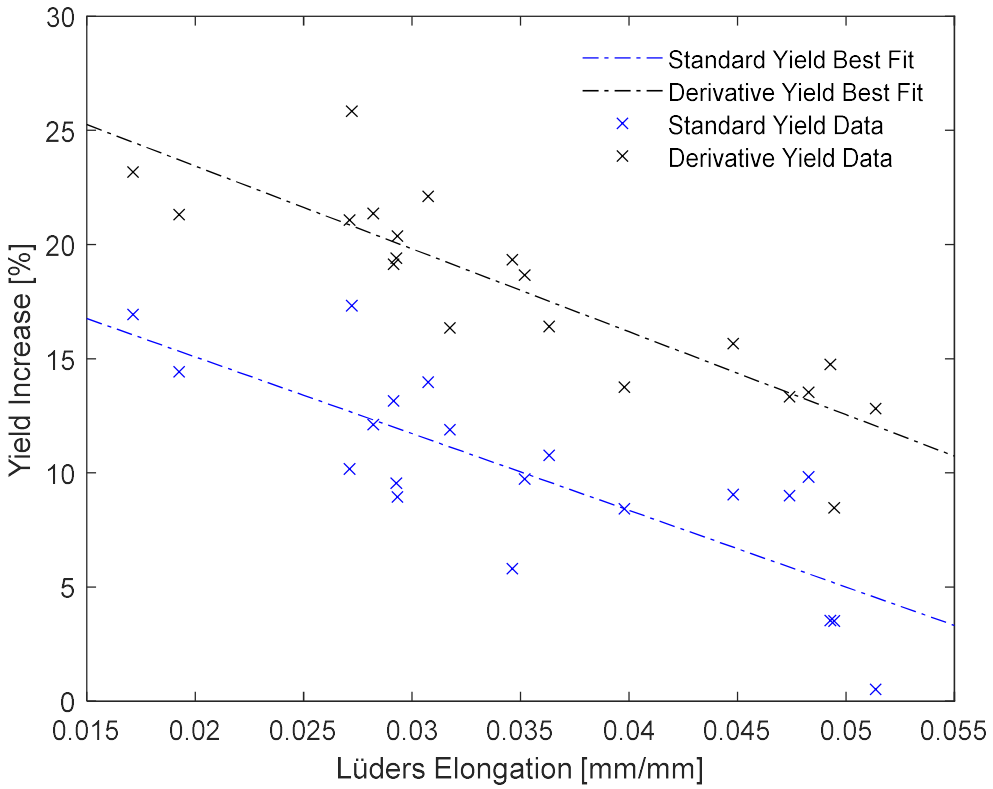

Figure 6.16 – Comparison of the trends between the yield strength increase and the Lüders elongation exhibited in the plain steel where the yield strength increase is calculated using either lower yield and offset yield or lower yield and derivative yield.

6.7 Summary

The standard methods for the measurement of yield as defined by the ASTM [41, 44] and BSI [12, 116] have been presented in summary and the limitations of their application noted. In doing so, it was observed that the selection of the appropriate standard measure for yield first requires a qualitative assessment and categorisation of the nature of the yielding present which is not necessarily clear. Additionally, it was noted that the use of multiple, conflicting measures for yield confuses the matter of comparing yield strengths.

It was observed that the literature regarding yield criteria features a trend towards tailored yield criteria for individual cases, leaving the need for a broadly applicable

yield criterion unaddressed. Noting that macroscopic yield manifests graphically as a localised change in the tangent modulus, a novel criterion based on the second derivative of stress with respect to strain was proposed. This is referred to here as the 'derivative yield'.

This criterion was applied alongside the appropriate standards to cases exhibiting discontinuous (plain steel), continuous (steel lattice and porous Ti_6Al_4V), and severely continuous (dimpled steel) yield behaviours. 'Severely' is used here to distinguish cases featuring a substantial departure from linearity in the stress-strain curve prior to macroscopic yield. In this way, it has been shown that the novel criterion is in good agreement with the standard upper yield for discontinuous yielding. Similarly, derivative yield non-arbitrarily identifies the point of first substantial departure from linearity for continuous yielding, shown to be a more representative measure than the offset approximation. Additionally, the derivative yield identifies a yield point for severely continuous yielding that is clearly more representative of the loading response than the result produced by the standard offset method. Furthermore, it has been shown that the applicability of the novel derivative yield independent of yield behaviour results in a more accurate comparison of strengths for materials exhibiting different types of yield behaviour.

The implications of the use of derivative yield in place of the standard offset yield on the results from Chapter 3 and Chapter 4 have been discussed.

Chapter 7 Finite Element Modelling of the Dimpling Process to Explore Novel Dimple Tooling Geometries

7.1 Introduction

The dimpling process, preceding cold roll forming, improves the mechanical properties of the product. As has been discussed in previous chapters, this is achieved through a combination of strain hardening, grain boundary strengthening, and geometric changes. The previous chapters have considered only the current standard dimple geometry (tooth profile), UltraSTEEL 3®, which features a spherical contact geometry. However, UltraSTEEL® has, to date, been in production using 3 distinct dimple geometries (US1, US2, and US3). Few other tooth profiles have been assessed as possible improvements on the past and present geometries. Therefore, this chapter will seek to evaluate the potential benefits regarding the strengthening of processed materials for several novel tooth profiles to provide targeted design improvements based on current understanding of the strengthening mechanisms at work. Ranging from minor adjustments to major redesigns, these novel profiles are assessed alongside the UltraSTEEL 3® profile in simulation to provide a comparison with the current standard.

7.2 Finite Element Simulation Setup

In preliminary testing, it was found that Nguyen-style models, while useful for simulating the UltraSTEEL® dimpling process as it is currently applied in industry, do not exhibit the flexibility required to reliably predict the yield stress for different tooth geometries and configurations. Therefore, a Collins-style model is applied here, using plastic strain distributions as an indication of local strengthening. To

facilitate clear illustrations of strain distributions, a dimple-centred unit cell geometry similar to that used by Nguyen *et al* [14] and illustrated in Figure 7.1 is used. The square base representing the dimpling rolls has a side length equal to the tooth pitch, spanning from dimple centre to dimple centre. Thus, the size of the
1690 geometry in the XZ plane is dependent on the dimple tooth geometry and configuration. The steel plate is similarly defined but with a sheet thickness of 0.5mm in all cases.

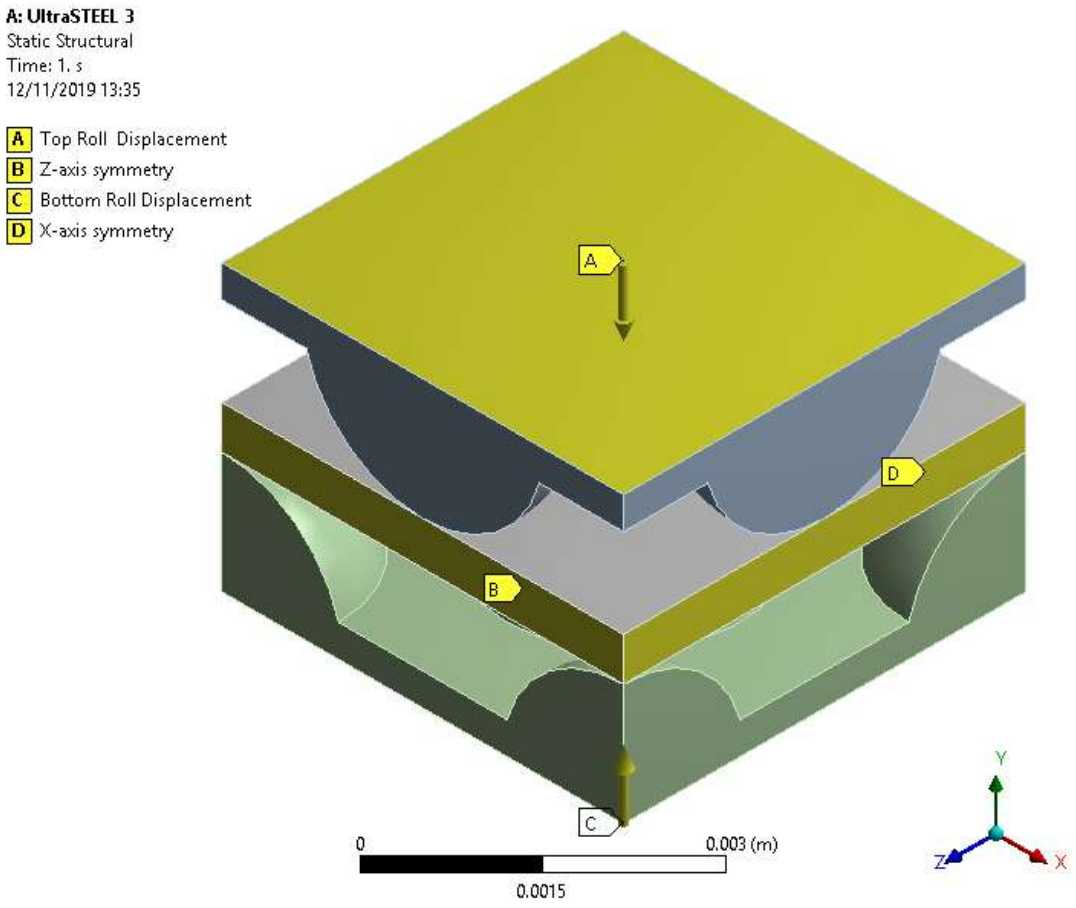

Figure 7.1 – Illustration of the Collins-style FE model and boundary conditions used to simulate the dimpling process in the present study

A bilinear isotropic material model similar to that presented in Chapter 5 and based on the data presented in Chapter 3 is applied here. This model is characterised as

follows: elastic modulus, 205 GPa; Poisson ratio, 0.3; density, 7810 kgm^{-3}; coefficient of friction, 0.3; yield stress, 320 MPa; tangent modulus, 876 MPa.

This material model is applied to the steel plate while both dimpling rolls are treated as rigid. As shown in Figure 7.1, the 'steel plate' is constrained with normal-direction symmetry conditions (zero displacement normal to the face) along the 4 vertical faces. The loading is applied as opposing vertical displacements of the blocks representing the forming rolls as indicated by 'A' and 'C' in Figure 7.1. These displacements result in a total forming depth of 0.5mm, equal to the sheet thickness, to conform with the standard double-depth forming as applied in industry [34, 37]. These simulations incorporate large deformation formulation.

7.3 Novel Profile Design Criteria

Similar to the study by Collins *et al* [13], both the plastic strain and material thinning will be considered. Thinning is simply a measure of the local reduction in thickness of the steel sheet due to the dimpling process and is measured as a percentage reduction from the specified gauge at the point of contact between the steel plate and the dimple teeth. This is a negative side-effect of the dimpling process as a reduction in the cross-sectional area of the steel amounts to a stress concentration due to non-uniform geometry that adversely affects the structural performance of dimpled steel. However, thinning is more relevant when considering tooth profiles with corners as compared with those employing curves instead since corners produce greater thinning. Therefore, since only curved geometries are considered here, the focus will be on plastic strain.

It has been discussed in previous sections that there is a strong relationship between plastic strain and material strengthening. Generally, increased plastic strain equates

to increased strengthening. Therefore, the plastic strain should be maximised. However, clearly excessive plastic strains result in material failure. Where this occurs during forming, this is referred to here as 'material pre-failure' since the forming results in localised regions of material failure, diminishing the mechanical performance of the product. Therefore, a maximum plastic strain will be imposed, the magnitude of which is based on the tensile data presented in Chapter 3 . The average strain to tensile strength of plain steel in this dataset is approximately 20% therefore, this will be used as an assumed maximum peak strain.

The upshot of these limiting points is that the minimum plastic strain should be maximised without resulting in the maximum plastic strain exceeding the pre-failure strain, 20%.

Additional considerations include any material thinning resulting from forming and the ease of alignment of the opposing tooth rolls in application. Since thinning results in geometric stress concentrations, it should be minimised.

7.4 Single-Form Dimple Tooth Profiles

Current understanding of the geometric effects of the tooth profiles on the plastic strains can be summarised as follows.

- Sharp edges
    - Result in increased peak plastic strains
    - Encourage grain size refinement
- Wide curves
    - Result in more uniform plastic strain distributions
    - Prevent excessive stress concentrations

Since these are all desirable, within the limitations discussed in the previous section, it is necessary to develop a satisfactory trade-off between edged and curved geometries. To this end, Figure 7.2 illustrates the novel single-form profiles considered in these simulations. These are referred to descriptively here as the 'plateau', and 'cross' profiles. These are profiles where, as has been the standard for the production profiles to date, a single tooth profile is used for the entire dimpled section. As shown, a spherical geometry equivalent to the UltraSTEEL 3® profile is also included. This is to provide a consistent basis for comparison with the simulated results pertaining to the application of novel tooth profiles. An ellipsoid profile has also been included for comparison.

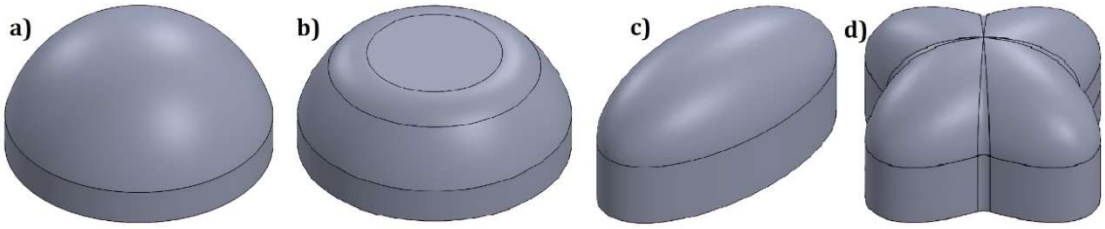

Figure 7.2 - Single-form dimple tooth profiles: a) US3®; b) Plateau; c) Ellipsoid; d) Cross

Figure 7.3 below illustrates the percentage of cells in the steel plate that experience more than a given level of plastic strain for each profile. At a glance, these strain distributions appear to suggest that all 3 novel geometries represent an improvement over UltraSTEEL 3®. This is because these curves all exhibit increased plastic strain at all levels compared to UltraSTEEL 3®. However, both the ellipsoid and the plateau profiles notably exceed the maximum peak strain. As illustrated by the grey bands in Figure 7.5 and Figure 7.6, this results in large regions of the material likely undergoing pre-failure. In the case of the ellipsoid profile, this is contained along the surface of the formed sample, as is the case for UltraSTEEL 3® (Figure 7.4), and may therefore minimally impact the performance of the dimpled

material under load. However, these pre-failure regions exist as full through-thickness bands in the case of the plateau profile, suggesting substantial damage to the material due to forming.

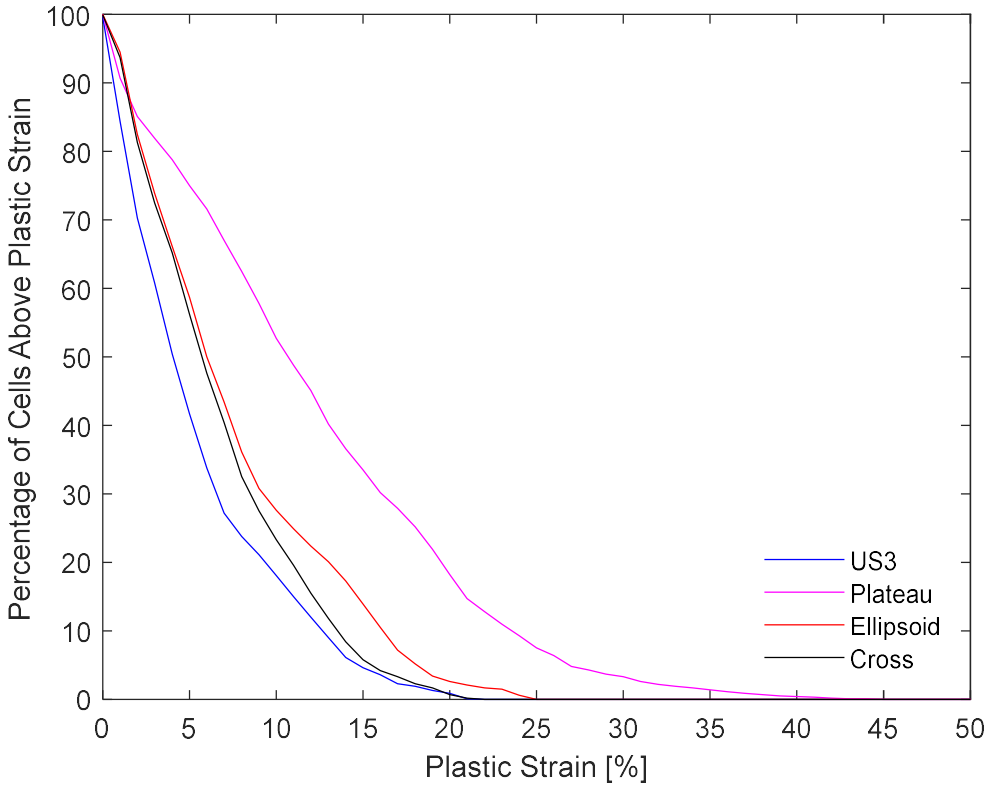

1770

Figure 7.3 - Plastic strain distribution curves for novel single-form tooth profiles compared to the standard UltraSTEEL 3®

The cross profile on the other hand, achieved a substantial increase to plastic strain for approximately 90% of the sample, as illustrated in Figure 7.3, with only a minor increase to the peak plastic strain (22%, as opposed to 21% for UltraSTEEL 3®). Despite this small increase in peak plastic strain, comparison of Figure 7.4 and Figure 7.7 indicates that the regions exceeding the maximum peak strain are notably smaller for the cross profile than for UltraSTEEL 3®.

Table 5 - Material thinning in simulation due to single-form novel tooth profiles

Profile	*US3*	*Plateau*	*Ellipsoid*	*Cross*
Thinning (%)	5.98	2.31	8.45	6.20

1780

Assessed at the maximum amplitude of the relevant dimples, the material thinning relating to each of these profiles is detailed in Table 5. Interestingly, this measure indicates that the plateau profile is superior to the others. However, this is a deceptive indication resulting from the same large flat surfaces that also result in the large areas of near-zero plastic strain illustrated in Figure 7.5. Most importantly, there is a negligible thinning difference (0.22%) between the UltraSTEEL 3® profile and the cross profile despite the notable improvement to plastic strain offered by the cross profile.

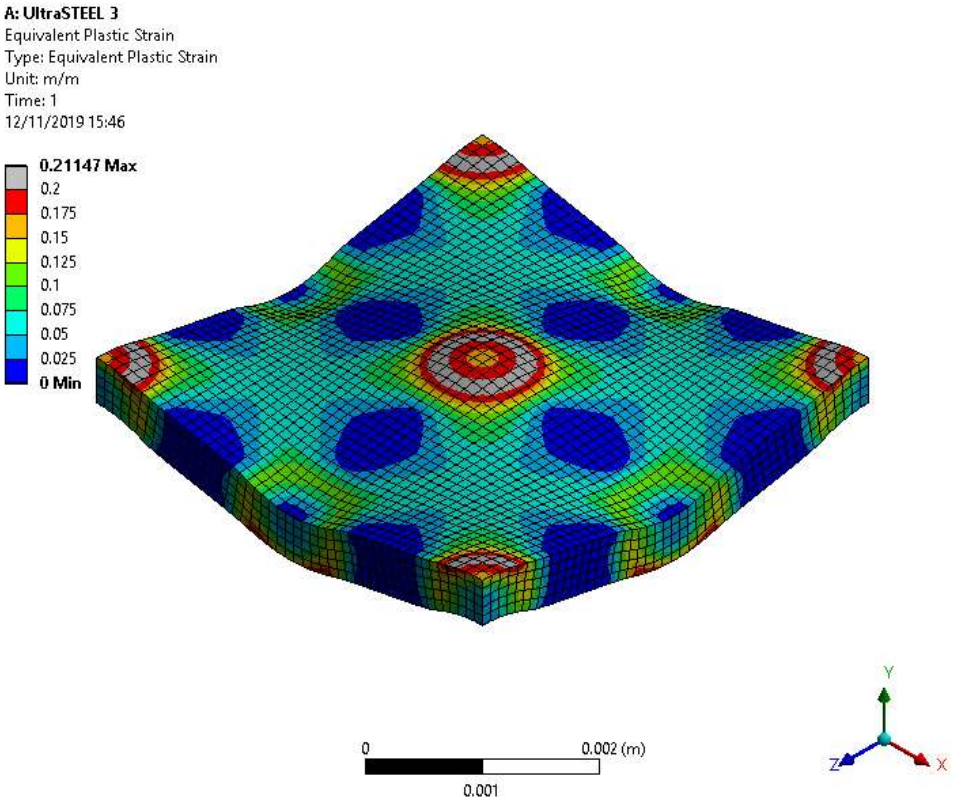

1790 *Figure 7.4 – Simulated plastic strain contour for UltraSTEEL 3®*

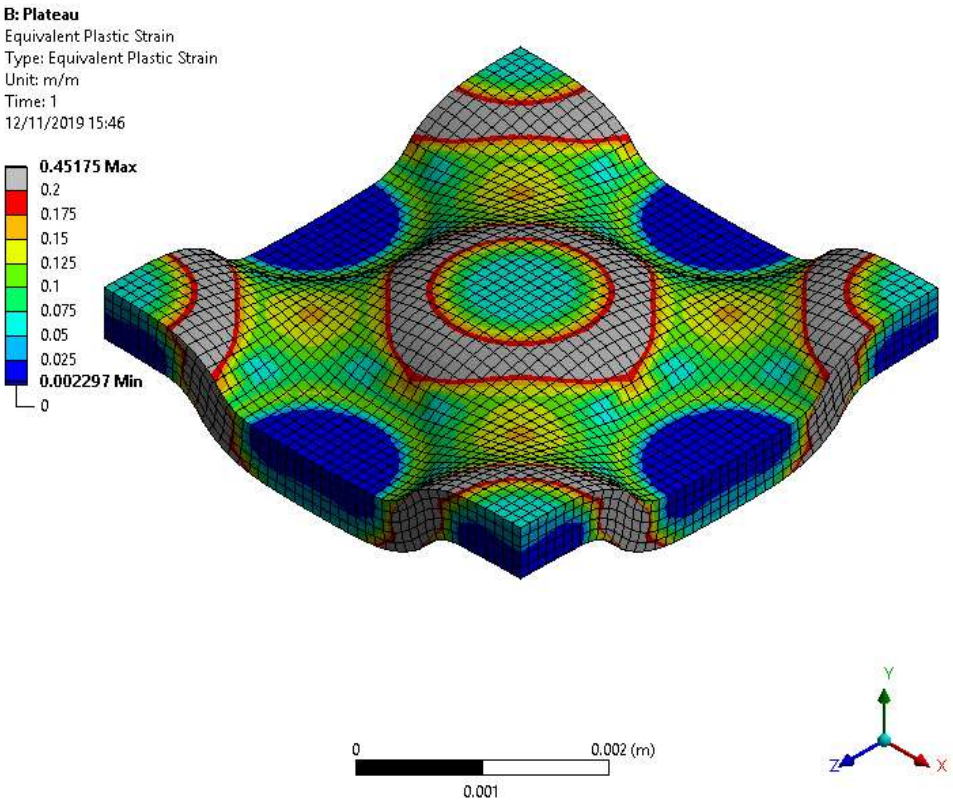

Figure 7.5 - Simulated plastic strain contour for the novel plateau profile

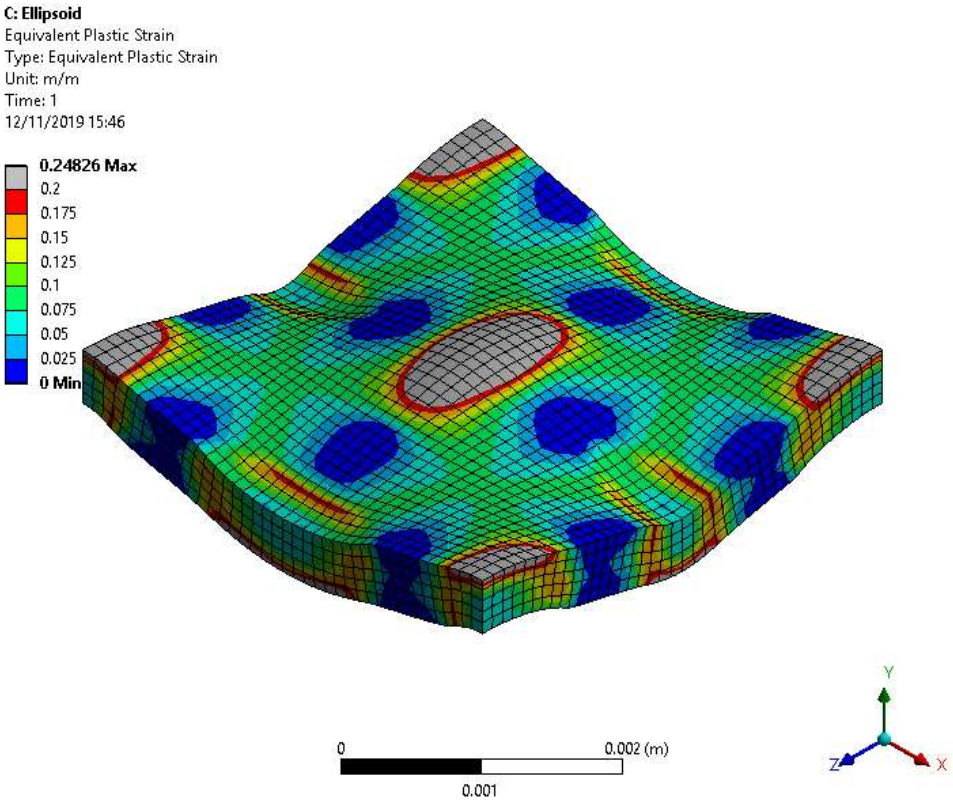

Figure 7.6 - Simulated plastic strain contour for an ellipsoid profile

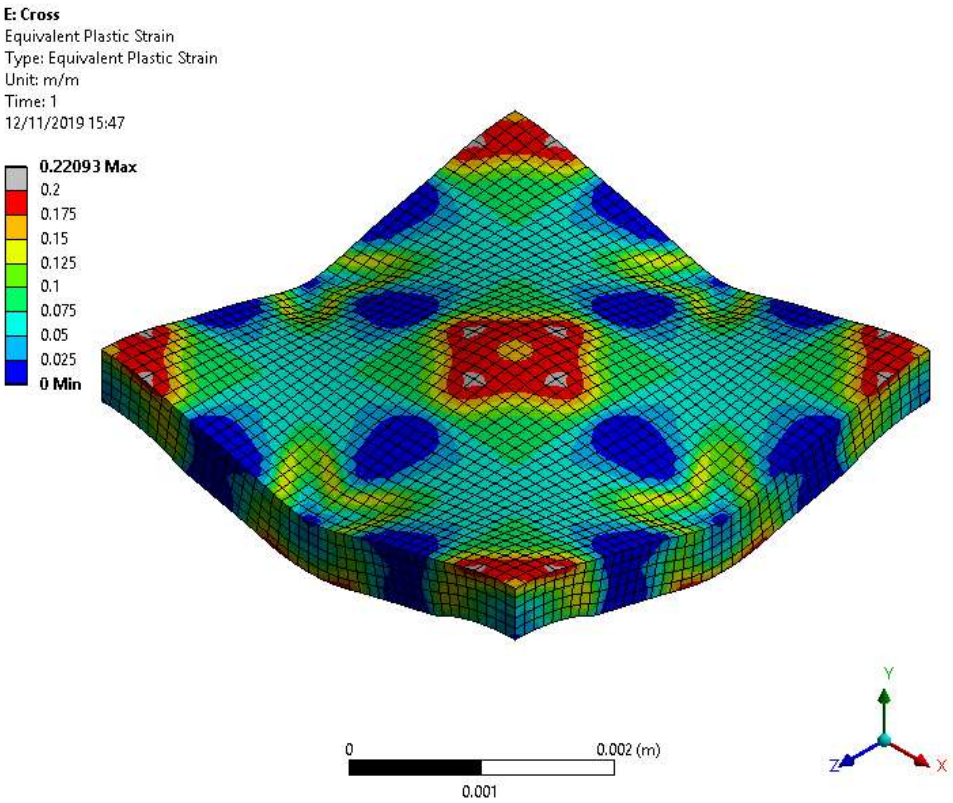

Figure 7.7 - Simulated plastic strain contour for the novel cross profile

7.5 Multi-Form Dimple Tooth Profiles

In addition to the traditional single-form profiles in the previous section, the possibility of multi-form profiles has been explored briefly. Two combination profiles have been considered here. Firstly, a tessellation motivated geometry was produced. The combination of the cross profile and a squared version of the plateau profile, as illustrated in Figure 7.8, should result in a more consistent inter-dimple region, effecting an increase in the proportion of the material undergoing plastic strain. While it should be no more difficult to align the top and bottom roll, in practice, than it is for the UltraSTEEL 3® profile, this profile may be more sensitive to deviation from the optimal alignment.

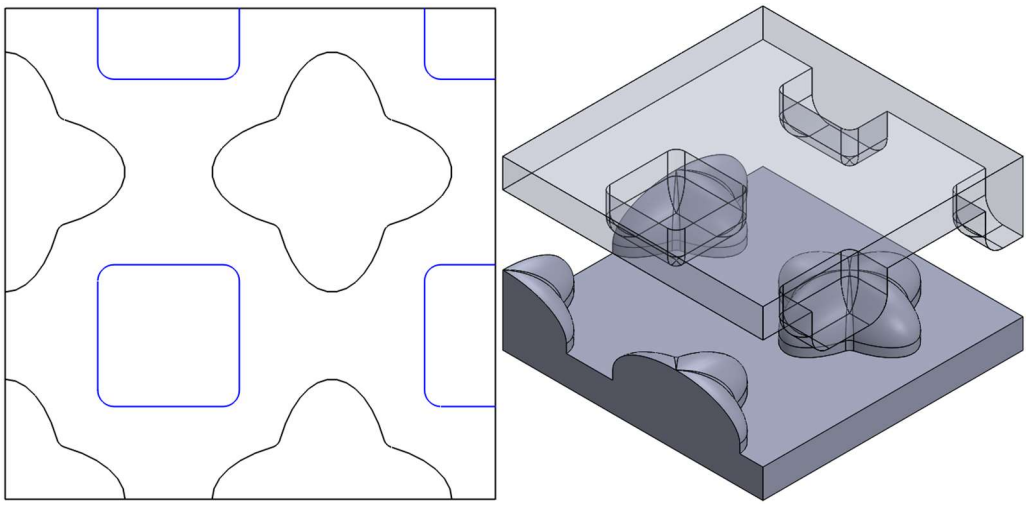

Figure 7.8 - Footprint and forming roll unit cell for the cross + plateau profile

Secondly, a nested geometry was produced. This profile, illustrated in Figure 7.9, sought to minimise the extent of the inter-dimple region while maximising the percentage of the material that is curved post-dimpling. In effect, this is a modification to the plateau profile to eliminate the large low-strain region introduced by the plateau itself. This should increase the proportion of highly strained material while trying to minimally impact the peak strain. To this end, a larger radius is used for the dimples than is used for the donuts. This is to mitigate the effects of the large shear strains present in this region on peak plastic strain. It is worth noting that this profile would likely result in an increased difficulty aligning the forming rolls and be more sensitive to misalignment than the current UltraSTEEL 3® profile.

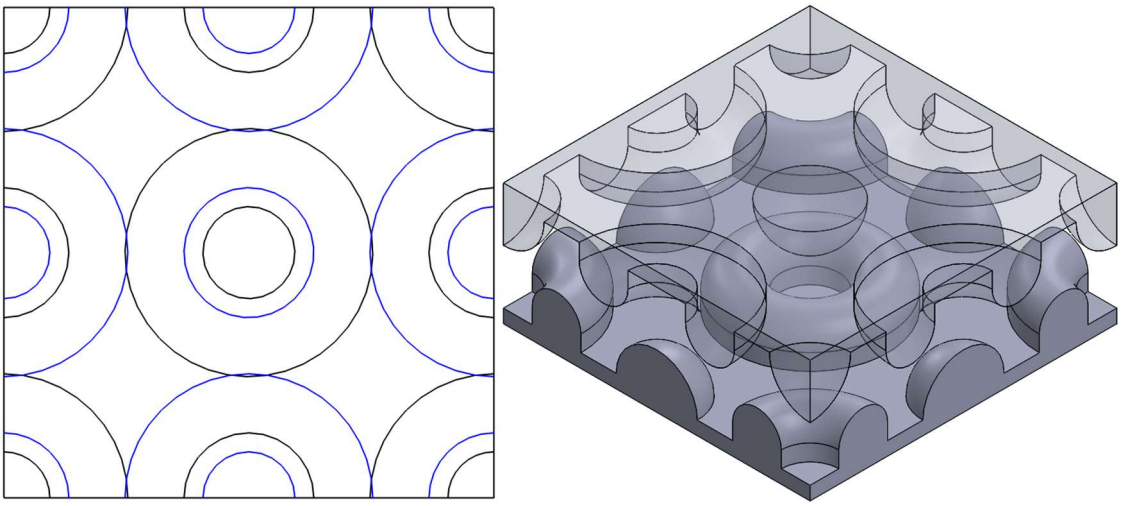

Figure 7.9 - Footprint and forming roll unit cell for the nested donut + dimple profile

The plastic strain distributions produced by the two multi-form profiles are illustrated in comparison with UltraSTEEL 3® in Figure 7.10. It is evident from this that the nested donut + dimple profile resulted in minimal strain increases for most of the material and succeeded only in increasing the peak plastic strain above the 20% limit. Conversely, and as expected, the cross + plateau combination results in a substantial increase to the proportion of highly strained material. However, this is accompanied by an increase to the peak plastic strain to match that of the donut + dimple profile.

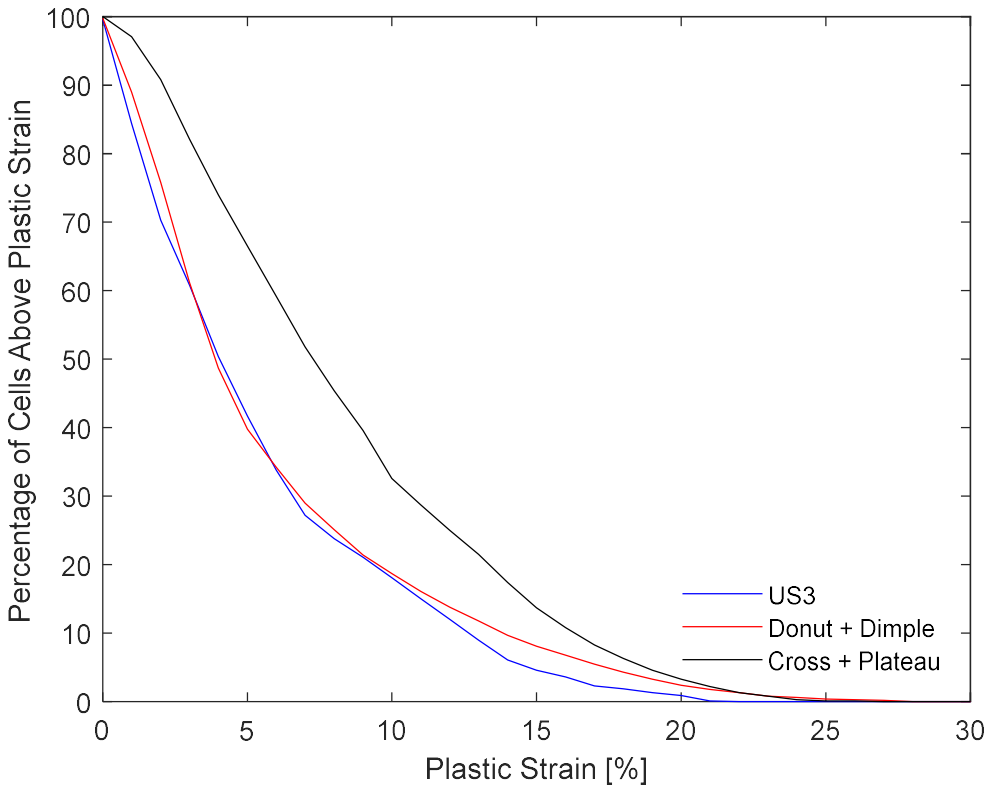

Figure 7.10 - Plastic strain distribution curves for novel multi-form tooth profiles compared to the standard UltraSTEEL 3®

In the case of the cross + plateau profile, the greatest thinning was observed at the peak of the cross. This is likely due to the sharper curves of the plateau offsetting the effect of shear stresses in the plateau region. This maximum thinning, detailed in Table 6, was found to be greater than that exhibited by UltraSTEEL 3® but only by a relatively small margin. Improving on this, the donut + dimple profile results in approximately the same level of thinning as UltraSTEEL 3®.

Table 6 - Material thinning in simulation due to multi-form novel tooth profiles

Profile	*US3*	*Cross + Plateau*	*Donut + Dimple*
Thinning (%)	5.98	6.49	6.00

Figure 7.11 more clearly illustrates the increased magnitude of plastic strain for most of the material compared to UltraSTEEL 3®. This also reveals however, that combination of the cross + plateau profile results in a substantial increase to both the peak plastic strain and the size of the regions exceeding the maximum peak plastic strain compared to the cross profile alone. These regions of excessive plastic strain, much like UltraSTEEL 3®, are however limited to the material surface and may therefore not substantially impact the loading response of a dimpled sample.

Inspection of Figure 7.12 reveals that although the donut + dimple profile results in approximately the same maximum plastic strain as the cross + plateau profile, the regions exceeding the maximum acceptable plastic strain permeate much of the material thickness. This indicates an increased likelihood of a sub-optimal loading response.

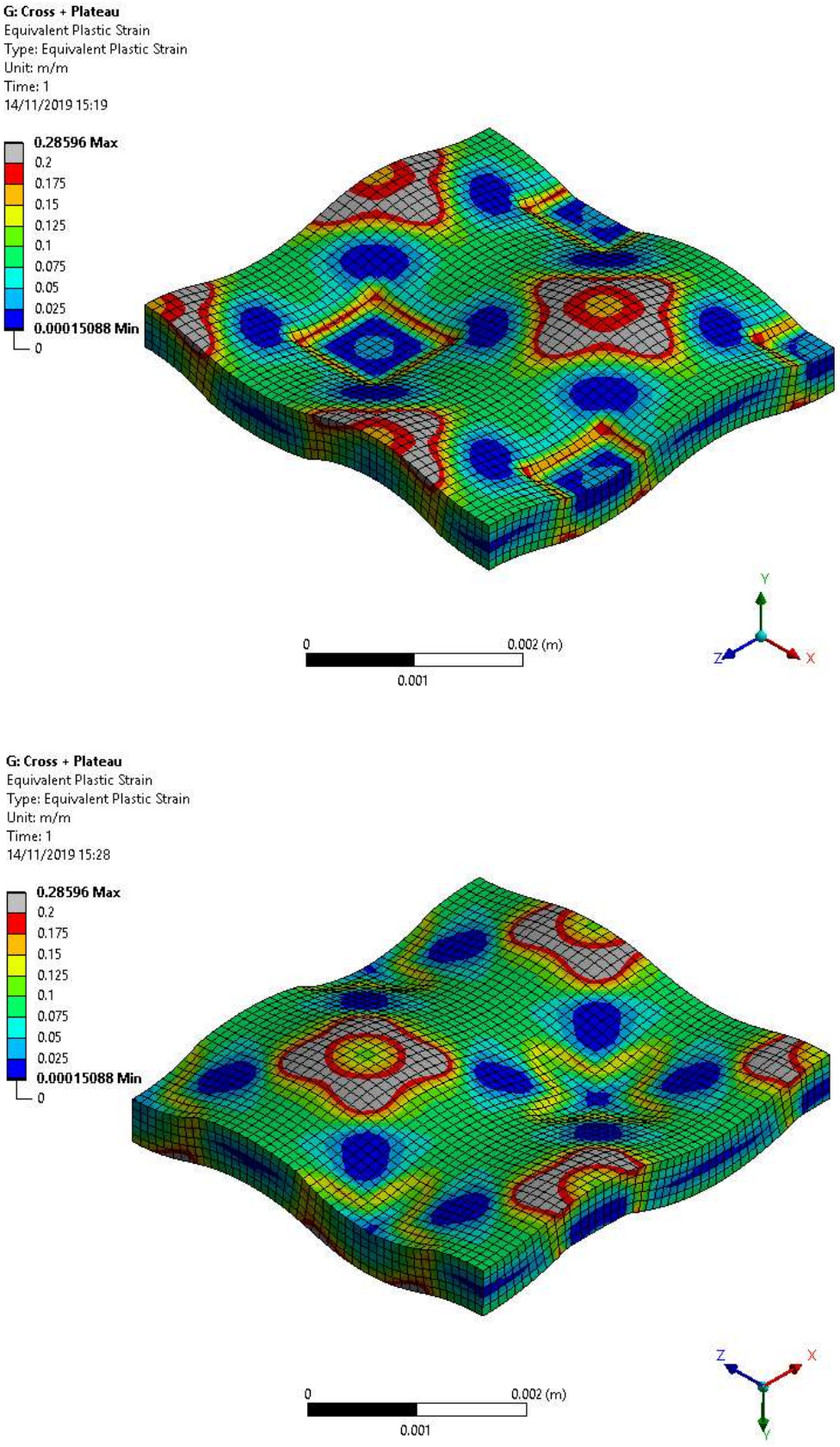

Figure 7.11 - Simulated plastic strain contour for the novel cross + plateau profile (top: isometric view, bottom: inverted isometric view)

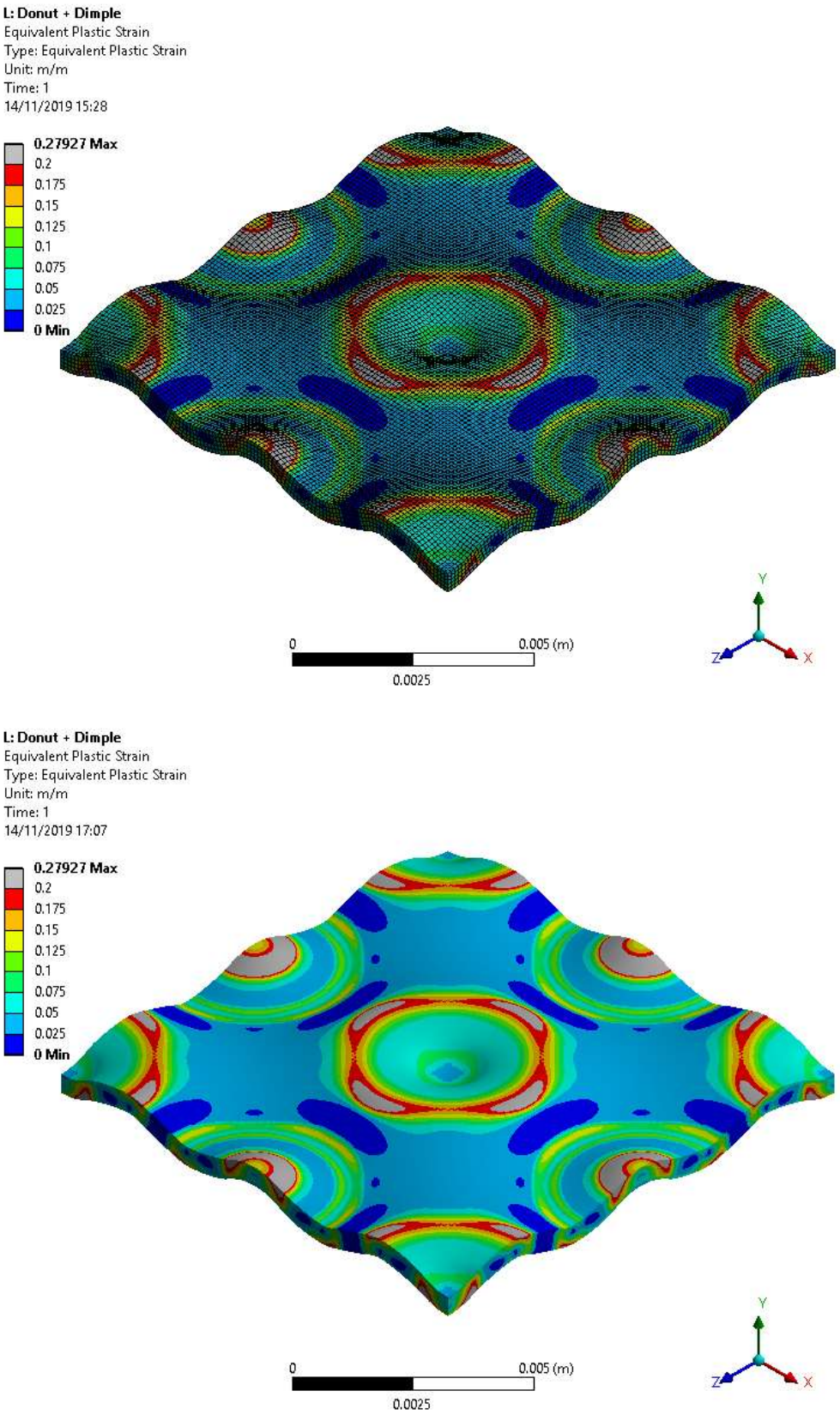

Figure 7.12 - Simulated plastic strain contour for the novel donut + dimple profile (top: with wireframe, bottom: without wireframe)

7.6 Proposed Profile

The observations from the previous sections are summarised in Table 7 below. Both the plateau and donut + dimple profiles can be disqualified for implementation due solely to the extent of the regions of excessive plastic strain developed. The ellipsoid profile, while developing regions of excessive plastic strain somewhat similar to those due to the UltraSTEEL 3® profile, results in the greatest thinning of the profiles considered. The most promising of the remaining profiles is the cross profile. This was found to exhibit almost no excessive plastic strain while increasing the desirable plastic strain across approximately 90% of the sample. This was achieved with only a minor increase to thinning.

Table 7 - Summary of plastic strains and thinning due to single-form and multi-form profiles

Profile	*Regions of excessive plastic strain*	*Thinning (%)*
UltraSTEEL 3®	Surface of dimple peak	5.98
Plateau	Through-thickness at plateau edges	2.31
Ellipsoid	Surface of dimple peak	8.45
Cross	Partial surface of dimple peak	6.20
Cross + Plateau	Surface of dimple peaks (both profiles)	6.49
Donut + Dimple	Partial through-thickness at dimple peak	6.00

Comparison of the results for the UltraSTEEL 3®, ellipsoid, and cross profiles indicates that it is the ellipsoidal nature of the cross profile that effects the increased plastic strain across much of the material, particularly the inter-dimple region. The

use of multiple ellipsoids in a cross formation appears to be what counteracts the increased maximum plastic strain exhibited by the ellipsoid profile. Therefore, a 'star' profile is proposed and is illustrated in Figure 7.13. It is expected that the addition of another ellipsoid in the cross style should reduce the maximum plastic strain to acceptable levels while maintaining much of the desirable increased plastic strain seen in the case of the cross profile. Additionally, since the cross exhibits less thinning than the ellipsoid profile, the star may similarly improve upon this value.

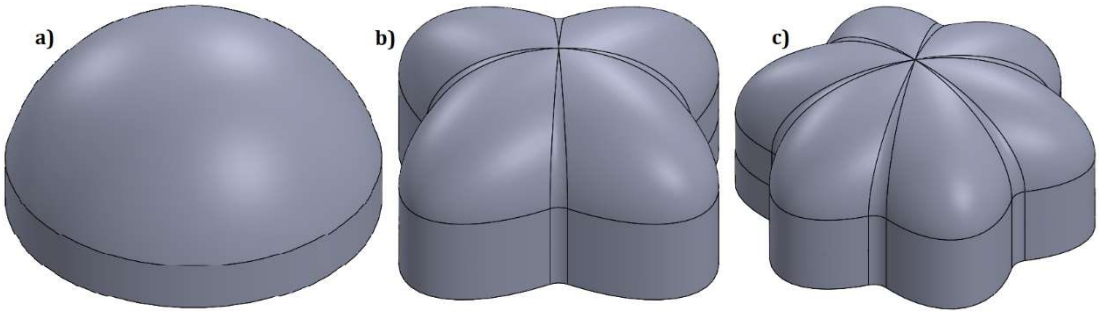

Figure 7.13 – Illustration of promising dimple tooth profiles: a) US3®; b) Cross; c) Star

Figure 7.14 indicates that the star profile successfully maintains much of the increased plastic strain achieved by the cross profile with some further improvement over approximately 50% of the material. However, this is at the cost of a small decrease in the proportion of the material formed to plastic strains greater than 11%.

As detailed in Table 8 the star profile not only improves upon the thinning exhibited by the cross profile, it results in an improvement of 0.36% compared to UltraSTEEL 3®.

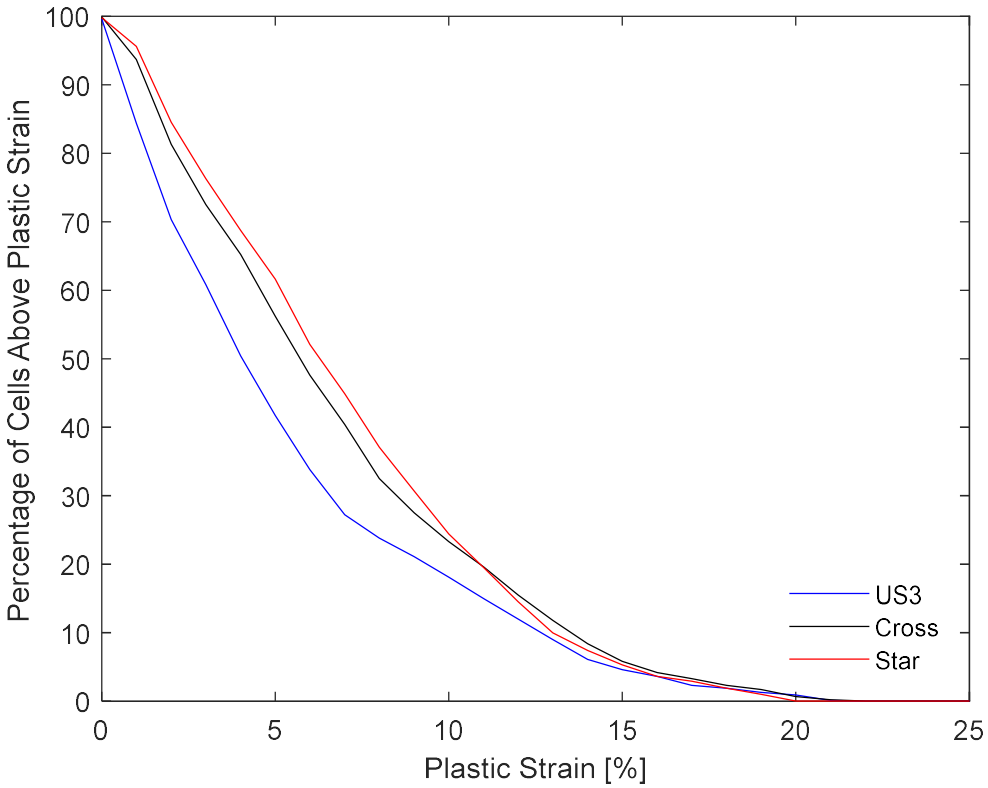

Figure 7.14 - Plastic strain distribution curves for the cross and star profiles compared to the standard UltraSTEEL 3® profile

Table 8 - Material thinning in simulation due to the cross and star tooth profiles

Profile	*US3*	*Cross*	*Star*
Thinning (%)	5.98	6.20	5.62

Illustrated in Figure 7.17, as compared to Figure 7.15 and Figure 7.16, the cross profile exhibits the usual trends in strain distribution. The maximum strain is achieved in a ring surrounding the dimple peak with minimums found in the inter-dimple region. Notably, the regions of maximum strain are larger, and the regions of minimum strain are smaller for the star profile than for either the UltraSTEEL 3® or cross profiles. Furthermore, the regions exceeding the 20% maximum plastic strain have been all but eliminated in the case of the cross profile.

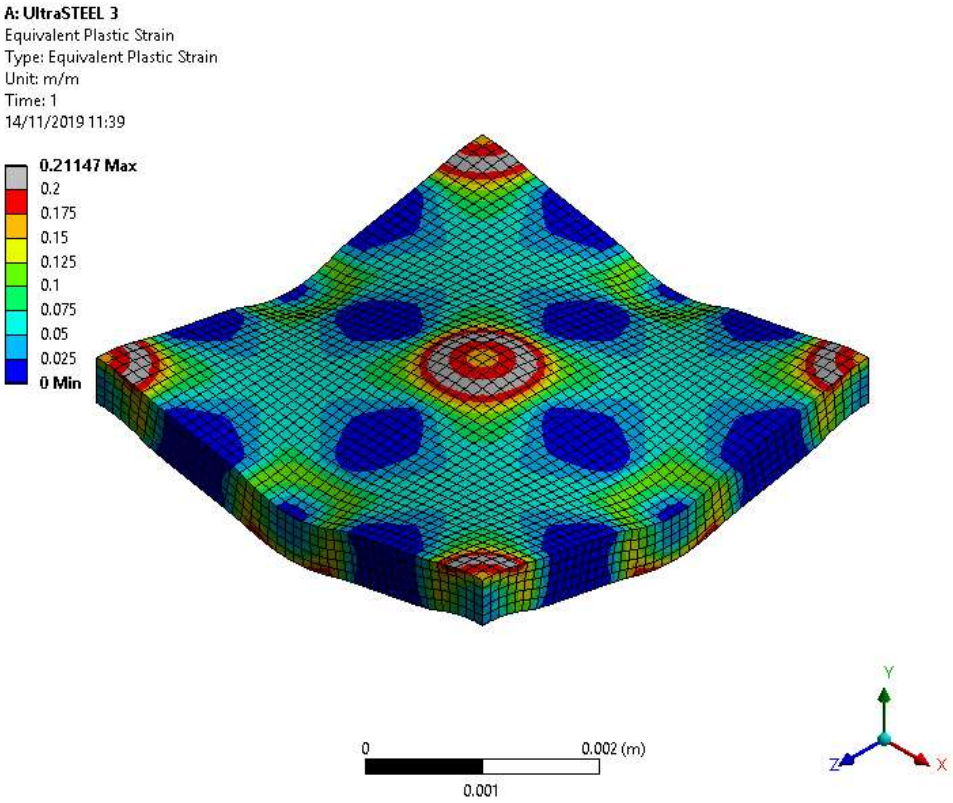

Figure 7.15 – Simulated plastic strain contour for the UltraSTEEL 3® profile

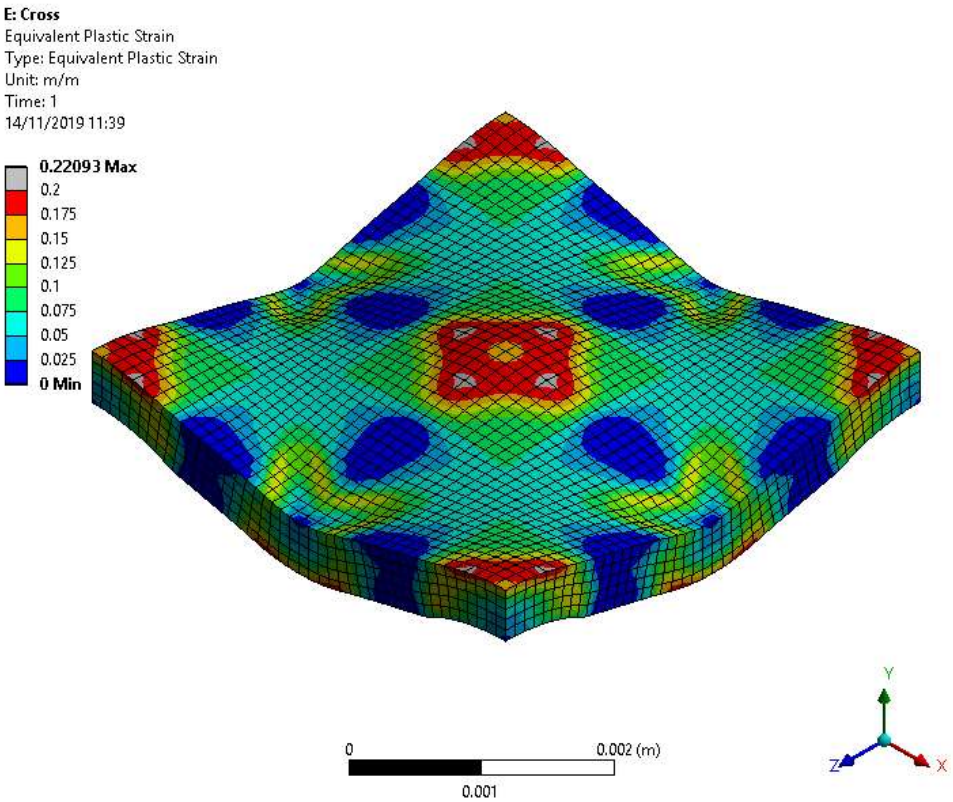

Figure 7.16 - Simulated plastic strain contour for the novel cross profile

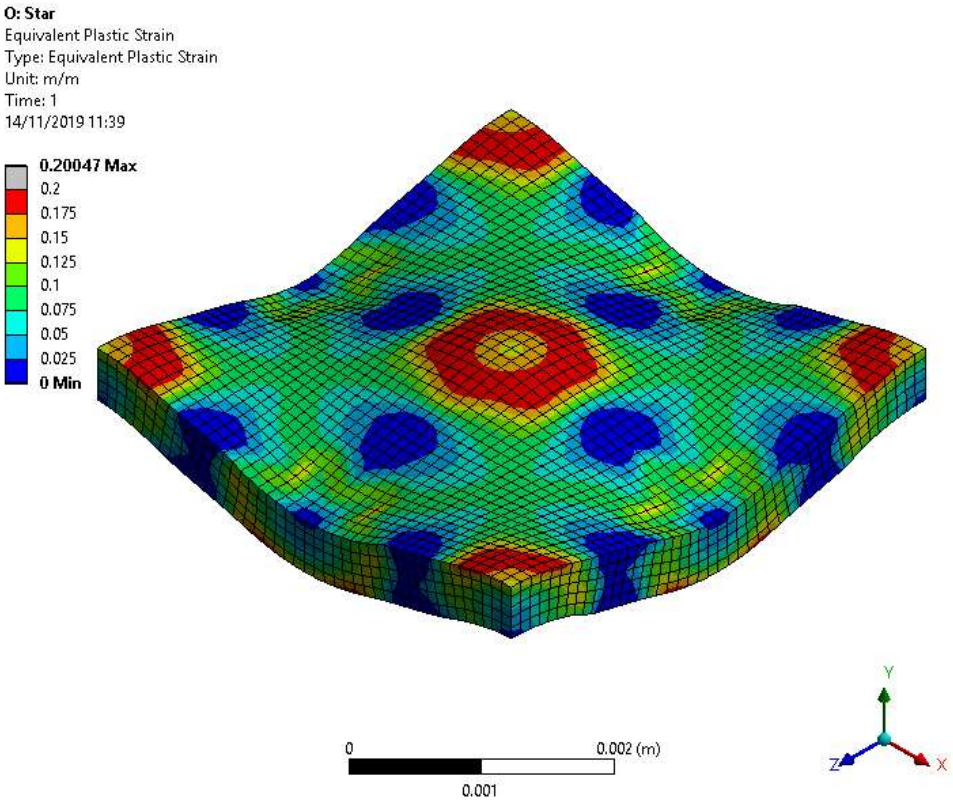

Figure 7.17 - Simulated plastic strain contour for the novel star profile

7.7 Summary

Several novel single-form and multi-form dimple tooth profiles have been analysed in comparison with a spherical profile equivalent to the current standard, UltraSTEEL 3®, as well as the previously considered ellipsoid profile using the finite element method. These have been assessed based on the resulting plastic strain distribution curves, plastic strain contours, and resultant material thinning.

It was determined that, with the exception of the star profile, all the profiles considered result in greater material thinning than the UltraSTEEL 3® profile. The star profile was found to exhibit a marginal reduction in thinning, approximately 0.36%.

Regarding the plastic strain distribution curves, all the profiles considered result in higher levels of plastic strain than UltraSTEEL 3®. However, for most, this included unacceptable increases to the maximum plastic strain. The exceptions to this are the cross profile, which produces a maximum plastic strain similar to that due to the UltraSTEEL 3® profile, and the star profile, which reduces the maximum strain to eliminate the over-strained regions while maintaining desirable increases to plastic strain.

Thus, exhibiting improved thinning and plastic strain characteristics, the present data indicates that the star profile will likely improve upon the structural performance of dimpled steel compared to the UltraSTEEL 3® profile without any modification to the cold roll forming process necessary and without any additional difficulty ensuring correct roll alignment.

Chapter 8 Conclusions and Future Work

In this thesis, the effect of the dimpling process, in the form of UltraSTEEL®, on the microstructure and mechanical properties of steel has been investigated. This work included microstructural examinations (SEM), extensive tensile testing, statistical modelling, and detailed finite element analysis. The new understanding developed was then applied alongside existing knowledge to the design of novel tooth profiles which were analysed and assessed using the finite element method.

8.1 Summary of Findings

- Extensive experimental tensile testing of both plain steel and dimpled steel dogbone samples revealed that the dimpling process results in average increases of 9.9% and 9.3% for yield and ultimate tensile stress, respectively.
- Microstructural investigation by SEM of the dimpled steel through-thickness cross-section in the rolling direction provided indications of some degree of grain size refinement due to the dimpling process. This suggests that grain boundary strengthening is also a relevant consideration for strengthening due to the dimpling process.
- An expression linking the Lüders Elongation in the plain steel to the yield strength increase due to the dimpling process was developed. This enables greater control over product yield strengths in industry.

$$Y_{inc} = -336Y_e + 21.8$$

- FE and analytical methods were used to illustrate that the non-uniform stress distributions resulting from the non-uniform geometry of dimpled samples

results in a necessary reduction in stiffness. This was determined to be counteracted by the material property changes resulting from the dimpling process.

- Experimental testing revealed that the sample-wide average Elastic Modulus decreases with increasing axial strain for both plain steel and dimpled steel. It was observed that these average Elastic Moduli for corresponding plain and dimpled samples converge with increasing axial strain. This was attributed to a combination of diminishing geometric effects due to unfolding dimples and local material failure due to stress concentrations negating the strengthening effects of dimpling in dimpled steels.
- A novel yield criterion was presented and applied to cases exhibiting discontinuous, continuous, and severely continuous yield (no substantial linear-elastic region in the stress-strain curve) behaviours. Based on the second derivative of stress with respect to strain, this method is applicable independent of yield behaviour and macroscopic geometric non-uniformities and has been shown to produce a more representative measure of the behaviour of dimpled steel than current standards.
- The novel 'star' dimple geometry was proposed as an alternative to the current standard UltraSTEEL 3®. Assessed using FE methods, this novel geometry has been shown to increase plastic strain over approximately 90% of the material without causing an unacceptably high peak plastic strain. Furthermore, the novel geometry exhibits a marginally reduced thinning compared to UltraSTEEL 3® and is likely to present no additional difficulties regarding roll alignment.

8.2 Discussion and Recommendations for Further Investigation

The present study has explored, and sought to maximise, the beneficial effects of the dimpling process on the mechanical properties of steel. In the course of the constituent investigations, questions beyond the scope of this thesis have revealed themselves. These are detailed below alongside recommendations for future work.

- The SEM investigation presented in Chapter 3 provided indications of grain size refinement due to dimpling. However, this assumed that the inter-dimple region can be considered somewhat representative of the plain steel microstructure. The benefit of this assumption is that variations within the source material need not be considered when comparing plain and dimpled samples since no such comparison is necessary. However, this does also limit the validity of the indications produced. Therefore, a more extensive microstructural study is recommended. This should include imaging of several corresponding plain and dimpled samples to explicitly assess the effects of dimpling on the microstructure of processed material. This may serve to provide standalone proof of grain boundary refinement due to dimpling.
- Additionally, due to the identified relevance of the initial grain size of the source material, it is expected that different metals will perform differently. Thus, a more extensive study may seek to include consideration for materials such as other grades of steel or aluminium, for example. This would determine whether the observed link between Lüders elongation and strengthening can be extended to other source materials either with or without modification to the predictive expression developed here.

- An experimental study of novel dimple tooth profile(s) is also recommended. This would allow not only direct assessment of the potential strengthening effect of the proposed profile(s) on the relevant source material, it would also allow assessment of the stiffness implications. Furthermore, a more extensive study of the dimple tooth geometry would allow optimisation of the profile for both yield strength and stiffness. This is because the slightly interwoven nature of the cross and star profiles presented here may allow disruption of the plain steel mean-line discussed in section 5.5 . It is expected that optimisation of the ellipsoids of which the cross and star profiles are composed may provide stiffness gains regardless of sample orientation relative to the bending line while maintaining the potential increases to yield strength discussed here.

References

1 Tahir, M.M., Siang, T.C., Ngian, S.P.: 'Typical tests on cold-formed steel structures', in 'Proceedings of the 6th Asia-Pacific Structural Engineering and Construction Conference (APSEC 2006)., Kuala Lumpur, Malaysia' (2006), pp. 246–258

2 Nguyen, V.B., Wang, C.J., Mynors, D.J., English, M.A., Castellucci, M.A.: 'Dimpling process in cold roll metal forming by finite element modelling and experimental validation'*J. Manuf. Process.*, 2014, **16**, (3), pp. 363–372.

3 Bramley, A.N., Mynors, D.J., English, M., Castellucci, M.: 'Controlling the Cold Roll Forming Design Process'*CIRP Ann. - Manuf. Technol.*, 2006, **55**, (1), pp. 271–274.

4 Collins, J., Castellucci, M.A., Hartley, P., Pillinger, I.: 'Formation and performance of dimpled steel sheet', in 'ADVANCES IN MANUFACTURING TECHNOLOGY-CONFERENCE-' (TAYLOR & FRANCIS LTD, 2003), pp. 87–92

5 Hadley Group: 'Hadley Industries PLC, PO Box 92, Downing Street, Smethwick, Birmingham, B66 2PA, United Kingdom' (2018)

6 Hadley Group: 'Hadley Group - Cold Rollforming', https://www.hadleygroup.com/capabilities/cold-rollforming, accessed September 2018

7 Liang, C., Wang, C., Nguyen, B., Mynors, D.: 'Explicit dynamics finite element analysis of energy absorption characteristics of thin-walled ultrasteel columns'2016.

8 Nguyen, V.B., English, M.: 'Effects of cold roll dimpling process on mechanical properties of dimpled steel'*Procedia Eng.*, 2017, **207**, pp. 1290–1295.

9 Ng, R. (Research and D.E.-H.Ind.): 'Phone Call - Ng, R. of Hadley Industries Research and Development' (2018)

10 British Standards Institution: 'BS EN 10346:2015 - Continuously hot-dip coated steel flat products for cold forming' (BSI, 2015)

11 Ng, R. (Research and D.E.-H.Ind.): 'E-mail - Ng, R. of Hadley Industries Research and Development' (2016)

12 British Standards Institution: 'BS EN 10002-1:2001 - Metallic Materials - Tensile Testing. Part 1' (BSI, 2001)

13 Collins, J., Castellucci, M., Pillinger, I., Hartley, P.: 'The influence of tool design on the development of localised regions of plastic deformation in sheet metal formed products to improve structural performance'*Met. Form.*, 2004.

14 Nguyen, V.B., Wang, C.J., Mynors, D.J., English, M.A., Castellucci, M.A.: 'Mechanical Properties and Structural Behaviour of Cold-roll Formed Dimpled Steel'*Spec. Top.*, 2011, p. 6.

15 Nguyen, V.B., Wang, C.J., Mynors, D.J., Castellucci, M.A., English, M.A.: 'Finite element simulation on mechanical and structural properties of cold-formed dimpled steel'*Thin-Walled Struct.*, 2013, **64**, pp. 13–22.

16 Nguyen, B., English, M., Castellucci, M.: 'FE Simulation Techniques for New Process and Product Developments in Metal Forming Industry', in International Cold Forming Congress, (2015)

17 Nguyen, V.B., Mynors, D.J., Wang, C.J., Castellucci, M.A., English, M.A.: 'Analysis and design of cold-formed dimpled steel columns using Finite Element techniques'*Finite Elem. Anal. Des.*, 2016, **108**, pp. 22–31.

18 Wang, C.J., Mynors, D.J., English, M.A.: 'Simulating the UltraSTEEL surface dimpling process'*Key Eng. Mater.*, 2009, **410/411**.

19 Liang, C.: 'Impact response analysis of structures incorporating novel design features'. University of Sussex, 2017

20 Callister Jr., W.D.: '4. Imperfections in Solids', in 'Materials Science and Engineering: An Introduction' (John Wiley & Sons, 2003, 6th Edition), pp. 65–90

21 Toribio, J., Ovejero, E.: 'Microstructure evolution in a pearlitic steel subjected to progressive plastic deformation'*Mater. Sci. Eng. A*, 1997, **234–236**, pp. 579–582.

22 Li, H., Feng, L., Yang, H.: 'Deformation mechanism of cold ring rolling in view of texture evolution predicted by a newly proposed polycrystal plasticity model'*Trans. Nonferrous Met. Soc. China*, 2013, **23**, (12), pp. 3729–3738.

23 Jin, L., Dong, J., Sun, J., Luo, A.A.: 'In-situ investigation on the microstructure evolution and plasticity of two magnesium alloys during three-point bending'*Int. J. Plast.*, 2015, **72**, pp. 218–232.

24 Tang, X., Wang, B., Zhang, H., Fu, X., Ji, H.: 'Study on the microstructure evolution during radial-axial ring rolling of IN718 using a unified internal state variable material model'*Int. J. Mech. Sci.*, 2017, **128–129**, pp. 235–252.

25 Guan, K., Yang, Q., Bu, F., *et al.*: 'Microstructures and mechanical properties of a high-strength Mg-3.5Sm-0.6Zn-0.5Zr alloy'*Mater. Sci. Eng. A*, 2017, **703**, pp. 97–107.

26 Alizadeh, R., Mahmudi, R., Pereira, P.H.R., Huang, Y., Langdon, T.G.: 'Microstructural evolution and superplasticity in an Mg–Gd–Y–Zr alloy after processing by different SPD techniques'*Mater. Sci. Eng. A*, 2017, **682**, pp. 577–585.

27 Minárik, P., Veselý, J., Král, R., *et al.*: 'Exceptional mechanical properties of ultra-fine grain Mg-4Y-3RE alloy processed by ECAP'*Mater. Sci. Eng. A*, 2017, **708**, pp. 193–198.

28 Zhang, J., Xie, H., Lu, Z., Ma, Y., Tao, S., Zhao, K.: 'Microstructure evolution and mechanical properties of AZ80 magnesium alloy during high-pass multi-directional forging'*Results Phys.*, 2018, **10**, pp. 967–972.

29 Wang, B., Liu, C., Gao, Y., Jiang, S., Chen, Z., Luo, Z.: 'Microstructure evolution and mechanical properties of Mg-Gd-Y-Ag-Zr alloy fabricated by multidirectional forging and ageing treatment'*Mater. Sci. Eng. A*, 2017, **702**, pp. 22–28.

30 Toribio, J.: 'Relationship between microstructure and strength in eutectoid steels'*Mater. Sci. Eng. A*, 2004, **387–389**, pp. 227–230.

31 Dieter, G.E.: '7 Fracture', in 'Mechanical Metallurgy' (1988, SI Metric Edition), pp. 241–274

32 Wang, Q., Mu, Y., Lin, J., Zhang, L., Roven, H.J.: 'Strengthening and toughening mechanisms of an ultrafine grained Mg-Gd-Y-Zr alloy processed by cyclic extrusion and compression'*Mater. Sci. Eng. A*, 2017, **699**, pp. 26–30.

33 Liu, W.Y., Suzuki, Y., Iizuka, T., Shiratori, T., Komatsu, T.: 'Variation of tensile and bending rigidities of a duplex embossed steel sheet by small uniaxial tensile deformation'*J. Mater. Process. Technol.*, 2018, **261**, pp. 123–139.

34 'UltraSTEEL® - Hadley Group', https://www.hadleygroup.com/capabilities/ultrasteel, accessed February 2019

35 Wang, Y., Guan, B., Mu, L., Zang, Y.: 'Equivalent Tensile Properties Analysis of the Dimpled Sheet'*J. Fail. Anal. Prev.*, 2018.

36 Nguyen, V.B., Wang, C.J., Mynors, D.J., English, M.A., Castellucci, M.A.: 'Compression tests of cold-formed plain and dimpled steel columns'*J. Constr. Steel Res.*, 2012, **69**, (1), pp. 20–29.

37 Hadley Group: 'Hadley Group - Construction', https://www.hadleygroup.com/markets/construction, accessed October 2019

38 Dieter, G.E.: '1 Introduction', in 'Mechanical Metallurgy' (1988, SI Metric Edition), pp. 3–16

39 Johnson, W.: '4: Plasticity theory and some quasi-static analyses', in 'Impact Strength of Materials' (1972), pp. 121–211

40 Mac Donald, B.J.: '2 Fundamentals of Stress Analysis', in 'Practical Stress Analysis with Finite Elements' (Glasnevin Publishing, 2011, Second Edition), pp. 17–46

41 'ASTM International - Standards Worldwide', https://www.astm.org/, accessed October 2019

42 Dieter, G.E.: '6 Strengthening Mechanisms', in 'Mechanical Metallurgy' (1988, SI Metric Edition), pp. 184–240

43 Rosenberg, H.M.: '4. Dislocations in crystals', in 'The Solid State' (Oxford University Press, New York, 1988, Third Edition), pp. 53–77

44 ASTM: 'Standard Test Methods for Tension Testing of Metallic Materials'2016, **E8/E8M-16a**.

45 Dieter, G.E.: '3 Elements of the Theory of Plasticity', in 'Mechanical Metallurgy' (1988, SI Metric Edition), pp. 69–99

46 Donovan, P.E.: 'A yield criterion for Pd40Ni40P20 metallic glass'*Acta Metall.*, 1989, **37**, (2), pp. 445–456.

47 Cowin, S.C., He, Q.-C.: 'Tensile and compressive stress yield criteria for cancellous bone'*J. Biomech.*, 2005, **38**, (1), pp. 141–144.

48 Karafillis, A.P., Boyce, M.C.: 'A general anisotropic yield criterion using bounds and a transformation weighting tensor'*J. Mech. Phys. Solids*, 1993, **Vol. 41**, (No. 12), pp. 1859–1886.

49 Banabic, D., Kuwabara, T., Balan, T., Comsa, D.S., Julean, D.: 'Non-quadratic yield criterion for orthotropic sheet metals under plane-stress conditions'*Int. J. Mech. Sci.*, 2003, **45**, (5), pp. 797–811.

50 Cazacu, O., Barlat, F.: 'A criterion for description of anisotropy and yield differential effects in pressure-insensitive metals'*Int. J. Plast.*, 2004, **20**, (11), pp. 2027–2045.

51 Cazacu, O., Plunkett, B., Barlat, F.: 'Orthotropic yield criterion for hexagonal closed packed metals'*Int. J. Plast.*, 2006, **22**, (7), pp. 1171–1194.

52 Plunkett, B., Cazacu, O., Barlat, F.: 'Orthotropic yield criteria for description of the anisotropy in tension and compression of sheet metals'*Int. J. Plast.*, 2008, **24**, (5), pp. 847–866.

53 Gopu, V.K.A.: 'Validity of Distortion-Energy-Based Strength Criterion for Timber Members'*J. Struct. Eng.*, 1987, **113**, (12), pp. 2475–2487.

54 Kuroda, M., Tvergaard, V.: 'Forming limit diagrams for anisotropic metal sheets with different yield criteria'*Int. J. Solids Struct.*, 2000, p. 23.

55 Sevostianov, I., Kachanov, M.: 'On the yield condition for anisotropic porous materials'*Mater. Sci. Eng. A*, 2001, **313**, (1–2), pp. 1–15.

56 Keralavarma, S.M., Benzerga, A.A.: 'An approximate yield criterion for anisotropic porous media'*Comptes Rendus Mécanique*, 2008, **336**, (9), pp. 685–692.

57 Liao, K.-C., Pan, J., Tang, S.C.: 'Approximate yield criteria for anisotropic porous ductile sheet metals'*Mech. Mater.*, 1997, **26**, (4), pp. 213–226.

58 Madou, K., Leblond, J.-B.: 'A Gurson-type criterion for porous ductile solids containing arbitrary ellipsoidal voids—II: Determination of yield criterion parameters'*J. Mech. Phys. Solids*, 2012, **60**, (5), pp. 1037–1058.

59 McElwain, D.L.S., Roberts, A.P., Wilkins, A.H.: 'Yield criterion of porous materials subjected to complex stress states'*Acta Mater.*, 2006, **54**, (8), pp. 1995–2002.

60 Narayanasamy, R., Ponalagusamy, R., Subramanian, K.R.: 'Generalised yield criteria of porous sintered powder metallurgy metals'*J. Mater. Process. Technol.*, 2001, **110**, (2), pp. 182–185.

61 Wang, D.-A., Pan, J., Liu, S.-D.: 'An Anisotropic Gurson Yield Criterion for Porous Ductile Sheet Metals with Planar Anisotropy'*Int. J. Damage Mech.*, 2004, **13**, (1), pp. 7–33.

62 Gurson, A.L.: 'Continuum Theory of Ductile Rupture by Void Nucleation and Growth: Part I - Yield Criteria and Flow Rules for Porous Ductile Media'*US Energy Res. Dev. Adm.*, 1975.

63 Gurson, A.L.: 'Porous Rigid-Plastic Materials Containing Rigid Inclusions - Yield Function, Plastic Potential, and Void Nucleation'*US Energy Res. Dev. Commision*, 1976.

64 da Silva, M.G., Ramesh, K.T.: 'The rate-dependent deformation and localization of fully dense and porous Ti-6Al-4V'*Mater. Sci. Eng. A*, 1997, **232**, (1–2), pp. 11–22.

65 Kee, A., Matic, P., K. Everett, R.: 'A mesoscale computer simulation of multiaxial yield in gasar porous copper'*Mater. Sci. Eng. A*, 1998, **249**, (1–2), pp. 30–39.

66 Chawla, N., Deng, X.: 'Microstructure and mechanical behavior of porous sintered steels'*Mater. Sci. Eng. A*, 2005, **390**, (1–2), pp. 98–112.

67 Wang, L., Kang, J., Sun, C., Li, D., Cao, Y., Jin, Z.: 'Mapping porous microstructures to yield desired mechanical properties for application in 3D printed bone scaffolds and orthopaedic implants'*Mater. Des.*, 2017, **133**, pp. 62–68.

68 Clausen, B., Lorentzen, T., Bourke, M.A.M., Daymond, M.R.: 'Lattice strain evolution during uniaxial tensile loading of stainless steel'*Mater. Sci. Eng. A*, 1999, **259**, (1), pp. 17–24.

69 Zhang, Y., Fan, H., Fang, D.: 'Constitutive relations and failure criterion of planar lattice composites'*Compos. Sci. Technol.*, 2008, **68**, (15–16), pp. 3299–3304.

70 Deshpande, V.S., Fleck, N.A., Ashby, M.F.: 'Effective properties of the octet-truss lattice material'*J Mech Phys Solids*, 2001, p. 23.

71 Hualin, F., Wei, Y.: 'An equivalent continuum method of lattice structures'*Acta Mech. Solida Sin.*, 2006, **19**, (2), pp. 103–113.

72 Ashby, M.F.: 'The properties of foams and lattices'*Philos. Trans. R. Soc. Math. Phys. Eng. Sci.*, 2006, **364**, (1838), pp. 15–30.

73 Shen, Y., Mckown, S., Tsopanos, S., Sutcliffe, C.J., Mines, R.A.W., Cantwell, W.J.: 'The Mechanical Properties of Sandwich Structures Based on Metal Lattice Architectures'*J. Sandw. Struct. Mater.*, 2010, **12**, (2), pp. 159–180.

74 Li, M., Wu, L., Ma, L., Wang, B., Guan, Z.: 'Mechanical Response of All-composite Pyramidal Lattice Truss Core Sandwich Structures'*J. Mater. Sci. Technol.*, 2011, **27**, (6), pp. 570–576.

75 Chen, H., Zheng, Q., Zhao, L., Zhang, Y., Fan, H.: 'Mechanical property of lattice truss material in sandwich panel including strut flexural deformation'*Compos. Struct.*, 2012, **94**, (12), pp. 3448–3456.

76 Vigliotti, A., Pasini, D.: 'Stiffness and strength of tridimensional periodic lattices'*Comput. Methods Appl. Mech. Eng.*, 2012, **229–232**, pp. 27–43.

77 Khaderi, S.N., Deshpande, V.S., Fleck, N.A.: 'The stiffness and strength of the gyroid lattice'*Int. J. Solids Struct.*, 2014, **51**, (23–24), pp. 3866–3877.

78 Dieter, G.E.: 'Mechanical Metallurgy' (1988, SI Metric Edition)

79 Pagano, N.J.: 'Distortional Energy of Composite Materials'*J. Compos. Mater.*, 1975, **9**.

80 Barlat, F., Lian, K.: 'Plastic behavior and stretchability of sheet metals. Part I: A yield function for orthotropic sheets under plane stress conditions'*Int. J. Plast.*, 1989, **5**, (1), pp. 51–66.

81 Kuwabara, T., Van Bael, A.: 'Measurement and Analysis of Yield Locus of Sheet Aluminium Alloy 6xxx', in 'Proceedings of Numisheet '99' Numisheet '99, (1999), p. 8

82 Kuwabara, T., Ikeda, S., Kuroda, K.: 'Measurement and analysis of differential work hardening in cold-rolled steel sheet under biaxial tension'*J. Mater. Process. Technol.*, 1998, **80–81**, pp. 517–523.

83 Ide, T., Tane, M., Ikeda, T., Hyun, S.K., Nakajima, H.: 'Compressive properties of lotus-type porous stainless steel'*J. Mater. Res.*, 2006, **21**, (1), pp. 185–193.

84 Máthis, K., Horváth, K., Farkas, G., Choe, H., Shin, K., Vinogradov, A.: 'Investigation of the Microstructure Evolution and Deformation Mechanisms of a Mg-Zn-Zr-RE Twin-Roll-Cast Magnesium Sheet by In-Situ Experimental Techniques'*Materials*, 2018, **11**, (2), p. 200.

85 Tvergaard, V., Needleman, A.: 'Analysis of the cup-cone fracture in a round tensile bar'*Acta Metall.*, 1984, **32**, (1), pp. 157–169.

86 Sonmez, F.O., Demir, A.: 'Analytical relations between hardness and strain for cold formed parts'*J. Mater. Process. Technol.*, 2007, **186**, (1–3), pp. 163–173.

87 English, M. (Director of T.-H.Ind.), Wang, C. (Senior L. in M.E.-U. of S., Ng, R. (Research and D.E.-H.Ind.): 'Research Meeting - Hadley Industries Research and Development' (2017)

88 Dieter, G.E.: '5. Plastic Deformation of Polycrystalline Aggregates', in 'Metallurgy and Metallurgical Engineering Series: Mechanical Metallurgy' (McGraw-Hill Book Company, 1961), pp. 118–157

89 Edelglass, S.M.: '10 Dislocations and Plastic Flow', in 'Engineering Materials Science: Structure and Mechanical Behavior of Solids' (The Ronald Press Company, 1966), pp. 321–365

90 Callister Jr., W.D.: '7. Dislocations and Strengthening Mechanisms', in 'Materials Science and Engineering: An Introduction' (John Wiley & Sons, 2003, 6th Edition), pp. 162–191

91 Callister Jr., W.D.: '3. The Structure of Crystalline Solids', in 'Materials Science and Engineering: An Introduction' (John Wiley & Sons, 2003, 6th Edition), pp. 31–64

92 English, M. (Director of T.-H.Ind.), Wang, C. (Senior L. in M.E.-U. of S., Ng, R. (Research and D.E.-H.Ind.): 'Research Meeting - Hadley Industries Research and Development' (2016)

93 English, M. (Director of T.-H.Ind.), Ng, R. (Research and D.E.-H.Ind.): 'Conference Call - Hadley Industries Research and Development' (2017)

94 Dieter, G.E.: '8 The Tension Test', in 'Mechanical Metallurgy' (1988, SI Metric Edition), pp. 275–324

95 Mac Donald, B.J.: '5 Material Modelling', in 'Practical Stress Analysis with Finite Elements' (Glasnevin Publishing, 2011, Second Edition), pp. 163–189

96 SAS IP, Inc: '3.4. Plasticity Models', https://www.sharcnet.ca/Software/Fluent14/help/ans_mat/amp8sq21dldm.html#biso, accessed March 2019

97 SAS IP, Inc: '3.4. Rate-Independent Plasticity', https://www.sharcnet.ca/Software/Ansys/16.2.3/en-us/help/ans_mat/amp8sq21dldm.html#biso, accessed March 2019

98 Tovee, J.-P.: 'Microstructural influence on the effects of forward and reverse mechanical deformation in HSLA X65 and X80 linepipe steels'. University of Birmingham, 2014

99 Field, A.: '14 GLM 3: factorial Designs', in 'Discovering Statistics Using IBM SPSS Statistics' (SAGE Publications Ltd, 2018, 5th Edition), pp. 607–648

100 Dieter, G.E.: '16. Statistics Applied to Materials Testing', in 'Metallurgy and Metallurgical Engineering Series: Mechanical Metallurgy' (McGraw-Hill Book Company, 1961), pp. 419–452

101 Field, A.: '8 Correlation', in 'Discovering Statistics Using IBM SPSS Statistics' (SAGE Publications Ltd, 2018, 5th Edition), pp. 333–368

102 Field, A.: '9 The Linear Model (Regression)', in 'Discovering Statistics Using IBM SPSS Statistics' (SAGE Publications Ltd, 2018, 5th Edition), pp. 369–436

103 'F Statistic / F Value: Definition and How to Run an F-Test', https://www.statisticshowto.datasciencecentral.com/probability-and-statistics/f-statistic-value-test/, accessed April 2019

104 Field, A.: '2 The SPINE of Statistics', in 'Discovering Statistics Using IBM SPSS Statistics' (SAGE Publications Ltd, 2018, 5th Edition), pp. 47–93

105 Brown, A.M.: 'A step-by-step guide to non-linear regression analysis of experimental data using a Microsoft Excel spreadsheet'*Comput. Methods Programs Biomed.*, 2001, **65**, (3), pp. 191–200.

106 'Microsoft Excel' (Microsoft, 2019)

107 'IBM SPSS Statistics 25' (IBM, 2019)

108 Hadley Group: 'Standard Operation Sheet - Tensile Testing' (Hadley Group Technology, 02/18)

109 Liang, C., Wang, C.J., English, M., Mynors, D.: 'Optimization of the UltraSTEEL Dimpling Forming Process for Energy Absorption'*Procedia Eng.*, 2017, **207**, pp. 1284–1289.

110 Nguyen, V.B. (Senior L. in C.E.-U. of D., Wang, C. (Senior L. in M.E.-U. of S.: 'Phone Call - V. B. Nguyen of Derby University' (2018)

111 'ANSYS Workbench version 19.2' (ANSYS Inc., 2019)

112 'Beam Stress & Deflection | MechaniCalc', https://mechanicalc.com/reference/beam-analysis, accessed May 2019

113 Patnaik, S.N., Hopkins, D.A.: 'Chapter 3 - Simple Beam', in Patnaik, S.N., Hopkins, D.A. (Eds.): 'Strength of Materials; A Unified Theory' (Butterworth-Heinemann, 2004), pp. 129–215

114 'International Organization for Standardization', http://www.iso.org/cms/render/live/en/sites/isoorg/home.html, accessed October 2019

115 'European Committee for Standardization', https://www.cen.eu/Pages/default.aspx, accessed October 2019

116 ‘British Standards Institution | BSI Group’, https://www.bsigroup.com/en-GB/, accessed October 2019

117 ‘Standards Australia - Standard Organisation in Australia’, http://www.standards.org.au/, accessed October 2019

Appendix – Quasi-Static Uniaxial Tensile Testing: Summary of Results

Table 9 and Table 10 are summaries of the variables measured for plain steel and dimpled steel, respectively. These were measured from the tensile stress-strain curves produced during the testing presented in Chapter 3 (engineering strain and strain). Each value is the average of the samples taken from the corresponding material source coil and is presented in the form 'Mean ± *SD*'.

Table 9 – Plain steel - summary of variables measured from the tensile stress-strain curves.

Coil	$\sigma_{Y,0.2}$ *(MPa)*	σ_{UY} *(MPa)*	σ_{LY} *(MPa)*	*UTS (MPa)*	*E (GPa)*	T_m *(P) (MPa)*	Y_d *(MPa)*	Y_e *(mm/mm)*	$\varepsilon_{y,0.2}$ *(mm/mm)*	ε_{UTS} *(mm/mm)*	Δ_σ *(MPa)*	Δ_ε *(mm/mm)*
1	323 ± 3	327 ± 6	318 ± 1	387 ± 1	172 ± 40	486 ± 83	9 ± 7	0.02712 ± 0.00058	0.00390 ± 0.00047	0.20667 ± 0.00144	64 ± 3	0.20277 ± 0.00138
2	326 ± 4	327 ± 4	320 ± 6	386 ± 3	167 ± 21	483 ± 1	7 ± 1	0.03074 ± 0.00285	0.00390 ± 0.00021	0.20583 ± 0.00161	60 ± 1	0.20194 ± 0.00161
3	323 ± 4	325 ± 4	321 ± 2	386 ± 2	176 ± 55	516 ± 45	4 ± 2	0.02932 ± 0.00453	0.00410 ± 0.00011	0.20750 ± 0.00087	63 ± 2	0.20340 ± 0.00096
4	327 ± 1	331 ± 2	325 ± 2	391 ± 2	152 ± 31	499 ± 21	7 ± 2	0.02821 ± 0.00188	0.00416 ± 0.00039	0.20817 ± 0.00225	64 ± 2	0.20401 ± 0.00187
5	332 ± 3	334 ± 4	328 ± 4	391 ± 5	174 ± 18	489 ± 16	6 ± 1	0.03462 ± 0.00298	0.00391 ± 0.00013	0.19933 ± 0.00153	59 ± 3	0.19543 ± 0.00159
6	326 ± 3	331 ± 1	320 ± 4	374 ± 5	181 ± 21	274 ± 38	11 ± 4	0.05137 ± 0.00081	0.00390 ± 0.00017	0.22333 ± 0.00189	48 ± 4	0.21944 ± 0.00189
7	335 ± 6	339 ± 6	332 ± 7	389 ± 4	146 ± 18	417 ± 17	6 ± 2	0.03519 ± 0.00439	0.00419 ± 0.00025	0.20600 ± 0.00786	54 ± 2	0.20181 ± 0.00796
8	335 ± 1	337 ±2	332 ± 1	396 ± 3	175 ± 21	465 ± 16	5 ± 1	0.02927 ± 0.00240	0.00389 ± 0.00019	0.21317 ± 0.00126	60 ± 3	0.20927 ± 0.00143
9	329 ± 3	330 ± 3	325 ± 2	394 ± 5	161 ± 20	560 ± 76	5 ± 3	0.02722 ± 0.00583	0.00413 ± 0.00054	0.20825 ± 0.00417	64 ± 5	0.20412 ± 0.00461
10	329 ± 4	336 ± 3	321 ± 1	376 ± 2	183 ± 28	251 ± 15	15 ± 3	0.04928 ± 0.00434	0.00395 ± 0.00035	0.22333 ± 0.00437	47 ± 3	0.21939 ± 0.00409
11	320 ± 9	323 ± 9	318 ± 10	369 ± 8	189 ± 16	310 ± 23	5 ± 2	0.04828 ± 0.00252	0.00369 ± 0.00015	0.19451 ± 0.01571	50 ± 4	0.19082 ± 0.01576
12	327 ± 6	329 ± 6	323 ± 6	379 ± 3	184 ± 2	425 ± 22	6 ± 2	0.03632 ± 0.00397	0.00379 ± 0.00006	0.19463 ± 0.00194	52 ± 3	0.19084 ± 0.00192
13	316 ± 3	317 ± 3	310 ± 3	366 ± 2	177 ± 13	351 ± 21	7 ± 1	0.04480 ± 0.00343	0.00376 ± 0.00009	0.18954 ± 0.01296	50 ± 2	0.18578 ± 0.01296
14	304 ± 2	306 ± 4	301 ± 2	365 ± 1	161 ± 15	455 ± 29	5 ± 3	0.03979 ± 0.00332	0.00393 ± 0.00018	0.18711 ± 0.00951	61 ± 1	0.18318 ± 0.00965
15	293 ± 3	294 ± 3	291 ± 3	363 ± 3	170 ± 12	631 ± 22	3 ± 1	0.01926 ± 0.00297	0.00373 ± 0.00013	0.19669 ± 0.00556	70 ± 2	0.19296 ± 0.00562
16	329 ± 2	332 ± 2	327 ± 2	396 ± 1	182 ± 14	670 ± 26	5 ± 2	0.02915 ± 0.00194	0.00381 ± 0.00012	0.16683 ± 0.00343	67 ± 2	0.16302 ± 0.00338
17	299 ± 6	301 ± 5	298 ± 5	375 ± 4	182 ± 30	801 ± 105	3 ± 1	0.01713 ± 0.00226	0.00367 ± 0.00029	0.18100 ± 0.00411	76 ± 2	0.14186 ± 0.07939
18	310 ± 3	312 ± 4	305 ± 2	360 ± 3	206 ± 35	332 ± 80	7 ± 4	0.04740 ± 0.00891	0.00356 ± 0.00022	0.22430 ± 0.01393	49 ± 2	0.22074 ± 0.01383
19	361 ± 3	362 ± 3	358 ± 4	430 ± 4	236 ± 12	679 ± 24	4 ± 2	0.03174 ± 0.00160	0.00362 ± 0.00022	0.14741 ± 0.01461	69 ± 2	0.14380 ± 0.01476
20	325 ± 2	326 ± 2	319 ± 2	368 ± 1	221 ± 21	281 ± 11	7 ± 1	0.04946 ± 0.00205	0.00348 ± 0.00014	0.20514 ± 0.00894	43 ± 1	0.20166 ± 0.00894

Table 10 – Dimpled steel - summary of variables measured from the tensile stress-strain curves.

Coil	$\sigma_{Y,0.2}$ *(MPa)*	$\sigma_{\Delta Y}$ *(MPa)*	*UTS (MPa)*	*E (GPa)*	$\varepsilon_{y,0.2}$ *(mm/mm)*	$\varepsilon_{y,\Delta}$ *(mm/mm)*	ε_{UTS} *(mm/mm)*	Δ_σ *(MPa)*	Δ_ε *(mm/mm)*
1	350 ± 7	385 ± 6	414 ± 1	180 ± 18	0.00384 ± 0.00027	0.75745 ± 0.14079	0.09630 ± 0.01795	64 ± 6	0.09246 ± 0.01769
2	364 ± 11	390 ± 5	412 ± 2	161 ± 28	0.00418 ± 0.00051	0.73223 ± 0.10339	0.09073 ± 0.01171	48 ± 11	0.08656 ± 0.01122
3	349 ± 5	386 ± 4	416 ± 3	188 ± 13	0.00377 ± 0.00012	0.72695 ± 0.01655	0.11848 ± 0.00392	67 ± 3	0.11471 ± 0.00382
4	364 ± 2	394 ± 4	423 ± 2	158 ± 46	0.00471 ± 0.00043	0.79543 ± 0.12363	0.09722 ± 0.02018	59 ± 2	0.09251 ± 0.01985
5	347 ± 5	391 ± 9	431 ± 7	164 ± 10	0.00404 ± 0.00015	0.77813 ± 0.05118	0.10247 ± 0.00339	84 ± 4	0.09843 ± 0.00341
6	322 ± 9	361 ± 8	405 ± 8	180 ± 30	0.00364 ± 0.00041	0.75329 ± 0.13360	0.10870 ± 0.03003	83 ± 13	0.10506 ± 0.02984
7	365 ± 2	394 ± 3	424 ± 3	171 ± 27	0.00402 ± 0.00039	0.72124 ± 0.07506	0.10605 ± 0.00657	59 ± 3	0.10203 ± 0.00687
8	363 ± 5	396 ± 9	428 ± 6	184 ± 45	0.00391 ± 0.00060	0.68996 ± 0.03209	0.09670 ± 0.01245	65 ± 2	0.09279 ± 0.01202
9	381 ± 6	409 ± 9	430 ± 5	159 ± 16	0.00430 ± 0.00017	0.74180 ± 0.02227	0.08818 ± 0.01887	49 ± 1	0.08389 ± 0.01874
10	332 ± 14	368 ± 3	409 ± 3	163 ± 26	0.00404 ± 0.00025	0.78900 ± 0.23678	0.11501 ± 0.03038	76 ± 14	0.11097 ± 0.03013
11	349 ± 6	361 ± 8	426 ± 1	275 ± 55	0.00328 ± 0.00028	0.41776 ± 0.11756	0.07384 ± 0.01207	77 ± 6	0.07056 ± 0.01212
12	358 ± 6	376 ± 5	422 ± 2	207 ± 34	0.00375 ± 0.00026	0.47966 ± 0.22227	0.06621 ± 0.00330	64 ± 6	0.06246 ± 0.00339
13	339 ± 2	359 ± 8	410 ± 1	285 ± 26	0.00319 ± 0.00013	0.46381 ± 0.03878	0.07179 ± 0.00510	72 ± 1	0.06860 ± 0.00518
14	327 ± 6	343 ± 6	411 ± 5	215 ± 22	0.00353 ± 0.00012	0.51941 ± 0.04742	0.08137 ± 0.00525	85 ± 2	0.07784 ± 0.00526
15	333 ± 7	353 ± 7	392 ± 3	215 ± 56	0.00363 ± 0.00050	0.54704 ± 0.07893	0.08810 ± 0.01144	59 ± 5	0.08448 ± 0.01163
16	370 ± 5	390 ± 11	432 ± 2	241 ± 40	0.00358 ± 0.00024	0.46844 ± 0.08403	0.06198 ± 0.00713	62 ± 4	0.05840 ± 0.00723
17	348 ± 1	367 ± 5	403 ± 3	211 ± 17	0.00369 ± 0.00013	0.51054 ± 0.06778	0.09916 ± 0.00177	55 ± 3	0.09548 ± 0.00179
18	332 ± 5	345 ± 3	404 ± 3	205 ± 16	0.00365 ± 0.00015	0.47613 ± 0.03726	0.09081 ± 0.01103	72 ± 5	0.08716 ± 0.01100
19	401 ± 3	417 ± 4	469 ± 1	212 ± 20	0.00392 ± 0.00016	0.51654 ± 0.06733	0.05786 ± 0.00557	68 ± 2	0.05394 ± 0.00556
20	330 ± 4	346 ± 5	388 ± 4	236 ± 7	0.00340 ± 0.00004	0.48445 ± 0.06979	0.11926 ± 0.01068	58 ± 5	0.11586 ± 0.01068